I. ACOUSTIC RADIATION AND REFLECTION FROM SPHERES

II. SOME EFFECTS OF THERMAL CONDUCTION AND COMPRESSIBILITY IN THE COLLAPSE OF A SPHERICAL BUBBLE IN A LIQUID

Thesis by

Robert Hickling

In Partial Fulfillment of the Requirements

For the Degree of

Doctor of Philosophy

California Institute of Technology

Pasadena, California

1962

ACKNOWLEDGEMENTS

The author would like to express his grateful appreciation to Professor M. S. Plesset for his encouragement and supervision of the work presented here. He is also indebted to Professor T. K. Caughey for several useful discussions.

The work was supported by the Office of Naval Research and by the International Nickel Company Inc. of America. The author is especially indebted to the latter for fellowships received during the years 1957 - 59, and 1960 - 61.

A large portion of the computation was performed at the Western Data Processing Center at the University of California at Los Angeles. Thanks are due to the International Business Machine Corporation and to the University of California for making this facility available. Thanks are also due to the Computing Facility group at University of California at Los Angeles for advice and assistance. The remainder of the calculations were carried out at the California Institute of Technology Computing Center.

Finally the author would like to express his especial thanks to Mrs. Barbara Hawk for her typing of the manuscript and to Mrs. Zora Harrison for preparation of the drawings.

ABSTRACT

This thesis presents the results of computations for four problems: two in the field of acoustics and two on the collapse of a cavity in a liquid. The first is an analysis of echoes from a solid homogeneous sphere in water, and demonstrates that the vibrations induced in the solid material by incident sound waves have an important effect on the form of the echo. Various materials are examined and the theory is shown to provide a satisfactory explanation for echoes observed in sonar work. The second problem deals with the far-field radiation patterns formed by different types of source distributions on the surface of a rigid sphere, and demonstrates the effect of the shape of a transducer and its housing on such radiation patterns. The problem of the binaural localization of sound sources is also considered. The third problem is concerned with the behavior of a thermally conducting gas inside a collapsing cavity in a liquid. It is shown that, for bubbles of an appropriate size, thermal conduction in the gas can account for the varying intensities of sonoluminescence which have been observed when different gases are dissolved in water. In the final problem, the shock waves which form in the liquid as a result of a cavity collapse are investigated. It is estimated that such shock waves could be a potent cause of cavitation damage.

TABLE OF CONTENTS

GENERAL INTRODUCTION

The results presented in this thesis were obtained largely through the use of a high speed computer. The problems considered come from two areas of basic engineering interest, namely the radiation and scattering of acoustic waves, and cavitation in liquids. These problems have previously been subjected to a certain amount of analytical work. In the case of cavitation several simplified solutions have been obtained, although no solutions have been found for the more generalized equations of motion, while in the acoustic problems generalized closed solutions have been derived but these are so complicated that their implications are clear only in certain simple cases. In essence both these difficulties amount to the same thing in that although the basic physical processes are reasonably well understood, the behavior and interaction of those processes under circumstances of even minor complexity cannot be analyzed in a simple way. This situation is one which has always confronted the research engineer. If he has a good knowledge of basic scientific principles, he can formulate appropriate hypotheses. However, the complexities involved in most applications force him to introduce drastic simplifying assumptions which often reduce his estimates to the level of a well-educated guess. The advent of high speed computers provides the means of overcoming this difficulty. Intractable equations can be solved numerically and complicated closed solutions evaluated for relevant specific examples. This is illustrated in the work presented here. It is also shown how use of a computer can aid in the understanding of a physical process. For example in the first problem, which deals with the reflection of sound by a solid elastic sphere in water, the theory predicts quite closely the complicated echo

structures which have been observed in sonar work. Similarly in the third problem it is shown how thermal conduction in a gas inside a collapsing cavity can be a significant factor in determining the intensity of sonoluminescence.

In the numerical solution of a problem there is always concern with its correctness. A machine program will generally produce some numerical results and it has to be shown that these are the appropriate ones. Even if all known relevant numerical techniques and tests are used, there can often be no absolute assurance in this regard. It is necessary therefore to have additional ways of demonstrating the correctness of the results. It must be shown that the solutions are consistent within themselves and with any related physical law, no matter how trivial. It must also be shown that they include special simple cases and asymptotic solutions. The most satisfactory test will always be of course to obtain a good consistent agreement with observation. These procedures are illustrated in the present work.

Finally it is perhaps necessary to comment on the relation between analytical and numerical work. Numerical solutions can in no way be envisaged as an alternative or substitute for analysis. Analysis provides the formulation and the guide-lines while numerical computation by a high speed computer is the extension of analysis made necessary by the complexity of the problem.

Section A of Part I has been published in the October issue of the Journal of the Acoustical Society 1962. Section B of Part II will appear in the Physics of Fluids. It is expected that Section A of Part II will appear in the Journal of the Acoustical Society.

PART I - ACOUSTIC RADIATION AND REFLECTION FROM SPHERES

Introduction

It is possible to obtain closed solutions in terms of known functions for a large number of problems in acoustics where the symmetry allows the wave equation to be solved by the method of separation of variables. These solutions are generally quite complicated and it is only in the limits, when the wavelength is very large or when it is very small, that they can be simplified into a readily understandable form. Some work has been done to obtain higher order approximations in the neighborhood of these limiting cases, but the problem of understanding the behavior in the intermediate range of wavelengths has in general remained unresolved. This is unfortunate because most acoustic phenomena occur within this range.

There appear to be two possible ways of overcoming the difficulty. The first is to attempt to express the solutions in a more simple analytic form. The second is to accept the closed solutions as they stand and to proceed with a direct numerical evaluation in cases of particular interest. At present there has not been much success in the first approach, and it is uncertain whether it is really practicable. On the other hand not much progress has been made with the second method because of the labor involved in the calculations. However this can now be undertaken by high-speed computers and numerical solutions have therefore become readily obtainable.

The work presented here is concerned with the numerical evaluation of certain closed form solutions involving spherical symmetry.

Section A deals with the scattering of sound waves by a solid elastic sphere in water, and in Section B, far field radiation patterns are obtained for certain source distributions on the surface of a rigid sphere. These results are mainly of interest to the sonar engineer. It is demonstrated for instance in Section A that the multiple echoes which have been observed from a sonar target of regular shape, can be ascribed to the non-rigidity of the target - - a fact which has not been clearly appreciated by workers in the field. Also, the results of Section B demonstrate the importance of the shape of a transducer and its housing in determining the form of radiation patterns. Some of the results of Section B can also be applied to the problem of the binaural localization of sound sources.

SECTION A - AN ANALYSIS OF ECHOES FROM A SOLID ELASTIC SPHERE IN WATER

1. Acoustic Echoes

It is well-known in sonar work that the pulse form of the direct echo returned by a stationary insonified target in water is usually quite different from that of the original signal sent out by the transducer. This effect can be observed even when the target has a regular shape as in the case of a sphere. In the experiments which have been made, the incident sound has consisted of single frequency, constant amplitude pulses of various lengths, and the echo pulse generally appears in the form of multiple echoes of the original pulse; i.e. compared to the original pulse, the echo is generally longer and subject to amplitude modulation. Presumably there are also differences in frequency content, but there does not appear to be any quantitative data available on the subject.

If the body has an irregular shape it is possible to suppose that this effect is due to echoes returned by the individual irregularities. However in the case of regularly shaped bodies with no abrupt changes in curvature, such an explanation cannot be used. In this event it would seem reasonable to suppose that the distortion in the echo is caused either by diffraction or by vibrations occurring within the solid material of the target or by both. The frequencies used in sonar usually preclude the influence of diffraction, so that the observed effects would appear to be due mainly to vibrations in the solid. Since the density of any solid does not differ from that of water by much more than a factor of eight, it seems quite possible for the incident sound to cause vibrations in the solid material of the target. In air the corre-

sponding density ratio would be of the order of 10^4 so that a target would react more like a rigid body, with a consequent diminution in echo distortion.

It is the purpose of this paper to test the validity of this hypothesis in the case of a homogeneous solid sphere supporting shear and compressional waves. Suitable experimental data[1] has recently become available and this is compared with calculated results based on known formal solutions[2],[3]. These results were obtained using a high speed computer. Previous calculations have been made for fluid[4] and rigid[5] spheres.

2. Formulation of the Problem for the Solid Elastic Sphere in Water

The coordinate system for the sphere is shown in Fig. 1 where the relationship between the cartesian and spherical polar coordinates is

$$x = r \sin\theta \cos\phi \ ,$$
$$y = r \sin\theta \cos\phi \ ,$$
$$z = r \cos\theta \ . \qquad (1)$$

The sphere is assumed to consist of solid isotropic material supporting both compressional and shear waves. The displacement vector $\vec{u}$ can be expressed, using the vector and scalar potentials $\vec{A}$ and ψ, as follows[6]

$$\vec{u} = -\nabla\psi + \nabla\times\vec{A} \ , \qquad (2)$$

where

$$\nabla^2\psi = (1/c_1^2)\partial^2\psi/\partial t^2 \ , \qquad (3)$$

$$\nabla^2 \vec{A} = (1/c_2^2)\partial^2 \vec{A}/\partial t^2 \quad , \tag{4}$$

describe the motion of the compressional and shear waves respectively. c_1 and c_2 are the compressional and shear wave velocities defined by

$$c_1 = [E(1-\sigma)/\rho_1(1+\sigma)(1-2\sigma)]^{\frac{1}{2}}$$

$$c_2 = [E/2\rho_1(1+\sigma)]^{\frac{1}{2}} \quad , \tag{5}$$

where E, ρ_1, σ are the Young's modulus, density and Poisson's ratio of the solid material of the sphere.

Outside the sphere there is a limitless fluid of density ρ and sound velocity c in which there is a continuous train of waves emanating from a point source situated on the z axis at $r = r_o$, $\theta = \pi$. The time dependence of these waves is of the form $\exp(-i\omega t)$ from which the wave number k in the fluid is obtained by means of the relation

$$k = \omega/c = 2\pi/\lambda$$

where λ is the wave length. Similar relations

$$k_1 = \omega/c_1 \; ; \; k_2 = \omega/c_2$$

hold for the compressional and shear waves in the solid. The waves emanating from the point source can be expressed[7]

$$p_i = P_o \exp(ikD)/D$$

$$= ikP_o \sum_{n=0}^{\infty} (2n+1)(-1)^n P_n(\cos\theta) j_n(kr) h_n(kr_o) \quad 0 < r < r_o \tag{6}$$

where

$$D = [r_o^2 + 2r\, r_o \cos\theta + r^2]^{\frac{1}{2}}$$

and the P_n are Legendre polynomials, and the j_n, h_n are spherical Bessel functions[8]. Plane waves incident on the sphere are obtained by making r_o go to infinity. Using the two limits

$$\exp(ikD)/D \longrightarrow \exp(ik\, r_o)\exp(ik\, r\cos\theta)/r_o$$

$$h_n(kr_o) \longrightarrow i^{-(n+1)}\exp(ik\, r_o)/kr_o \tag{7}$$

and removing the common factor $\exp(ik\, r_o)/r_o$ gives

$$p_i = P_o \exp(ikr\cos\theta)$$

$$= P_o \sum_{n=o}^{\infty} (2n+1) i^n P_n(\cos\theta) j_n(kr) \quad . \tag{8}$$

The above waves, p_i, incident on the sphere result in scattered waves in the fluid which will be of the form

$$p_s = P_o \sum_{n=o}^{\infty} c_n h_n(kr) P_n(\cos\theta) \tag{9}$$

where the coefficients c_n have to be determined from the boundary conditions at the surface of the sphere. The appropriate conditions are:

(a) the pressure in the fluid is equal to the normal component of stress in the solid.

(b) the normal component of displacement of the fluid is equal to the normal component of displacement of the solid.

(c) the tangential components of shearing stress in the solid vanish at the surface.

These conditions can be expressed[9] in the relations

$$p_i + p_s + 2\rho_1 c_2^2 \left[\frac{\sigma}{(1-2\sigma)} \; div\vec{u} + \frac{\partial u_r}{\partial r} \right] = 0 \qquad (10)$$

$$u_{i,r} + u_{s,r} = u_r \qquad (11)$$

and

$$\frac{\partial u_\theta}{\partial r} - \frac{u_\theta}{r} + \frac{1}{r} \frac{\partial u_r}{\partial \theta} = 0 \qquad (12)$$

evaluated on the surface of the sphere at $r = a$. The displacement of the fluid in Eq. 11 is obtained from Eqs. 6 and 9 by using

$$u_{i,r} + u_{s,r} = (1/\rho\omega^2) \, \partial(p_i + p_s)/\partial r \quad . \qquad (13)$$

Because of the symmetry of the incident waves, the component of displacement u_ϕ is taken to be zero and the ϕ component of the shearing stress can also be neglected. The only non-zero component of the vector potential will be A_ϕ so that the potentials become

$$\psi = \sum_{n=o}^{\infty} a_n j_n(k_1 r) P_n(\cos\theta)$$

$$A_\phi = \sum_{n=o}^{\infty} b_n j_n(k_2 r) \frac{d}{d\theta} P_n(\cos\theta) \quad . \qquad (14)$$

Using Eq. 2 these expansions can be inserted into the boundary conditions 10 - 12 and the coefficients of each normal mode equated. The coefficients c_n of the scattered waves in the fluid given by Eq. 9 can then be expressed as follows,

$$c_n = k(-1)^n (2n+1) h_n(kr_o) \sin\eta_n \exp(-i\eta_n) \qquad (15)$$

where the angle η_n is given by

$$\tan \eta_n = - [j_n(x)F_n - j'_n(x)]/[n_n(x)F_n - n'_n(x)] \qquad (16)$$

with

$$F_n = \frac{\rho}{\rho_1} \frac{x_2^2}{2} \frac{\dfrac{x_1 j_n'(x_1)}{x_1 j_n'(x_1) - j_n(x_1)} - \dfrac{2(n^2+n) j_n(x_2)}{(n^2+n-2) j_n(x_2) + x_2^2 j_n''(x_2)}}{\dfrac{x_1^2 \left[\dfrac{\sigma}{1-2\sigma} j_n(x_1) - j_n''(x_1)\right]}{x_1 j'_n(x_1) - j_n(x_1)} - \dfrac{2(n^2+n)[j_n(x_2) - x_2 j_n'(x_2)]}{(n^2+n-2) j_n(x_2) + x_2^2 j_n''(x_2)}} \qquad (17)$$

and

$$x = ka \; ; \; x_1 = k_1 a \; ; \; x_2 = k_2 a \; .$$

The primes denote the derivative with respect to the argument. This result was first derived by Faran[2]. However there was an error in his presentation in which the factor $\sigma/(1-2\sigma)$ was misplaced. Finally it should be noted that the expression on the right hand side of Eq. 15 is of the form $f(x)/(f(x) + i\,g(x))$ where f, g are regular on the real axis. Hence there are no singularities when the argument is real, and the function can be integrated numerically in a straightforward manner. It also follows that the solution as presented is complete for all frequencies, i.e., the boundary conditions are fully satisfied by the shear and compressional waves postulated in Eq. 14.

Certain limiting cases are of interest. If $F_n \longrightarrow 0$, the solution would then apply to scattering by a rigid immovable sphere[10]. This would be the case for instance when the density of the solid was very much greater than that of the fluid. If $F_n \longrightarrow \infty$ the solution for

scattering by a free surface sphere is obtained[11]. This corresponds to the condition where the normal stress at the surface of the sphere vanishes, which would result for example when the density of the material inside the sphere was very much less than that of the fluid.

From the above it follows that the echo returned by the solid sphere to the source is given by

$$p_e = \frac{P_o}{2r_o}\left[-2x_o \sum_{n=o}^{\infty} (2n+1) \sin\eta_n \exp(-i\,\eta_n) h_n^2(x_o)\right] \exp(-i\omega t)$$

$$= \frac{P_o}{2r_o} f(x, x_o, x_1, x_2) \exp(-ix\tau) \qquad (18)$$

where $x_o = kr_o = xR$, and $\tau = ct/a$. When the source is a large distance from the sphere

$$p_e = \frac{P_o a}{2r_o^2}\left[\frac{2}{x} \sum_{n=o}^{\infty} (-1)^n (2n+1) \sin\eta_n \exp(-i\eta_n)\right] \exp[ik(2r_o - ct)]$$

$$= \frac{P_o a}{2r_o^2} f_\infty(x, x_1, x_2) \exp[ix(2R-\tau)] \quad . \qquad (19)$$

Removal of a factor $\exp(ik\,r_o)/r_o$ gives the solution for incident plane waves. Equations 18 and 19 can then be used to construct the echo due to a pressure pulse emanating from the source. Suppose the source emits a pulse of form $P_i(t)$. This can be expressed in terms of Fourier components as

$$P_i(t) = \frac{P_o c}{(2\pi)^{\frac{1}{2}} D} \int_{-\infty}^{\infty} g(k) \exp[ik(D-ct)]\, dk \qquad (20)$$

where D is as defined previously. The frequency spectrum $g(k)$ is

found by taking the Fourier transform of the given pulse, i.e.,

$$g(k)=\frac{1}{(2\pi)^{\frac{1}{2}}}\int_{-\infty}^{\infty} P_i(t)\exp\left[-ik(D-ct)\right]dt \quad . \tag{21}$$

With the new variable $x = ka$, the reflected pulse will be

$$P_e(\tau)=\frac{P_o c}{(2\pi)^{\frac{1}{2}} a r_o}\int_{-\infty}^{\infty} g(x)\, f(x, x_o, x_1, x_2)\exp(-ix\tau)\,dx \quad , \tag{22}$$

and when the point source moves to a large distance from the sphere

$$P_e(\tau) = \frac{P_o}{2(2\pi)^{\frac{1}{2}} r_o^2}\int_{-\infty}^{\infty} g(x)\, f_\infty(x, x_1, x_2)\exp\left[ix(2R-\tau)\right]dx \quad . \tag{23}$$

In general the echo given by (23) will differ in form from that of the incident pulse (20). Only for high frequencies in the special cases of a rigid and a free surface sphere will it be the same. It can be shown[12] that in the former case $f_\infty \longrightarrow \exp(-2ix)$ as x becomes large while for the free surface sphere $f_\infty \longrightarrow -\exp(-2ix)$. Hence if the frequencies contained in the pulse are in the high frequency range, Eq. 23 becomes

$$P_r(\tau)=\frac{P_o}{2(2\pi)^{\frac{1}{2}} r_o^2}\int_{-\infty}^{\infty} g(x)\exp\left[ix(2R-2-\tau)\right]dx$$

which means that the reflected pulse has the same form as the emitted pulse, but is returned time $2(r_o-a)/c$ later. This travel time indicates that the sound is reflected from a point source reflector at the point on the surface of the sphere nearest to the source of incident sound. A similar result holds for the free surface sphere except that the pulse

is inverted.

3. The Steady State Solutions

The steady state solutions given by the functions f in Eqs. 18, 19 were determined for a certain number of cases, the calculations being performed on a high speed computer. The results are shown in Figs. 2 - 13.

The first results obtained were for the special cases of the rigid[10] and free surface[11] spheres for a distant point source of continuous waves. These are shown in Figs. 2(a), (b). The agrument of the function f_∞ is presented divided by the variable $x = ka$. The results for the rigid sphere are in agreement with those of Stenzel[5]. For low frequencies the function is given by the initial terms in the series expansion which in the limit as x tends to zero are

$$\frac{2i}{x}\left[\frac{j_o'(x)}{h_o'(x)} - \frac{3j_1'(x)}{h_1'(x)}\right] \to 3x^2\left(1 - \frac{ix^3}{3}\right),$$

and

$$\frac{2i}{x}\frac{j_o(x)}{h_o(x)} \to 2(1-ix) \quad ,$$

for the rigid and free surface spheres respectively. For the rigid sphere this represents the well-known condition of Rayleigh scattering where the scattered intensity is proportional to the fourth power of the frequency. For the free surface sphere the results are quite different. Not only does the scattered intensity reach maximum values at low frequencies, but the scattering is uniform in all directions. For high frequencies both solutions tend to the form $\exp(-2ix)$, the free surface solution converging more rapidly than that of the rigid sphere. In the

previous section, it was shown that this indicates that at high frequencies the sound is mainly from a small area on the surface opposite the source and this would agree with physical intuition. At low frequencies the echo appears to come from the center of the rigid sphere and from a half radius position in the free surface sphere. As the frequency increases the apparent origin of the echo moves gradually towards the region on the surface opposite the source. This is shown in Fig. 2(b), where the phase of f_∞ divided by $x = ka$ represents distance along a radius inside the sphere. In the case of the rigid sphere these results can be readily understood by supposing that low frequency waves are intercepted by the entire cross section whereas high frequency waves behave as in geometrical optics and form a "bright spot" reflector on the surface opposite the source. With the free surface sphere the results at low frequencies are not so readily explainable except that as expected they differ from those for the rigid sphere.

The main body of results were derived for solid spheres supporting internal shear and compressional waves. The properties of the materials considered are given in Table I. The fluid outside the sphere was assumed to be water of density 1 gm/cc and compressional velocity 1,410 m/sec.

As an initial test of the programs, the results obtained by Faran[2] were recalculated. Since these were for $\sigma = \frac{1}{3}$ no error could result from the misplacing of the factor $\sigma/(1-2\sigma)$ mentioned in the previous section since this factor is unity. Good agreement was found.

Some of the results for the materials listed in Table I are given in detail in Figs. 3 - 11. As before these are for a distant source. Generally the range of frequency was for values of ka up to 30, but for

TABLE I [13]

Material	Density (gm/cc)	Poisson's Ratio σ	Compressional Velocity C_1 (m/sec)	Shear Velocity C_2 (m/sec)
Beryllium	1.87	0.05	12,890	8,880
Fused Silica	2.20	0.17	5,968	3,764
Heavy Silicate, Flint Glass	3.88	0.224	3,980	2,380
Armco Iron	7.70	0.29	5,960	3,240
Monel Metal	8.90	0.327	5,350	2,720
Aluminum	2.70	0.355	6,420	3,040
Yellow Brass	8.60	0.374	4,700	2,110
Lucite	1.18	0.40	2,680	1,100
Lead	11.34	0.43	1,960	690
Ice [14]	0.917	0.336	2,743	1,433

Armco Iron, ice and lucite the range extended to ka = 60, 20, 10 respectively. In addition to the pressure amplitude the phase variation is given for Armco Iron, and aluminum. In all cases the results begin at low frequencies as though the solid were a rigid body, changing in general into a fairly regular series of peaks and minima as the frequency increases. With a rigid, incompressible material such as beryllium, the change from the rigid body solution is not very great. However, as the material becomes more compressible and pliant, the resonances tend to become more pronounced and more closely spaced. In the case of lucite and ice the resonances have become quite sharp and close together. This general trend was investigated by considering

an average frequency interval between minima or between resonance peaks for each material. The results are shown in Fig. 12 plotted against the shear velocity c_2. Parameters other than c_2 were also considered such as Poisson's ratio σ, but with these the scatter of points was much greater. It appears therefore that this feature is most strongly dependent on the behavior of shear waves in the material. The successive peaks and minima which occur in the direct echo for a continuous frequency were shown by Faran[2] to be due to strong lobes of backscattered radiation forming and then splitting again into side lobes scattering in other directions. It seems therefore that shear waves play an important role in this process. Figs. 3 - 11 are arranged in order of decreasing shear velocity and a gradual process of transition seems to be apparent as this parameter is varied. As an independent parameter, the density of the material does not seem to have a very pronounced effect except at very low frequencies where the size of the first pressure amplitude peak appears to vary in direct relation with it. As the frequency increases there appears to be no tendency towards some constant limit as in the cases of the free surface and rigid spheres. The peaks seem to recur, but in an increasingly ragged form.

In the phase variations shown in Figs. 6 and 8 jumps in phase occur at frequencies corresponding to minima in the pressure amplitude. As with the rigid body the parameter $(-\arg f_\infty/ka)$ is zero at the low frequency limit and varies continuously as the frequency increases. Unlike the rigid sphere however this variation does not tend towards a limit where the apparent source of the echo corresponds to physical reality. The representation should therefore be regarded only as a convenient way of presenting the phase as a continuously varying function.

In order to determine the effect of distance of the sound source from the center of the sphere the function f in Eq. 18 was evaluated for a point source at various distances from a rigid, a free surface, and a brass sphere. The pressure amplitude $|f|$ multiplied by R is shown in Figs. 13 - 15, allowing a ready comparison with the solutions for a distance source $|f_\infty|$. In general it appears that f_∞ represents a satisfactory solution when the sound source is situated more than 10 radii from the center of the sphere.

4. Echo Pulse Forms

The most obvious general feature in the steady state solution for ordinary metals is the succession of peaks and minima in the pressure amplitude and it is of interest to determine how this affects the pulse form of the echo when the steady state solutions are used in the integral expression 23 for a distant source. The incident pulse form could be chosen arbitrarily. However in practice the incident sound is generally produced by making a transducer resonate over several cycles at a particular frequency. Mathematically the pressure variation which results at a point in the fluid can be represented as follows,

$$\begin{aligned} P_i(t) &= 0 && t < -\Delta t \\ &= \exp(-i\omega_o t) && -\Delta t < t < \Delta t \\ &= 0 && t > \Delta t \end{aligned} \qquad (24)$$

where ω_o is the angular frequency of the transducer at resonance, and $2\Delta t$ is the duration of the pulse. The frequency spectrum $g(\omega)$ is given by the transform

$$g(\omega) = \left[\frac{1}{2\pi}\right]^{\frac{1}{2}} \int_{-\Delta t}^{\Delta t} \exp\left[i(\omega-\omega_o)t\right] dt$$

$$= \left[\frac{2}{\pi}\right]^{\frac{1}{2}} \sin\left[(\omega-\omega_o)\Delta t\right] / (\omega-\omega_o)$$

which is the non-dimensionalized system of Eq. 23 becomes

$$g(x) = \left[\frac{2}{\pi}\right]^{\frac{1}{2}} \sin\left[(x - x_o)\,\Delta\tau\right] / (x - x_o) \qquad (25)$$

where $x_o = \omega_o a/c$ and is referred to as the dominant frequency. By use of Eq. 25 and the previously derived values of the function f_∞ it is then possible to obtain the pulse form of the echo by numerically integrating Eq. 23.

The nature of the function g in Eq. 25 is shown in Figs. 16 - 18 for different pulse lengths $\Delta\tau$. The height of the main peak occurring at the dominant frequency is equal to $\Delta\tau$ and its "spread" varies inversely with $\Delta\tau$. If the function $|f_\infty|$ is momentarily idealized as consisting of a series of similar, equally spaced peaks, it would appear that the form of the echo depends mainly on the pulse length and on the location of the dominant frequency relative to the maxima and minima of the $|f_\infty|$. Two extreme cases would then arise depending on whether the dominant frequency coincided with a maximum or with a minimum of $|f_\infty|$.

Using the data for Armco iron as shown in Figs. 5, 6 several echo pulse forms were computed for different lengths of the incident pulse and for dominant frequencies corresponding to values of x or ka at 24.5 and 25.5. The former frequency occurs at a peak of the pressure amplitude and the latter at a minimum. The range of integration over ka for the longer pulses was from 15 to 35, while for the

short 5 cycle pulse, it extended from 10 to 40. The incident pulse did not therefore have a perfectly rectangular form. However in comparison to experimental pulse forms, it could be considered a satisfactory approximation. In addition the irregularities introduced by restricting the range of integration facilitated the recognition of certain features of the incident pulse in the echo. The calculated echoes are shown in Figs. 16 - 18. The time scale for the incident pulse is chosen with respect to the time of arrival of the mid-point of the pulse at the center of the sphere, whereas the scale for the echo is chosen with respect to the time of arrival back at the source. All pulses are shown travelling from right to left. It can be seen from these figures that the leading edge of the echo precedes that of the incident pulse by a time difference of 2 in each case. In addition the leading edge of the echo is of the same form as the leading edge of the incident pulse. These features indicate that the first part of the echo consists of a rigid body reflection from the region of the surface of the sphere adjacent to the sound source. The subsequent parts of the echo are affected by the vibrations of the sphere. In the case of the five cycle pulse, the first echo is of identical form to the incident pulse, while the second echo is also of the same form, but inverted. Subsequent echoes diminish in amplitude and lose the characteristic features of the incident pulse. Whether the dominant frequency occurs at a minimum or a maximum of the function $|f_\infty|$ does not appear to make much difference to the form of the echo for the short five cycle pulse, but obviously it is important when the pulse is longer. The reason can be seen from the frequency spectra shown in Figs. 16 - 18. A change in ka of the order of 1 in the spectrum for the short pulse will not greatly affect the integral (23); however, this is not the case for the longer pulses. The differences in form of the

echoes shown in Figs. 17, 18 are in fact quite distinctive. It seems moreover that the changes which occur when the dominant frequency is moved from a maximum of $|f_\infty|$ to a minimum, are characteristic of any ordinary metal. Figure 19 shows the echoes from a sphere of aluminum for the same type of incident pulse, where these results were obtained experimentally[1]. With allowance for a change of scale and such effects as the response of the transducer, the differences in the echo resulting from a change in the dominant frequency are closely related to those shown in Figs. 16 - 18. The sphere in this case had a diameter of 5 inches and the change in dominant frequency was from 120 kc/sec to 123.5 kc/sec. This is equivalent to a change in ka of about 1, which according to Fig. 12 is the approximate distance between a peak and a minimum of the function $|f_\infty|$ for most metals including aluminum. Using the constants given above for water and aluminum, it is found that 120 kc/sec does not in fact coincide with a peak of the steady state reflection function $|f_\infty|$. However this is not surprising since the values used referred to rolled aluminum. In addition if the frequency is to be expressed in terms of ka with any accuracy, it would be necessary to know the velocity of sound in water under the conditions of the experiment, and also the diameter of the sphere, to within less than 1%. Echoes were calculated for rolled aluminum at values of ka equal to 34.6 and 35.6 corresponding to frequencies of 122.3 kc/sec and 125.8 kc/sec, these values occurring at a maximum and a minimum respectively of the reflection function $|f_\infty|$. The pulse lengths $\Delta\tau$ were the same as those in Figs. 16 - 18. Similarly echoes were calculated for a brass sphere for frequencies at ka = 20.2 and 21.0. These echoes were found to have the same features. The leading edge was a rigid body reflection and the same kind of transition in pulse form occurred

when the frequency and the pulse length were varied. With yellow brass the secondary echoes in the multiple echo forms had a bigger amplitude than the primary echo.

5. Discussion

Although this paper represents only a preliminary study, it may be worthwhile to consider the significance of the results in relation to the problem of using sonar echoes to obtain information about a target.

In the first place, it would seem that solid materials could be divided roughly into two groups, metallic flint-like substances and substances which are fairly pliant. This can be seen from the steady state solutions where the former is characterized by a succession of peaks and minima roughly the same distance apart, while the latter has sharper, stronger peaks more closely spaced. Although all the echo forms which were calculated belong only to the first type, it is evident from the steady state solutions that there would be a difference in the general nature of echoes between the two groups. Hence there would exist the possiblity of distinguishing for instance between a bare rock and a large fish.

Secondly, if the sonar target is known to be a homogeneous metallic sphere, then it is possible to determine its approximate radius by using data of the type shown in Fig. 19. The features of the transition between a peak and a minimum of the steady state reflection function $|f_\infty|$ for the long incident pulses is characteristic of most ordinary metals, as shown in the previous section. The transition is accomplished during a change in ka of the order of 1. Hence given an actual change in frequency in cycles per second, it is then possible to determine the radius a of the sphere. For example the transition in

pulse form shown in Fig. 19 is achieved through a frequency change of 3.5 kc/sec corresponding to a change in ka of about 1 which therefore makes the radius of the sphere approximately 2.5 inches. In general however such an estimate would not be quite so accurate. It also seems possible to estimate the size of the sphere by varying the pulse length rather than the frequency, since the individual echoes occurring in the short pulse become contingent when the incident pulse length is approximately equal to the diameter of the sphere, see Fig. 19.

Finally, it has been shown[15] that there are significant differences in the steady state reflection function f_∞ for rigid bodies of different shapes. Although these effects would be rendered more complicated by allowing for the vibrations of the solid material, it may be possible to use them to derive some information about the shape of a sonar target.

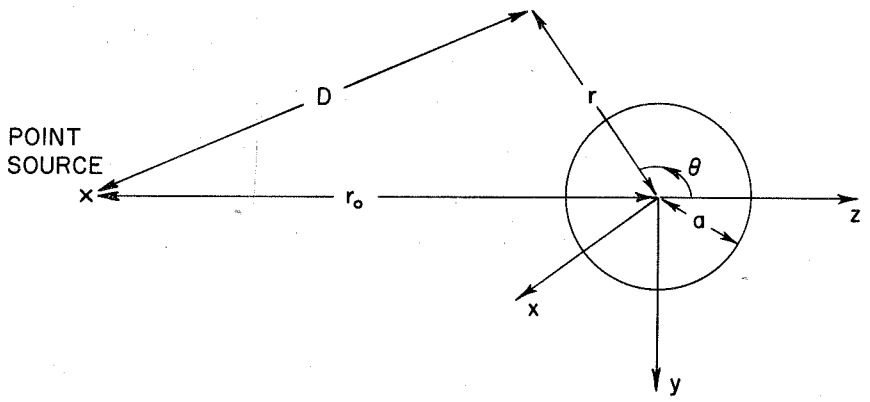

Fig. 1 Coordinate System

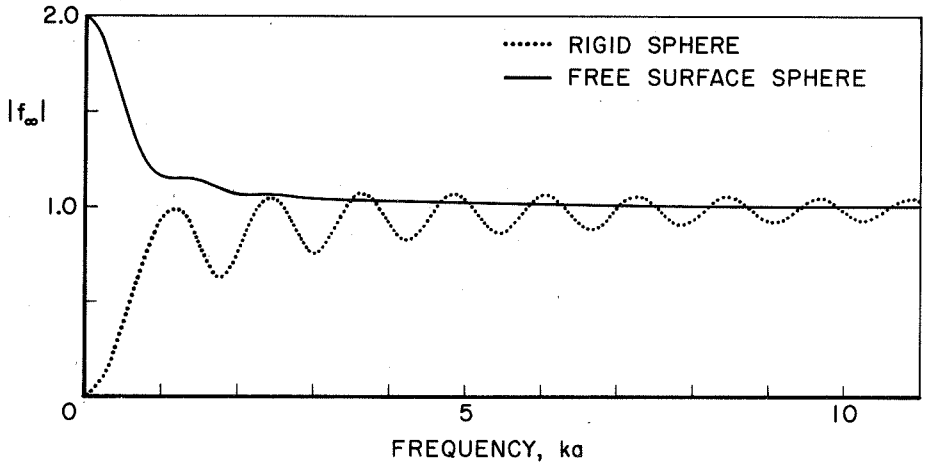

Fig. 2(a) The pressure amplitude as a function of frequency of the echo returned by rigid and free surface spheres to a distant source of continuous waves.

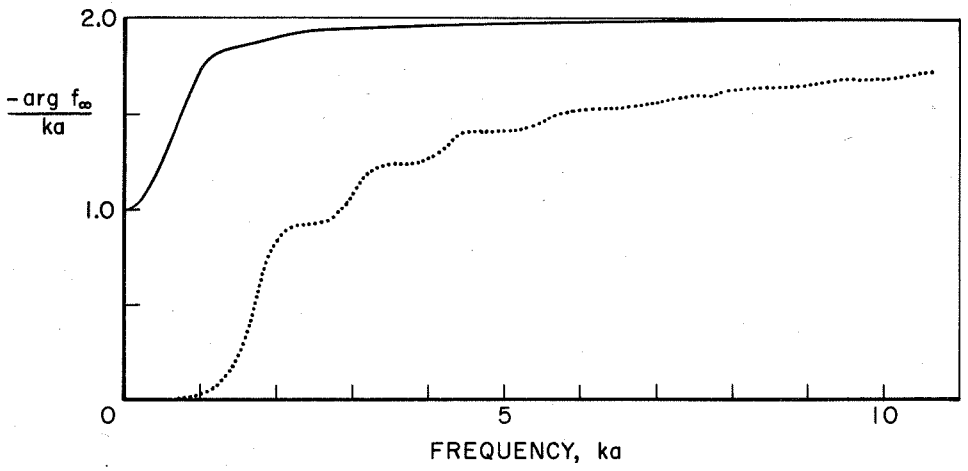

Fig. 2(b) The phase of the echo from rigid and free surface spheres as a function of frequency.

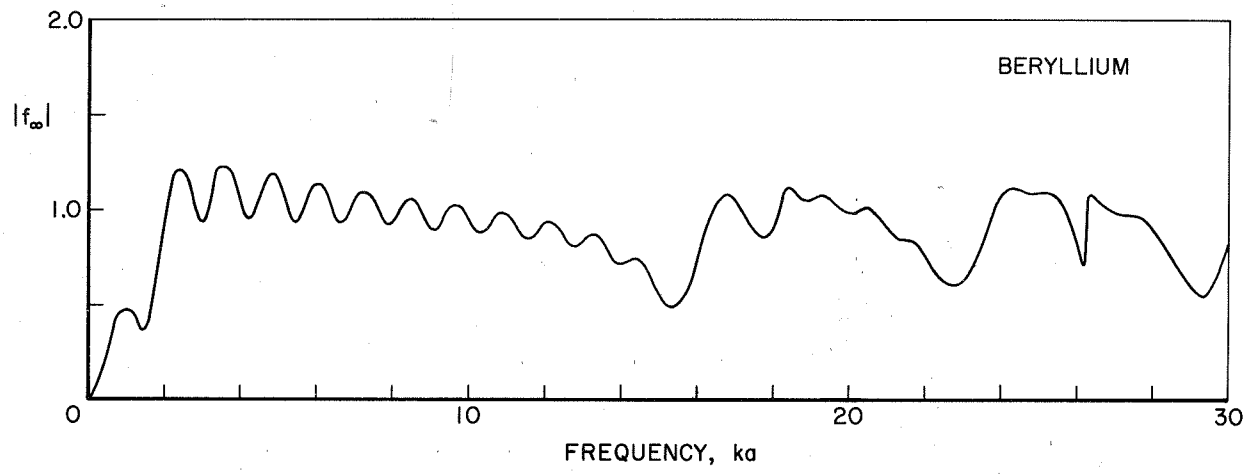

Fig. 3 The pressure amplitude as a function of frequency of the echo returned by a beryllium sphere to a distant source of continuous waves.

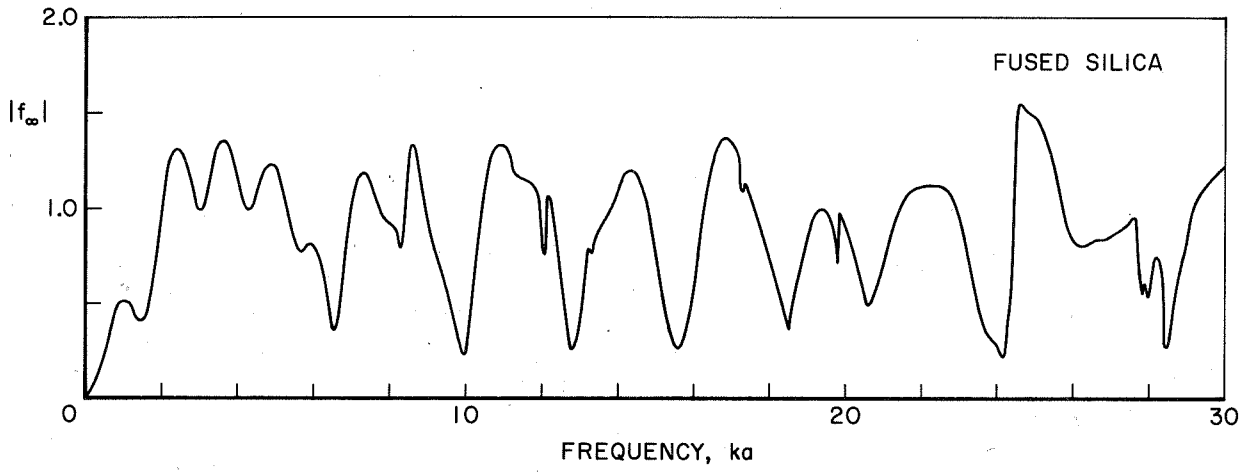

Fig. 4 The pressure amplitude as a function of frequency of the echo returned by a fused silica sphere to a distant source of continuous waves.

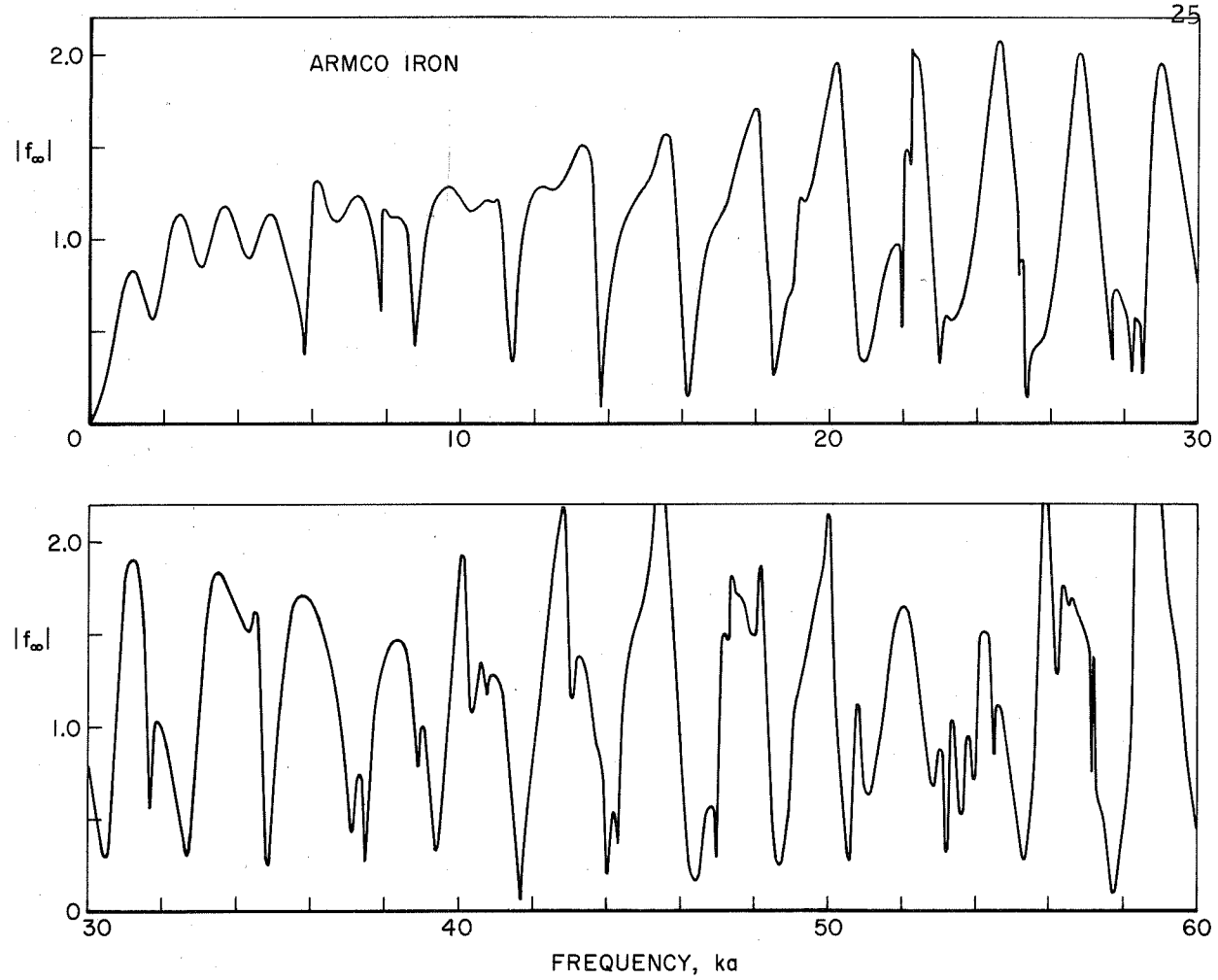

Fig. 5 The pressure amplitude as a function of frequency of the echo returned by a sphere of Armco iron to a distant source of continuous waves.

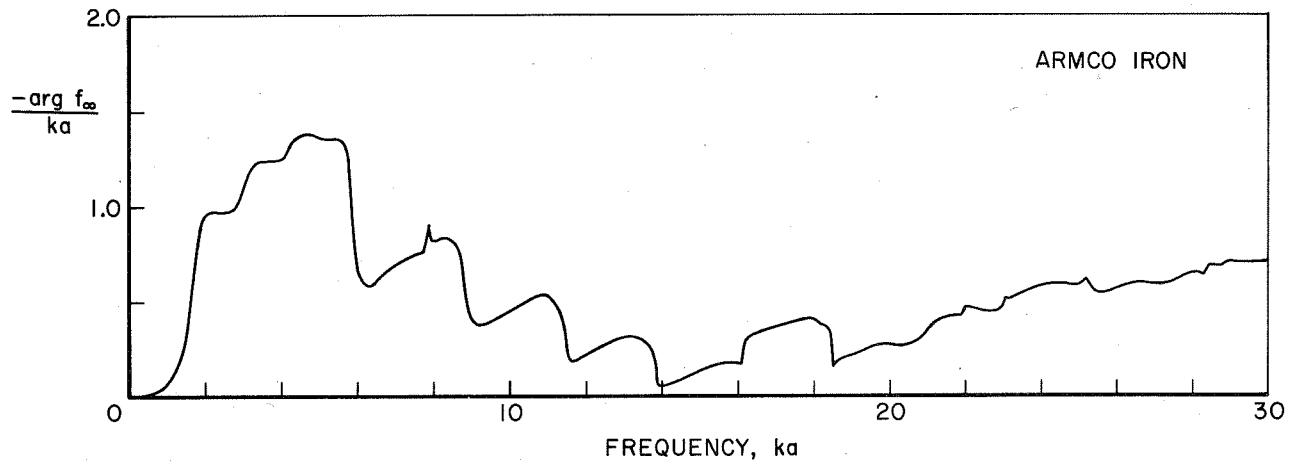

Fig. 6 The phase of the echo from the Armco iron sphere as a function of frequency.

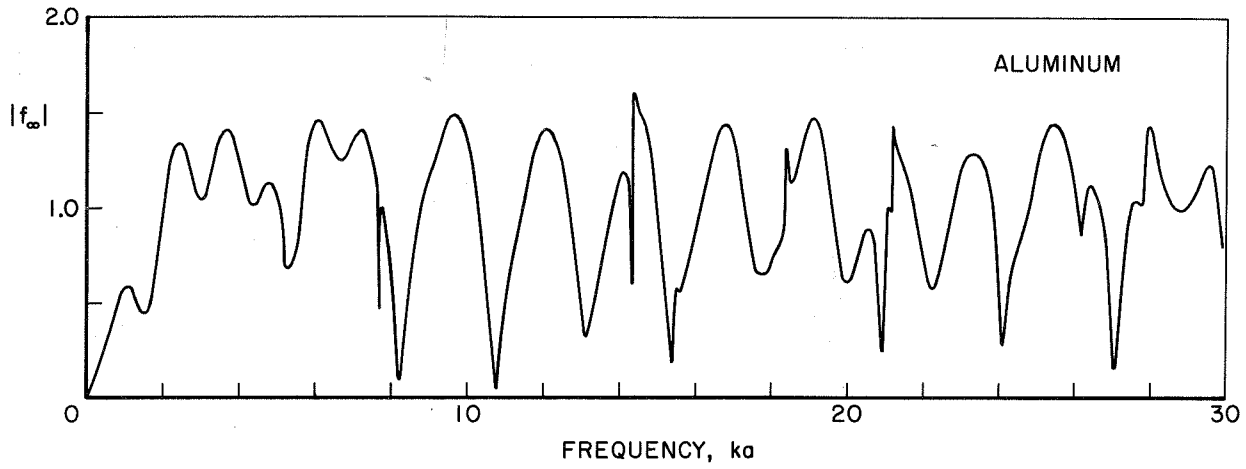

Fig. 7 The pressure amplitude as a function of frequency of the echo returned by an aluminum sphere to a distant source of continuous waves.

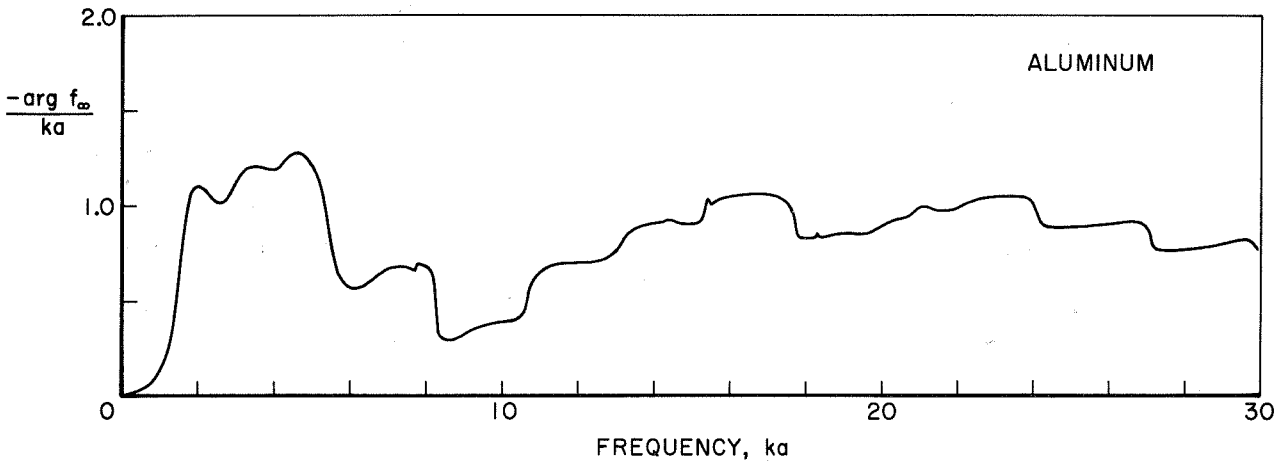

Fig. 8 The phase of the echo from the aluminum sphere as a function of frequency.

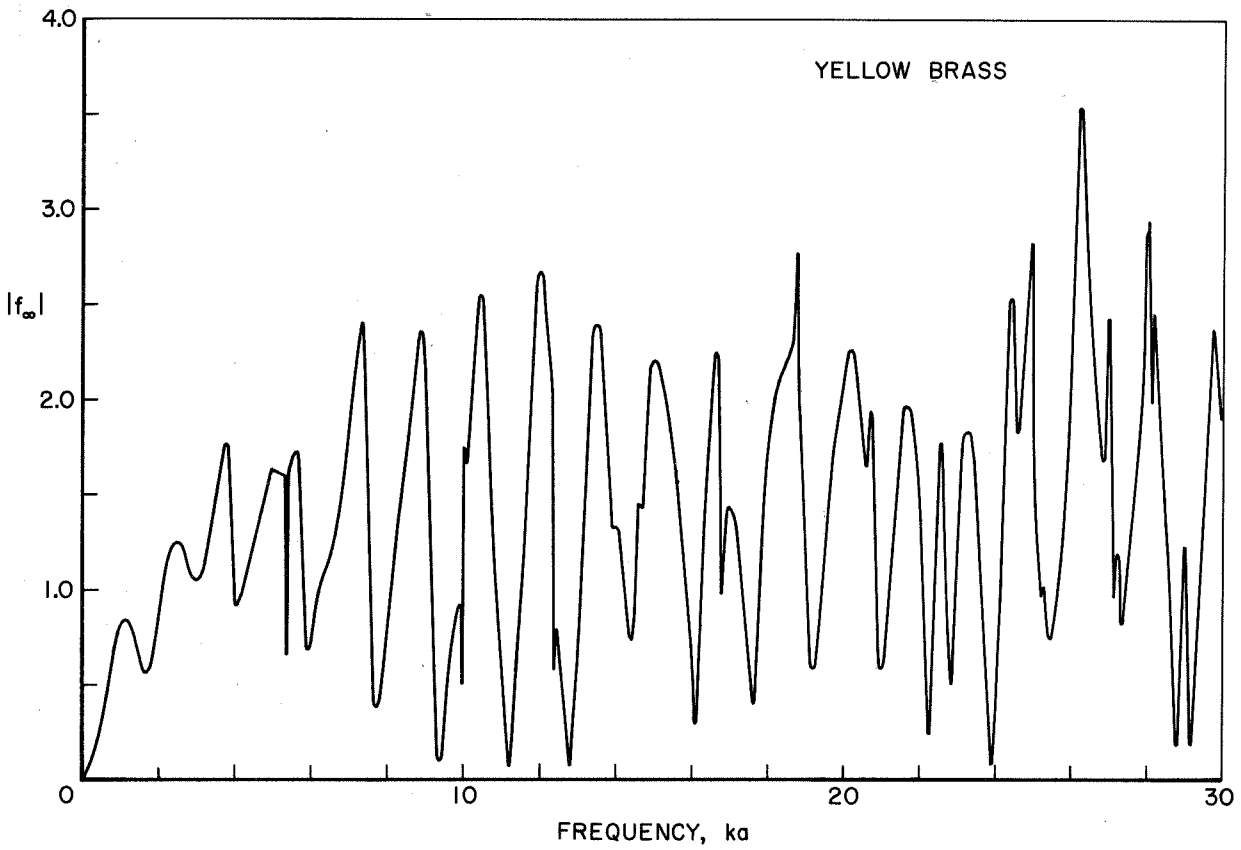

Fig. 9 The pressure amplitude as a function of frequency of the echo returned by a sphere of yellow brass to a distant source of continuous waves.

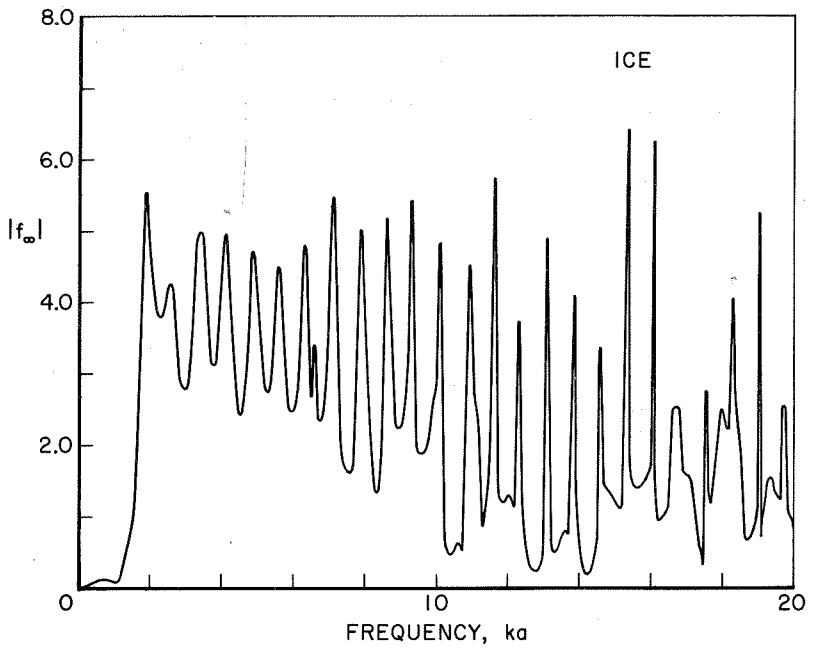

Fig. 10 The pressure amplitude as a function of frequency of the echo returned by an ice sphere to a distant source of continuous waves.

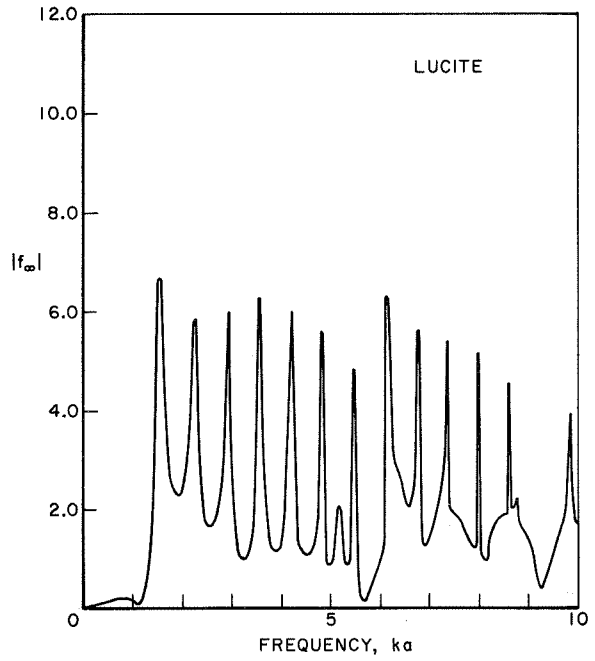

Fig. 11 The pressure amplitude as a function of frequency of the echo returned by a lucite sphere to a distant source of continuous waves.

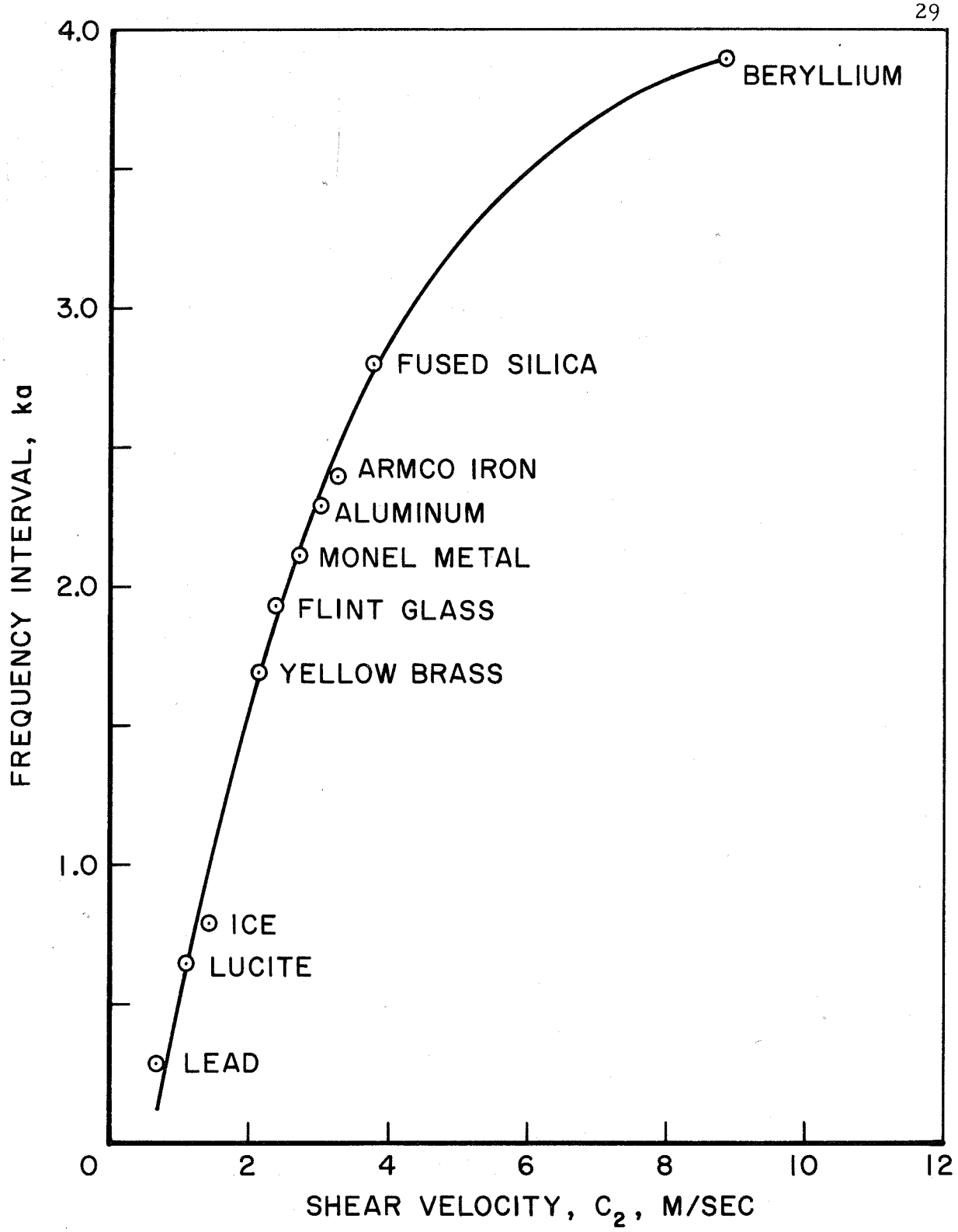

Fig. 12 Average interval in frequency between minima or between peaks in the pressure amplitude of the echo for different materials as a function of the shear velocity of the material.

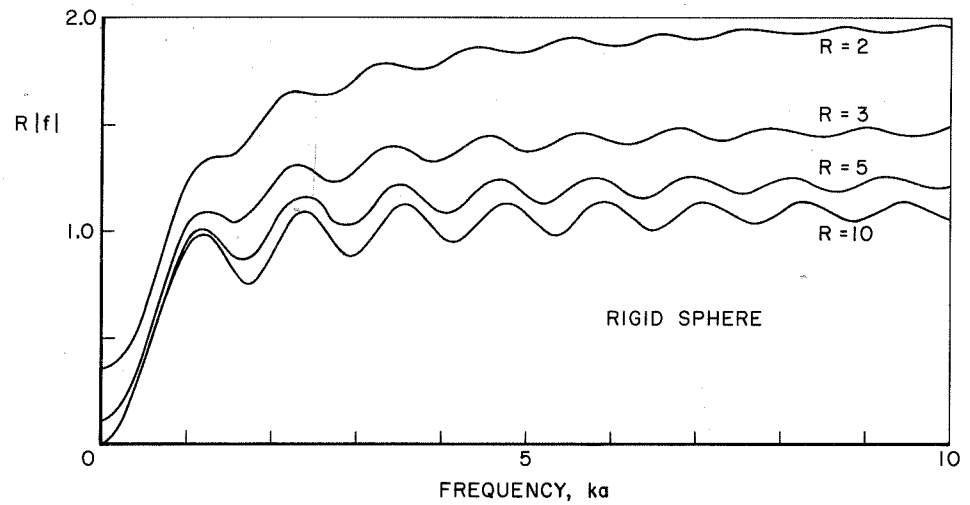

Fig. 13 The pressure amplitude as a function of frequency of the echo returned by a rigid sphere to a point source of continuous waves distance Ra from the center of the sphere.

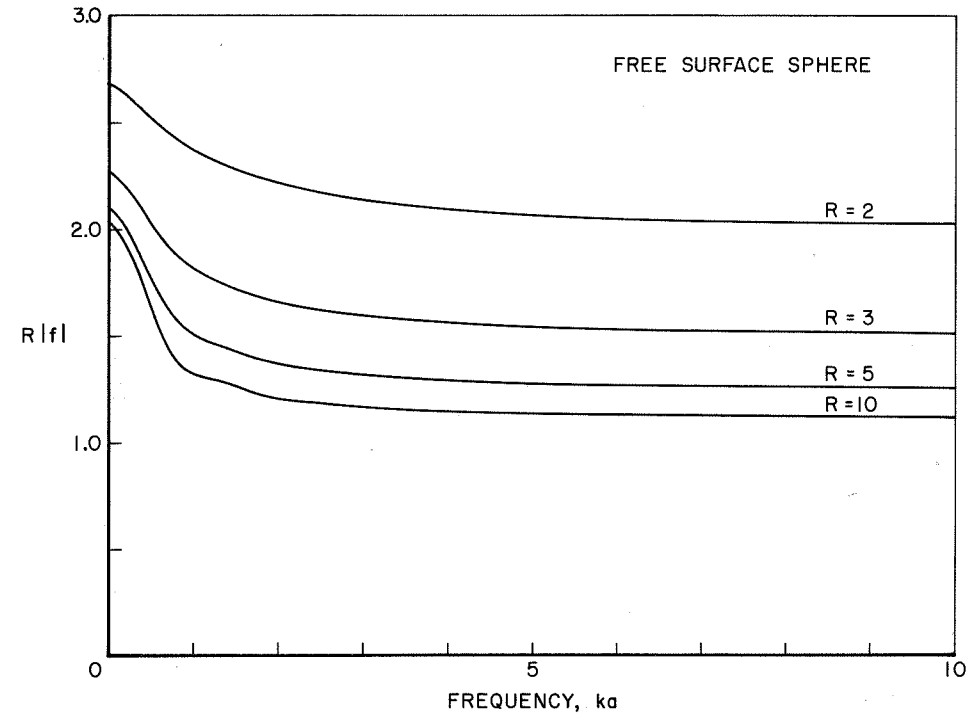

Fig. 14 The pressure amplitude as a function of frequency of the echo returned by a freee surface sphere to a point source of continuous waves distance Ra from the center of the sphere.

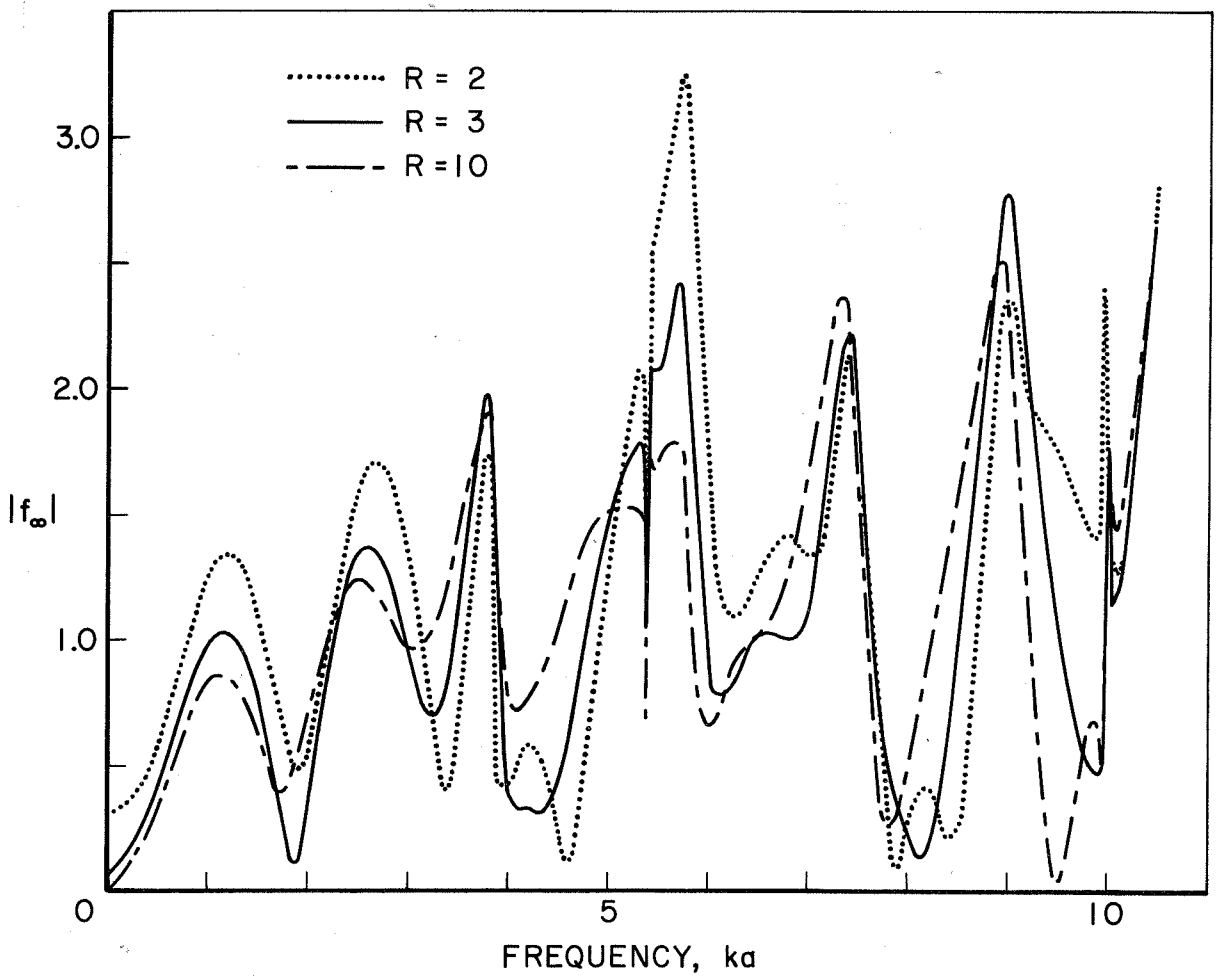

Fig. 15 The pressure amplitude as a function of frequency of the echo returned by a brass sphere to a point source of continuous waves distance Ra from the center of the sphere.

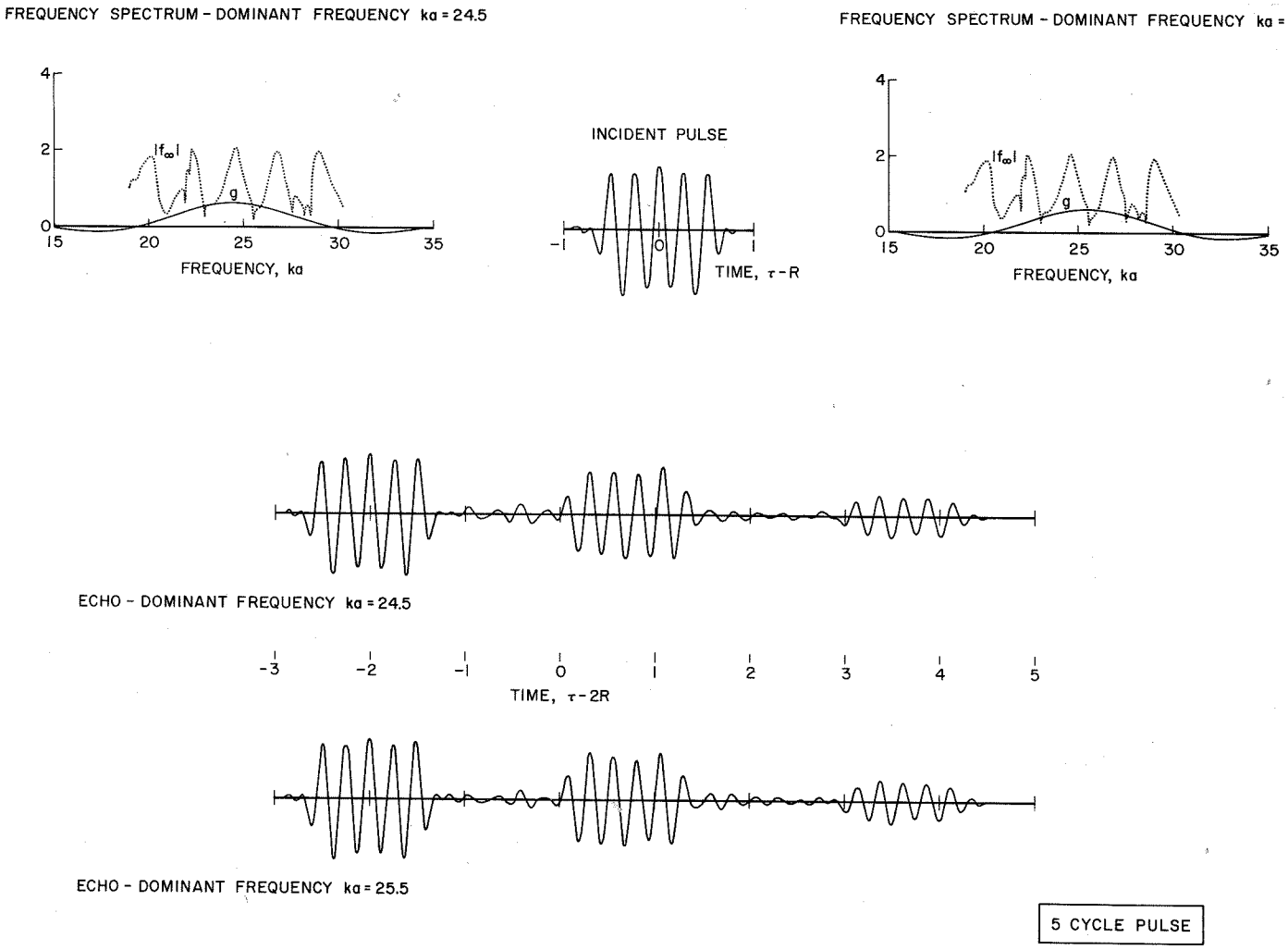

Fig. 16 Pulse forms of echoes returned by an Armco iron sphere for dominant frequencies at ka = 24.5 and 25.5 with an incident pulse of five cycles.

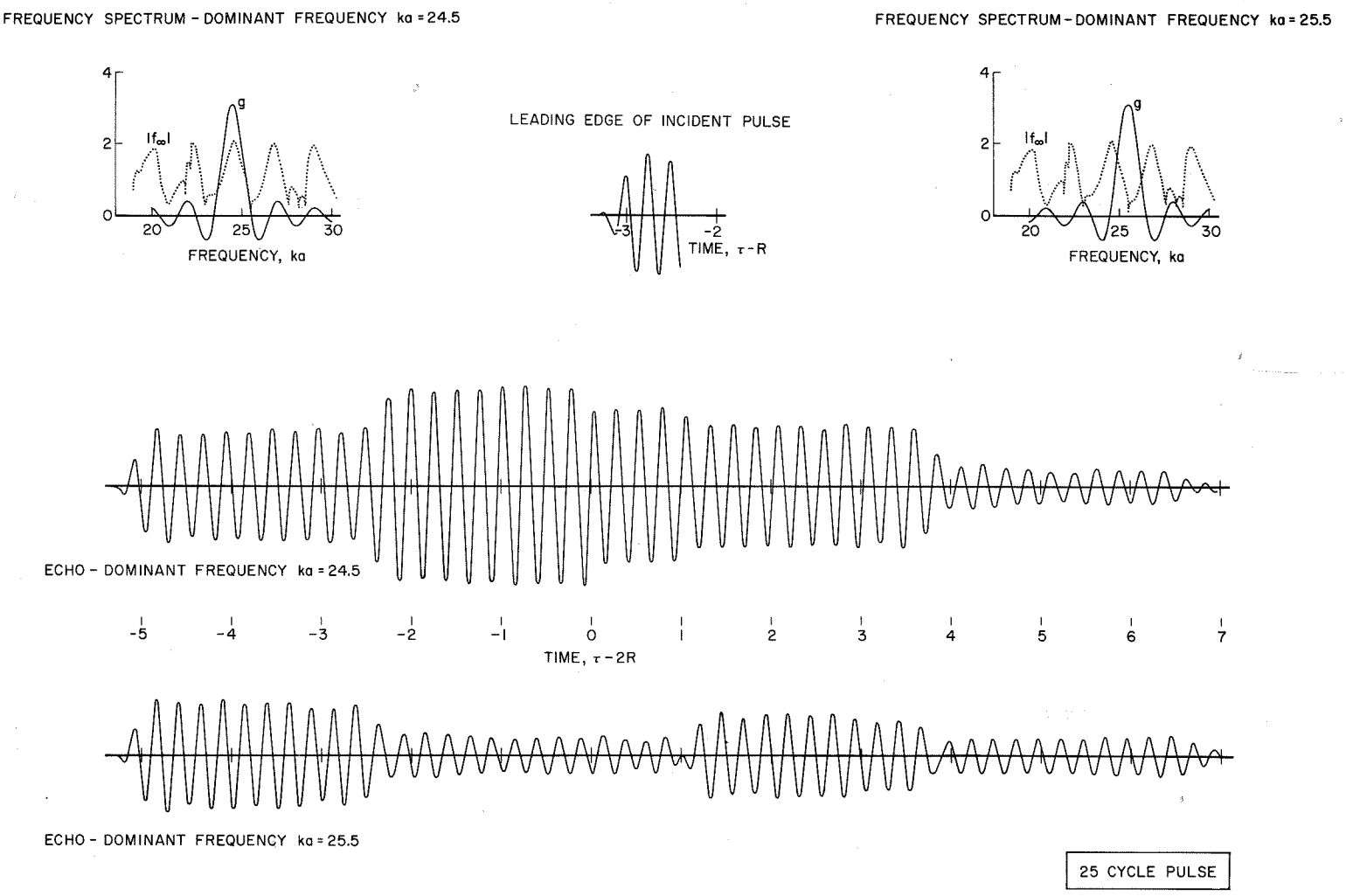

Fig. 17 Pulse forms of echoes returned by an Armco iron sphere for dominant frequencies at ka = 24.5 and 25.5 with an incident pulse of twenty-five cycles.

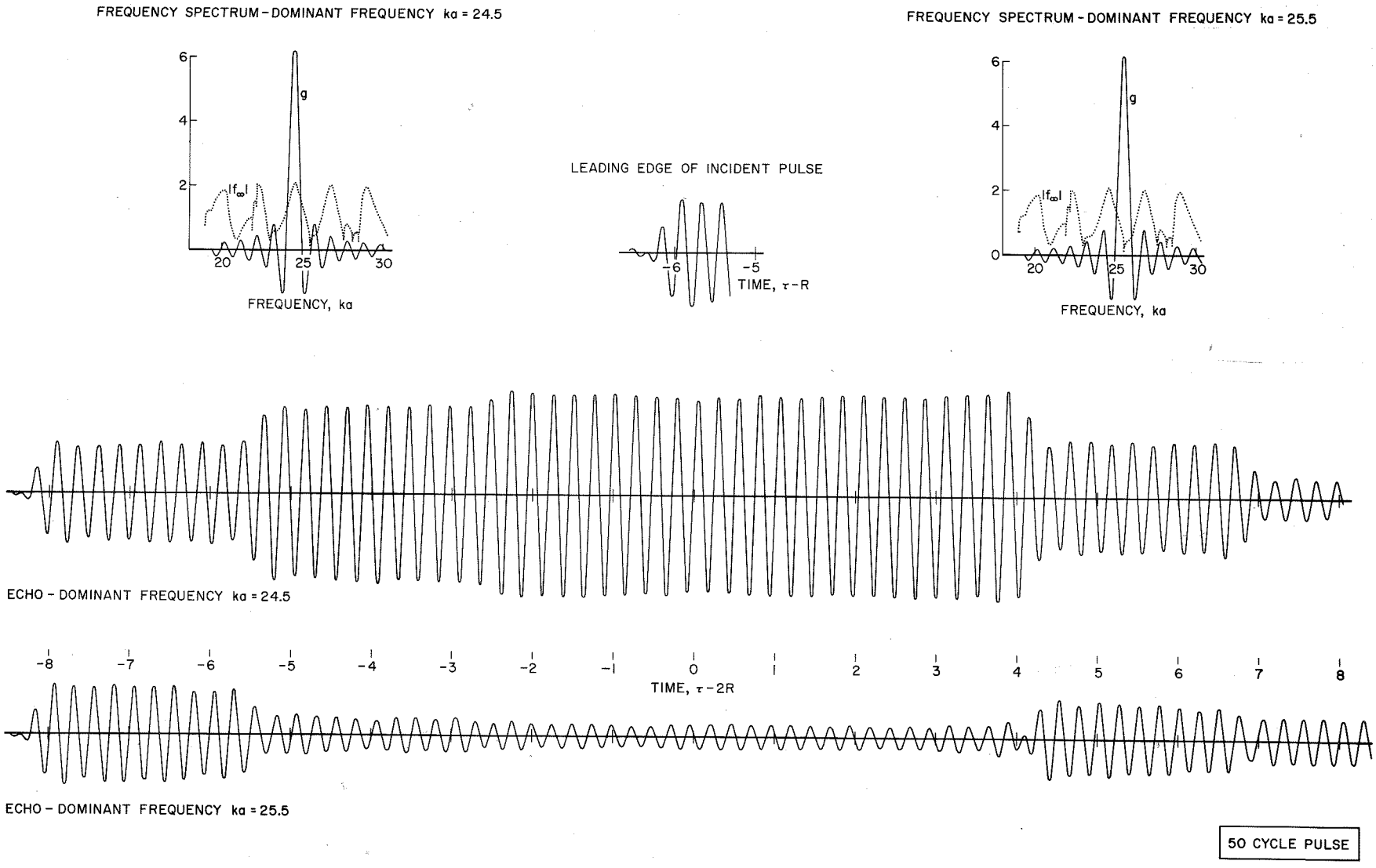

Fig. 18 Pulse forms of echoes returned by an Armco iron sphere for dominant frequencies at ka = 24.5 and 25.5 with an incident pulse of fifty cycles.

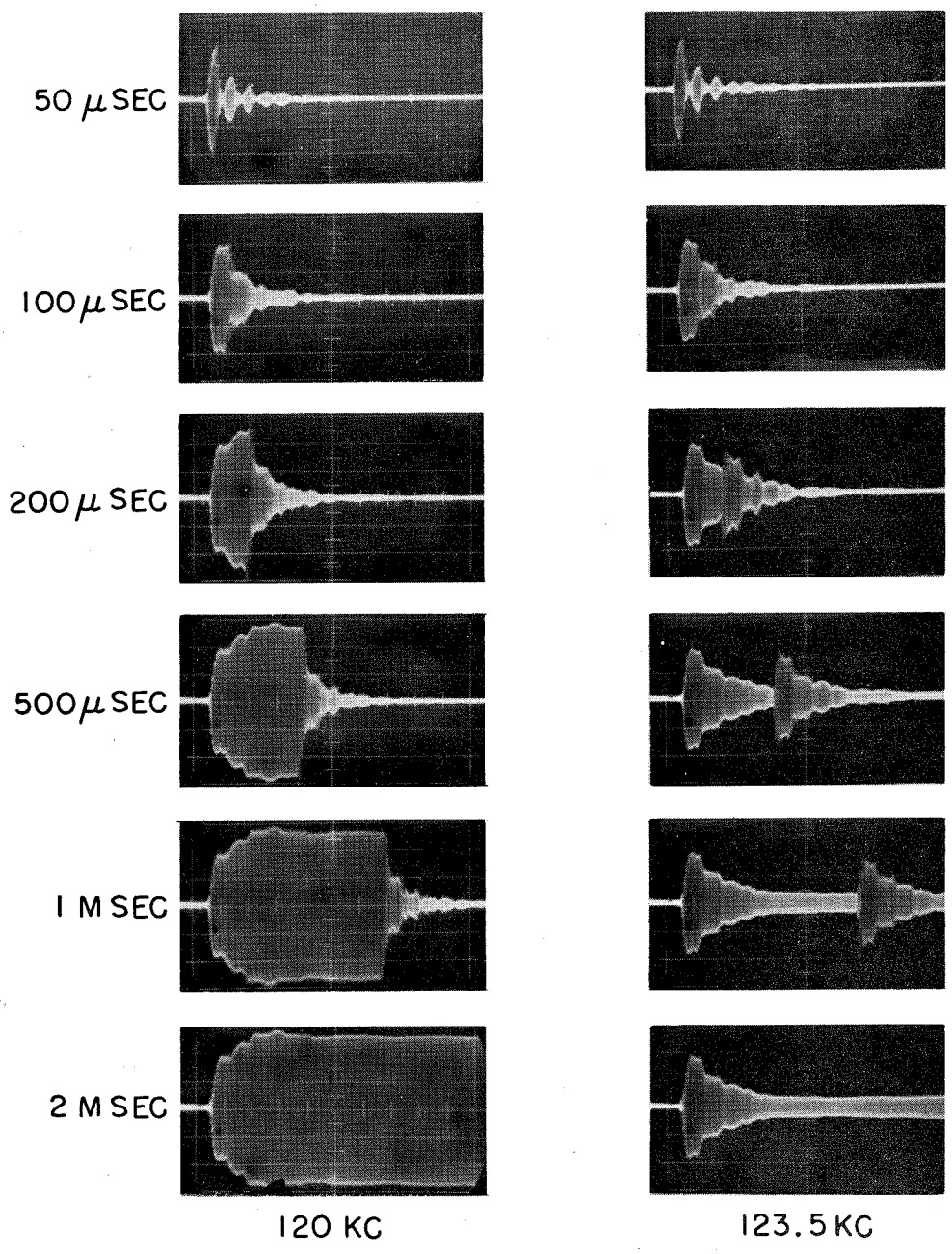

Fig. 19 Experimentally determined echo forms for a 5" diameter aluminum sphere for various incident pulse lengths. The sweep is 150 μ sec/cm.

SECTION B - UNIFORM DISTRIBUTIONS OF SOUND SOURCES ON THE SURFACE OF A RIGID SPHERE AND SOME APPLICATIONS

1. Introduction

Most of the available theoretical information about the acoustic radiation generated by sources of finite extent concerns pistons set in a plane infinite baffle. The case of a piston set in a rigid sphere has also been treated, [16] but the sound field has not been considered in great detail.

This section presents results of calculations for certain source distributions set in the surface of a rigid sphere, namely for uniformly vibrating spherical caps (pistons) and rings, and for plane line sources of constant strength. These elementary distributions can be superimposed to give more complicated systems. Radiation impedances are computed as well as the sound fields in the far zone.

The sphere has often been used as a model for the human head, and some of the results presented here can be considered to apply to hearing. In this regard use is made of the principle of reciprocity which equates the pressure in the far zone due to a point source set in the sphere to the pressure distribution over the sphere due to a point source at infinity. A subject of particular interest to sonar engineers as well as to psychologists is that of the binaural localization of sound, and this is discussed at the end of the section.

2. Source Distributions on the Surface of a Rigid Sphere

The spherical polar coordinate system is used which is related to a Cartesian system having the z-axis as the polar axis, by the relations

$$x = r \sin\phi \sin\theta$$
$$y = r \cos\phi \sin\theta \qquad (1)$$
$$z = r \cos\theta \ .$$

The center of the sphere, which is of radius a, coincides with the origin of the coordinate system. The sphere is immersed in a limitless fluid and its surface is assumed to vibrate continuously with a velocity of the general form $U(\theta, \phi) \exp(-i\omega t)$, where t is the time, c is the sound velocity, λ the wavelength, $k = 2\pi/\lambda$, and $\omega = kc$.

$U(\theta, \phi)$ can be expressed in terms of spherical harmonics[17]

$$U(\theta, \phi) = \sum_{m,\, n} [A_{mn} Y^{e}_{mn}(\theta, \phi) + B_{mn} Y^{o}_{mn}(\theta, \phi)] \qquad (2)$$

where

$$A_{mn} = \frac{(2n+1)}{4\pi} \epsilon_m \left[\frac{(n-m)!}{(n+m)!}\right] \int_0^{2\pi} d\phi \int_0^{\pi} U(\theta, \phi) Y^{e}_{mn} \sin\theta \, d\theta \qquad (3)$$

and the expression for B_{mn} is similar to that for A_{mn} except that Y^{o}_{mn} is substituted for Y^{e}_{mn}. Y^{e}_{mn} and Y^{o}_{mn} are defined as follows:

$$Y^{e}_{mn} = \cos(m\phi) P^{m}_{n}(\cos\theta)$$
$$m \leq n \qquad (4)$$
$$Y^{o}_{mn} = \sin(m\phi) P^{m}_{n}(\cos\theta)$$

where P^{m}_{n} is the unnormalized modified Legendre function. ϵ_m is unity when $m = 0$, and is equal to 2 otherwise.

The resulting outgoing pressure waves in the fluid can be expressed in the form,

$$p = \sum_{m,n} \left[C_{mn} Y^{e}_{mn}(\theta, \phi) + D_{mn} Y^{o}_{mn}(\theta, \phi) \right] h_n(kr) \exp(-i\omega t) \qquad (5)$$

and the corresponding radial velocity can be determined by using the formula

$$u_r = - \frac{i}{\rho\omega} \frac{\partial p}{\partial r} \qquad (6)$$

ρ being the density of the fluid. When $r = a$, u_r is equal to the velocity on the surface of the sphere given by Eq. 2, so that it follows that

$$C_{mn} = \frac{A_{mn}\rho c}{i h'_n(ka)} \quad ; \quad D_{mn} = \frac{B_{mn}\rho c}{i h'_n(ka)} \quad . \qquad (7)$$

The h'_n are the derivatives with respect to the argument of the spherical Bessel functions of the third kind[8].

The radiation impedance is given by

$$F = \int_o^{2\pi} d\phi \int_o^{\pi} \left(\frac{p}{u_r}\right)_{r=a} a^2 \sin\theta \, d\theta = a^2 q_a \rho c (\theta_p - i\chi_p) \qquad (8)$$

where p is obtained by inserting the relations 7 in Eq. 5, and $a^2 q_a$ denotes the area of the source distribution.

In the far zone, for a large distance r from the sphere

$$h_n(kr) \sim \exp(ikr)\, i^{-(n+1)}/r$$

and hence in this region

$$p = \rho c U_o (a/r) \exp\left[ik(r-ct)\right] \psi(\theta, \phi) \qquad (9)$$

where

$$\psi(\theta, \phi) = \frac{1}{kaU_o} \sum_{m,n} \frac{1}{i^{n+2}} \frac{1}{h_n'(ka)} \left[A_{mn} Y^e_{mn}(\theta, \phi) + B_{mn} Y^o_{mn}(\theta, \phi) \right] \tag{10}$$

ψ, θ_p, χ_p have then to be determined over a range of ka for different forms of vibration of the surface of the sphere. If the vibrations are axisymmetric, then the solutions are independent of ϕ. m is then zero, and it follows that

$$\begin{aligned} B_{mn} &= 0 \\ Y^e_{on} &= P_n(\cos\theta) \\ A_{on} &= (n + \tfrac{1}{2}) \int_o^\pi U(\theta)\, P_n(\cos\theta)\, \sin\theta\, d\theta \end{aligned} \tag{11}$$

where P_n is a Legendre polynomial. If the amplitude of the vibrations has a constant value U_o over a certain axisymmetric region $\theta_1 < \theta < \theta_2$ and is zero elsewhere, then

$$\begin{aligned} A_{on} &= (n + \tfrac{1}{2})\, U_o \int_{\theta_1}^{\theta_2} P_n(\cos\theta)\, \sin\theta\, d\theta \\ &= \tfrac{1}{2}\, U_o \left\{ \left[P_{n+1}(\cos\theta_1) - P_{n-1}(\cos\theta_1) \right] + \left[P_{n-1}(\cos\theta_2) - P_{n+1}(\cos\theta_2) \right] \right\} \end{aligned} \tag{12}$$

where P_{-1} is taken to be unity. This corresponds to a uniformly vibrating ring set in the surface of a rigid sphere. When $\theta_1 = 0$, the case of a uniformly vibrating spherical cap or piston is obtained and

$$A_{on} = \tfrac{1}{2}\, U_o \left[P_{n-1}(\cos\theta_2) - P_{n+1}(\cos\theta_2) \right] . \tag{13}$$

If in addition θ_2 is made to tend to a small quantity, say Δ/a, then Eq. 13 tends to the case of a point source set in a rigid sphere[16], namely

$$A_{on} = \frac{1}{2}\, U_o(n + \tfrac{1}{2})\left(\frac{\Delta}{a}\right)^2 \quad . \tag{14}$$

For the above cases 12 - 13, the radiation impedance is determined from

$$\theta_p - i\chi_p = \frac{1}{2(\cos\theta_1 - \cos\theta_2)} \sum_n \left[\frac{h_n(ka)}{ih'_n(ka)}\right] \frac{1}{(2n+1)} \left[\frac{A_{on}}{U_o}\right]^2 \quad . \tag{15}$$

When the surface vibrations are not axisymmetric the problem becomes more complicated, but certain examples can still be solved relatively easily. Consider a section of the uniformly vibrating ring already discussed, for values of ϕ lying between $\pm \phi_1$, with all the remainder of the surface held rigid. Since

$$\int_{-\phi_1}^{\phi_1} \sin(m\phi)\, d\phi = 0$$

$$\int_{-\phi_1}^{\phi_1} \cos(m\phi)\, d\phi = 2\sin(m\phi_1)/m \quad ; \quad m > 0$$
$$= 2\phi_1 \quad ; \quad m = 0$$

it follows that

$$B_{mn} = 0$$

$$A_{mn} = \frac{(2n+1)}{m\pi}\, U_o \left[\frac{(n-m)!}{(n+m)!}\right] \sin m\phi_1 \int_{\theta_1}^{\theta_2} P_n^m(\cos\theta) \sin\theta\, d\theta \qquad m > 0$$

$$A_{on} = \frac{(2n+1)}{2\pi}\, U_o \phi_1 \int_{\theta_1}^{\theta_2} P_n(\cos\theta) \sin\theta\, d\theta \quad .$$

If $\theta_2 = \theta_1 + \Delta\theta$ where $\Delta\theta$ is small, then

$$A_{mn} = \frac{(2n+1)}{m\pi} U_o \Delta\theta \left[\frac{(n-m)!}{(n+m)!}\right] \sin m\phi_1 P_n^m(\cos\theta_1) \sin\theta_1 \qquad m > 0$$

$$A_{on} = \frac{(2n+1)}{2\pi} U_o \Delta\theta \, \phi_1 P_n(\cos\theta_1) \sin\theta_1 \quad . \tag{16}$$

This is the case of a plane line source embedded in the surface of a rigid sphere. The radiation impedance cannot be determined as in Eq. 15 because the corresponding series does not converge.

For ease in calculation the modified Legendre polynomials were expressed in the semi-normalized form

$$\bar{P}_n^m = \left[\frac{(n-m)!}{(n+m)!}\right]^{\frac{1}{2}} P_n^m \quad . \tag{17}$$

Since it was necessary to have P_n, and P_n^m to very high orders (n, m about 40), the calculations had to be carried out in double precision.

The Bessel function subroutine which was carried out in single precision achieved an accuracy of about six figures in the range up to n = 35 when compared with standard tables[18]. A check on the derivatives showed a similar accuracy.

The sound pressure in the far zone given by the function ψ of Eq. 10 was obtained for a range of ka from 1 to 25 for the following source distribution:

(a) a point source;

(b) uniformly vibrating spherical caps for θ extending over the regions defined by: 0° - 20°, 0° - 40°, 0° - 60°;

(c) individual uniformly vibrating rings for θ in the regions defined by: 20° - 25°, 40° - 45°, 60° - 65°;

(d) a uniform line source situated along $\theta_1 = 45^\circ$, between the limits $\phi_1 = \pm 10^\circ$.

The results are presented in the form of the argument and modulus of ψ in Figs. 1 - 9. The modulus, of course, is the absolute value of the sound pressure in the far zone. The individual lines in the figures represent the variation with respect to ka at a particular point in the far zone sound field defined by the coordinates (θ, ϕ). The sound field for any particular frequency is thus obtained by reading off the values where the ordinate at that frequency intersects the lines. The argument of ψ could not be presented more accurately, since in general it changes quite rapidly over the range of ka considered. However, it can at least be shown how it changes qualitatively with changes in source configuration.

The impedances θ_p, χ_p were determined for a variety of rings and caps using Eq. 15 and are presented in Figs. 10 and 11.

The results of supplementary calculations are given in Figs. 12 - 17 and are described in the next sections.

3. Discussion of Results

Figure 1 gives the far zone pressure field* for a point source set in the surface of a rigid sphere. At very low frequencies, the sound is radiated uniformly in all directions. At very high frequencies, the sound is radiated mainly into the half space tangential to the sphere at the point source. This is presumably because the dimensions of the point source have been assumed to be much smaller than any given value of the wavelength. The variation of phase with frequency is linear as shown in Fig.1(b). At low frequencies, below about ka = 1.5, the lines

---

* The results for the pressure amplitude agree in general with those given in Fig. 66, ref. 10.

are not quite straight, but curve to a phase value of 90° at ka = 0. This is shown in Fig. 14(b). The initial slope for $ka << 1$ agrees with the relation[16] $-\frac{3}{2} \cos\theta / \left[1 + \left(\frac{3}{2} ka \cos\theta\right)^2\right]$.

Due to the principle of reciprocity [16] the pressure field in the far zone is proportional to the pressure distribution over a rigid sphere due to a point source at infinity. The factor of proportionality is i/ka, so that to obtain the solution of this problem from Fig. 1, the modulus of ψ is divided by ka as shown in Fig. 14(a). The phase remains the same except that the coordinate system is shifted vertically so that the origin coincides with the focus of the straight lines. The application of these results to binaural localization of sound will be discussed in the next section.

Figure 2 - 4 show the development of the sound field as the spherical cap changes size. As usual at the low frequency limit, the radiation is uniform in all directions. At very high frequencies, the situation is not so definite. It has been shown[19] that the radiation field at very high frequencies has the same form as that of the given velocity distribution over the surface of the sphere. This tendency is apparent in the figures showing the pressure amplitude. In the far zone outside the cone defined by the cap angle, the pressure amplitude lines can be seen to be going to zero. For values of θ lying inside the cone, the lines were found to be tending to settle around $|\psi|$ equal to unity, except for points directly on the axis $\theta = 0$. This was investigated as far out as ka = 70 for caps whose half angles went over the range from 10° to 170°. Some of the $\theta = 0$ pressure amplitude curves are shown in Fig. 12. The number of oscillations about the mean $|\psi| = 1$ increases very rapidly as the cap increases in size, but the amplitude decreases in size although only slowly at first. In the limit when the cap

covers the entire surface of the sphere, the expected result of a constant amplitude at all frequencies is attained. For values of θ near zero the pressure amplitude at first follows the $\theta = 0$ curve quite closely, but at very high frequencies it begins to settle down around $|\psi| = 1$. Hence, although according to calculation the oscillatory nature of the $\theta = 0$ pressure amplitude persists at very high frequencies, it will eventually have no existence in any physical sense.

As the cap decreases in size the radiation field resembles that of a point source over an increasingly greater part of the frequency range. However the behavior at high frequencies is eventually the same, because the wavelengths become much smaller than the dimensions of the cap.

The behavior of rings is similar to that of caps at the high and low ends of the frequency range. At the low frequencies the radiation is uniform and at very high frequencies all the radiation is concentrated uniformly in the region defined by the angle subtended by the thickness of the ring. Figures 5 - 7 show how the sound field varies as a 5° ring is moved backwards over the sphere. These results can also be used to analyze how the sound fields of the caps are built up as they are increased in size. For example, if the 40° - 45° ring is added to the 40° cap to produce a 45° cap, then the phase difference at about $ka = 25$ is approximately 180° for the $\theta = 0$ lines. This means that the sound intensity at $\theta = 0$ will be decreased by the addition of the ring hence assisting in the process of the formation of the rapid fluctuations shown in Fig. 12. The sound field in other directions and for other combinations of the elementary rings could be analyzed in a similar way.

The phase variation with frequency as shown in Figs. 2(b) - 7(b) indicates some general tendencies. As the cap grows larger or as the ring is moved backwards over the sphere the rate of change of phase with frequency grows smaller. Also, as might be expected, the abrupt changes of phase which occur coincide with sharp minima in amplitude. Other trends can also be observed.

It seems likely that certain desired sound fields which are axisymmetric and fairly simple in form could be approximated by arrays of rings whose relative phases and amplitudes are chosen specifically for the purpose. For example the directional beam of Fig. 13 is obtained by combining a 40° cap with a 40° - 45° ring at a frequency corresponding to $ka = 14.2$. The ring is made to vibrate 180° out of phase with the cap, while the amplitude of the caps vibrations is $\frac{1}{3}$ that of the ring.

The acoustic impedances of the caps and rings are shown in Figs. 10 and 11. As the cap increases in size the resistive part of its impedance approaches the high frequency limit ρc more rapidly, while the reactive part has its maximum at progressively lower frequencies. Rings behave roughly in the same manner as caps which subtend the same angle at the center of the sphere. Thus 5° rings behave similarly to the 5° cap, and a 40° rings is similar in behavior to the 40° cap. The number of oscillations increases as a ring moves backwards from its initial position as cap.

Figures 8 and 9 give the far zone pressure field due to a uniform plane line source situated on the plane $\theta_1 = 45^{\circ}$ between the limits $\phi_1 = \pm 10^{\circ}$. Figure 8 gives the results in the meridian half plane $\phi = 0$ directly ahead of the line source and Fig. 9 in the equatorial plane

$\theta = 90^{\circ}$. For higher frequencies the results in the in the $\phi = 0$ plane resemble those for a point source. The intensity at $\theta = 90^{\circ}$ is of the same order as that at $\theta = 0^{\circ}$ but has developed oscillations. The effect of the length of the line source on phase shows up at lower frequencies particularly in the equatorial plane $\theta = 90^{\circ}$. In the region ahead of the line source approximately $\phi = \pm 60^{\circ}$, the phase remains roughly constant over the range of frequencies from ka = 1 to 2, and linear at higher frequencies. Outside this region the phase variation is quite disturbed. As the length of the line source is increased the results tend gradually to those for a thin ring at $\theta = 45^{\circ}$.

4. Binaural Localization of Sources of Sound

As has been pointed out in the previous section, the far zone pressure field for the point source is the same as the pressure distribution over the surface of a rigid sphere due to a point source at infinity, i.e., due to plane waves incident on the sphere. It is possible therefore to examine mechanisms for localizing a source of sound using the amplitude and phase observed at two diametrically opposite points on the surface of the sphere. Such mechanisms might then be expected to be similar to the mechanisms employed by ears set in a human head. For this purpose it is usually assumed that the head and the sphere correspond roughly in size so that the radius of the sphere will be taken to be about 3.4 inches. Hence a frequency of approximately 620 cycles will be represented by a value of ka = 1, and proportionately for any other frequency. It should be pointed out, however, that due to the symmetry of the sphere a sound source can only be located as on the surface of a cone whose axis is the diameter at the ends of which the

measurements are made. In actuality sounds are localized a little more accurately by making use of the symmetry of the head and body and the sensations of sound experienced elsewhere than at the ears, although discrimination is well developed only in the horizontal plane[20].

The current view held by experimenters in the field is that localization is achieved at low frequencies by making use of the phase difference between the two ears and at high frequencies by using the intensity difference. This explanation was first proposed by Rayleigh[21] although the emphasis of his conclusions was somewhat modified later[22]. The experiments which have been performed use both pulses and pure tones, the latter having to be used very carefully in order to exclude transient effects. The direction of a pulsed sound was found to be quite readily distinguished. The results for pure tones are more conflicting, but some of the more successful experiments[23] have been carried out at frequencies of only a few hundred cycles.

In order to discuss the usefulness of intensity differences, some results should be quoted. Banister[24] found that in order to achieve a sensation of deviation from the median plane an intensity difference between the ears of more than 4db was necessary. In addition, phase differences of pure tones become ambiguous above 1,200 cycles[20] (also compare Figs. 15(b), 16(b)), so that it would seem that intensity differences should be the significant factor for the higher frequencies. However, if a direction of 15° to the median plane be accepted[20], [25] as the minimum deviation which can be readily perceived (the actual minimum angle is probably less than half this amount), then on the basis of Banister's findings, the results for a sphere show that intensity differences can never be of sufficient significance in determining the

direction of a distant source of sound. For example, in Fig. 16(a) (which gives the pressure distribution over the sphere when the frequency is about 6,200 cycles) for a source situated 15° from the median plane at $\theta = 90^{\circ}$, the ratio of the pressure amplitudes would be 3.95/2.55, an intensity difference somewhat less than 4db. Figure 1 does not hold out the possibility of improvement at higher frequencies. At very high frequencies it is clear that not much discrimination can be expected when one side of the sphere is illuminated and the other side in a shadow. For an actual head, it is clear that the pinna must play a role at higher frequencies, but it also seems apparent that over a wide section of the audible frequency range, intensity differences will at best be only marginally significant for a distant source of sound. This conclusion appears to be in contradiction to the known fact that intensity differences produce a sensation of "sidedness" or deviation from the median plane. However, it is apparent that larger intensity differences will occur when the deviations from the median are more than 15° so that a less accurate localization of distant sources of sound is still possible by means of intensity differences. Larger intensity differences are also obtained when the sound source is brought closer to the head. For example, Figure 17 which is obtained from the general Eq. 5, shows that for a 15° deviation the intensity difference for a tone of approximately 6,200 cycles is increased to a maximum of about 8 db as the source approaches the head. The distance at which the intensity difference rises to a sufficient degree above the 4 db threshold is not very certain, but it seems to be only a few feet at the most. Similar results hold down to about 2 k/cs. It would seem, therefore, that the higher frequency pure tones cannot be localized very accurately by means

of intensity differences unless the source is within a few feet of the head.

This conclusion has a bearing on the localization of pulsed sounds. As has already been stated, a pulsed sound can be localized very readily at all distances - certainly well within the 15^{o} deviation which has been set up as a criterion. In view of the apparent inaccuracy in localizing the constituent tones in the higher frequency range, it might be expected that additional properties inherent in the nature of a pulse are responsible for this enhanced ability. A pulse can be analysed by using the results in Fig. 14 which shows how the amplitude and phase of the different constituent tones in the pulse will vary with frequency when the sound source is more than several feet away. The phase variation with frequency is closely linear above about 1,500 cycles, each direction having a certain fixed slope, and this linearity provides a localization mechanism which has often been suggested for pulses, namely a difference in arrival time of the pulse at each ear. As might be expected, the differences in arrival time computed from Fig. 1(b) agree very well with the results given by Woodworth and Schlosberg[20], who use a simple path difference theory valid only for higher frequencies. The formula, therefore, which would give the phase difference between the ears in this range is of the form

$$\text{phase difference} = ka\,(\theta_d + \sin\theta_d) \qquad (18)$$

where θ_d is the angle which the incident sound waves make with the median plane at $\theta = 90^{o}$. The arrival time differences can be readily determined from this formula. From the results, it appears that the ears have to distinguish a difference of the order of 1/10 millisecond and from experiment this appears on the average to be the minimal

amount required to achieve an effective sensation of "sidedness"[20], [26]. However there is always the problem of determining the precise arrival time of a pulse, the time differences which are used being at the most about 1 per cent of pulse length[20]. In order to obviate this difficulty, it has been suggested that the time differences which the ears sense are obtained from a continuous comparison in the arrival time of different parts of the same pulse at each ear. However it would seem that the same pulse form will not occur at each ear. As shown in Fig. 14(b) the change of phase with frequency is not linear over the whole frequency range. The slope varies at lower frequencies so that the simple path difference theory breaks down when the sphere is smaller than about 1/3 the wave length of the incident waves. Hence for an actual head it would be expected that the non-linearity would persist to much higher frequencies, because the irregularities of the head and pinna provide much greater curvatures for the incident sound to contend with than the gross effect of the spherical model. Thus it would appear that a pulse would not only arrive at each ear at a somewhat different time but more generally in a somewhat different form. Figure 14(a) shows that the amplitude variation with frequency will also contribute to this effect. It is known[23] that the ear is quite sensitive to changes in pulse form and hence using more general differences of this type would seem a more sophisticated mechanism for sound localization than using only time and intensity differences. To reconcile two such sensations into a single impression is not an uncommon feature in nature, so that such an idea is not in such obvious conflict with experience as it might seem. The diffraction of sound around the head must surely be sufficiently complex to produce different pulse forms at each ear, thus requiring an automatic

reconciliation process in the brain, and if such a reconciliation process exists it must surely be combined with the ability to localize a sound. The fact that the calculated time and intensity differences are so minimal for such a large deviation as 15^{o} certainly leaves room for such a hypothesis. Unfortunately, it cannot be indicated as yet what changes in pulse form would be significant. The ear has obviously gone through a learning process of comparable complexity to that of the eye, but as yet there appears to be no clear insight into the kinds of recognition patterns which it uses.

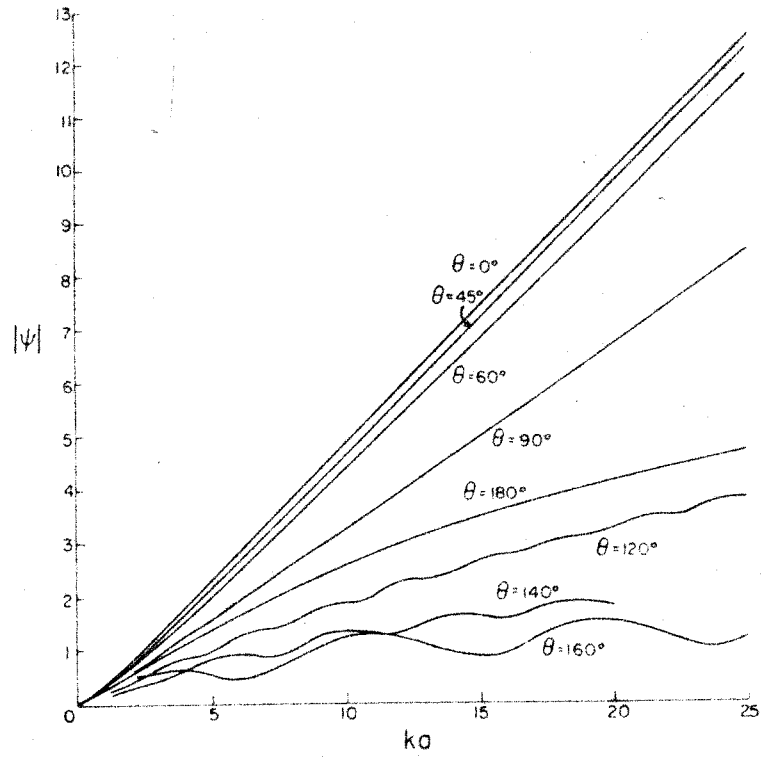

(a) The far zone pressure amplitude as a function of frequency due to a point source set in the surface of a rigid sphere.

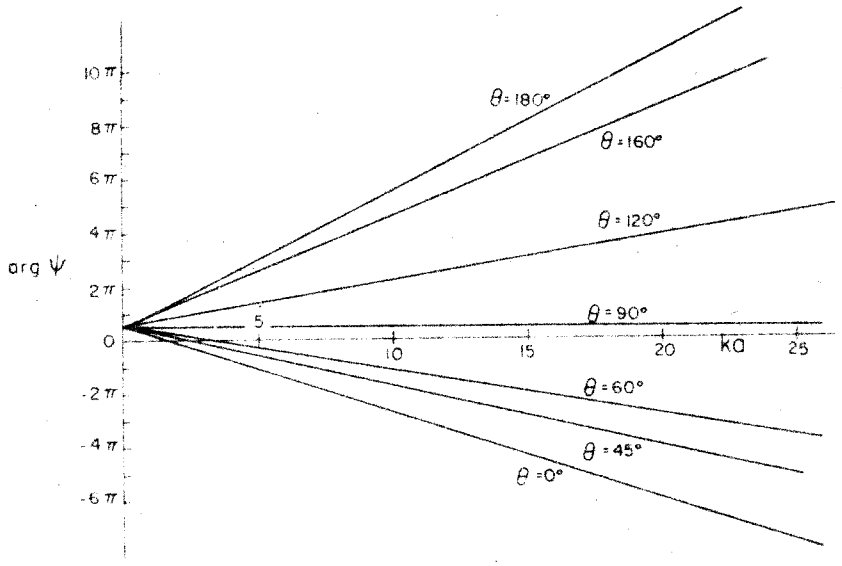

(b) The phase of the far zone pressure field as a function of frequency due to a point source set in the surface of a rigid sphere.

Fig. 1

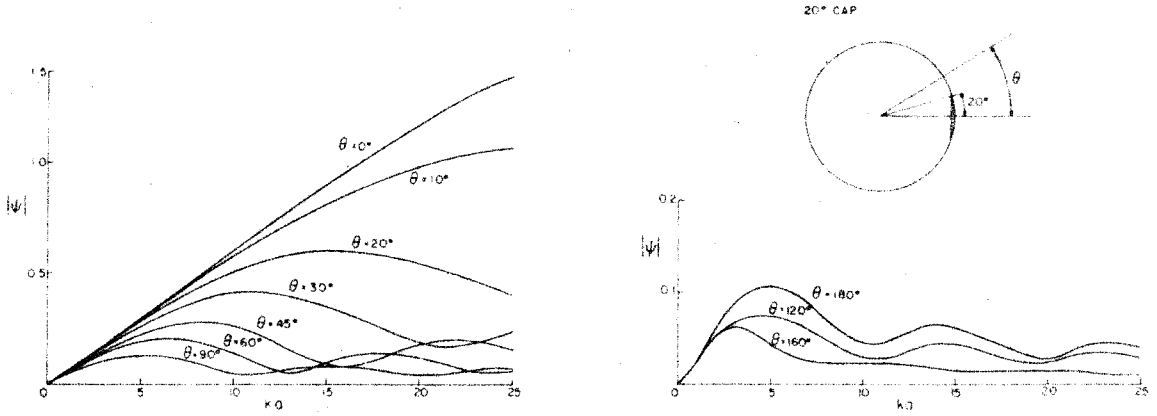

(a) The far zone pressure amplitude as a function of frequency due to a 20° cap set in the surface of a rigid sphere.

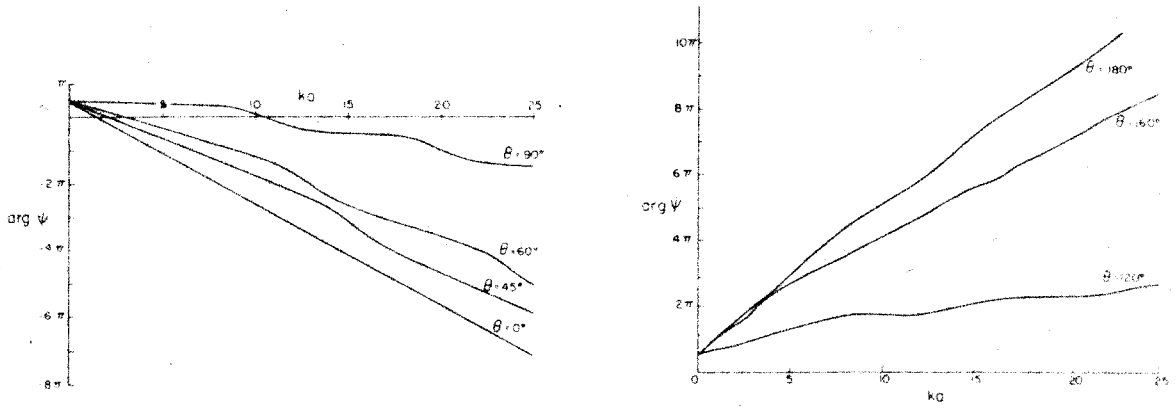

(b) The phase of the far zone pressure field as a function of frequency due to a 20° cap set in the surface of a rigid sphere.

Fig. 2

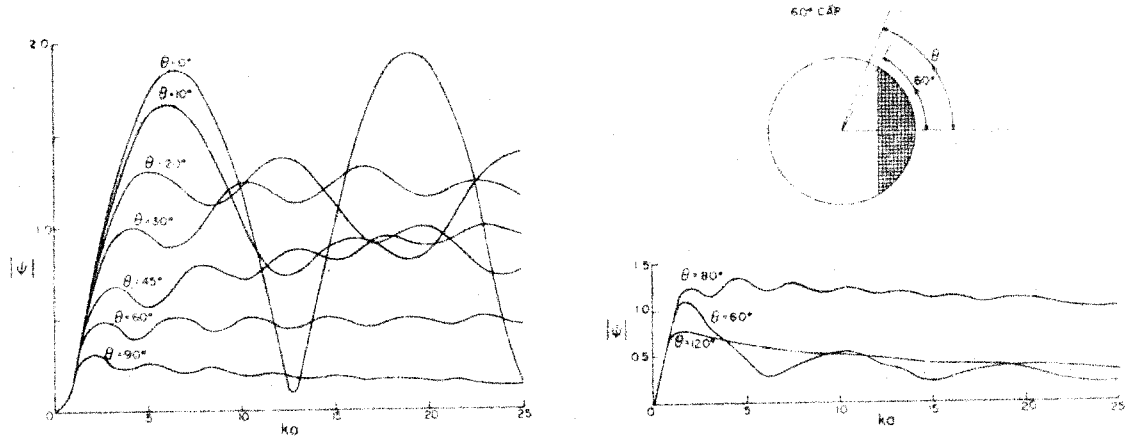

(a) The far zone pressure amplitude as a function of frequency due to a 60° cap set in the surface of a rigid sphere.

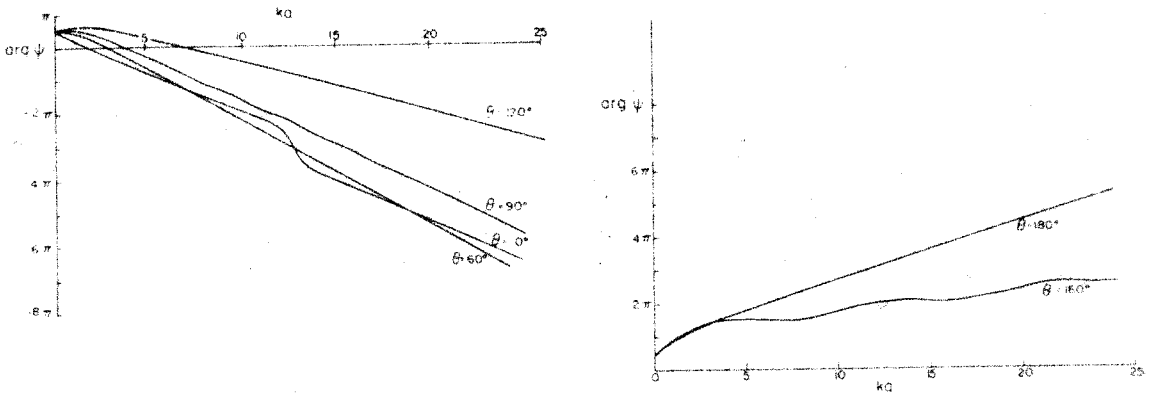

(b) The phase of the far zone pressure field as a function of frequency due to a 60° cap set in the surface of a rigid sphere.

Fig. 4

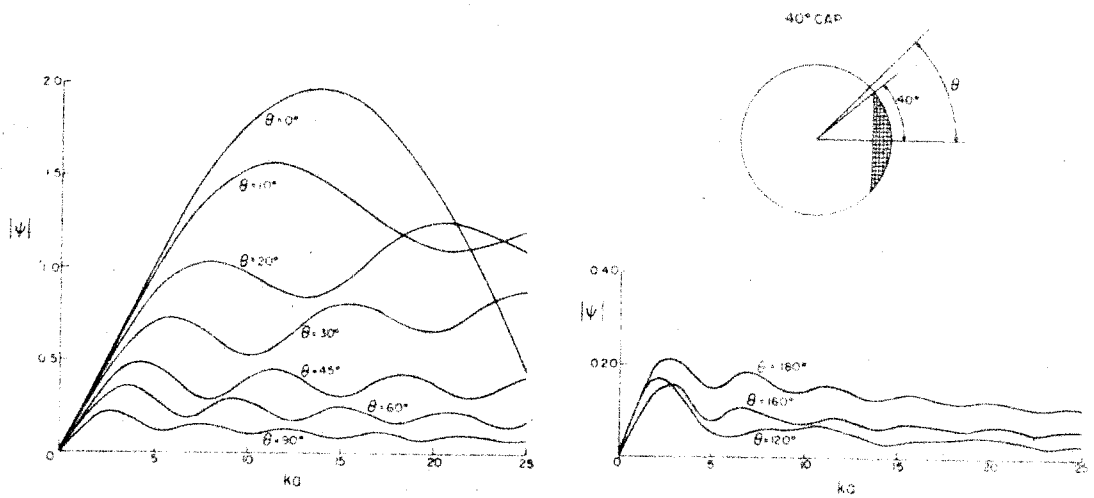

(a) The far zone pressure amplitude as a function of frequency due to a 40^{o} cap set in the surface of a rigid sphere.

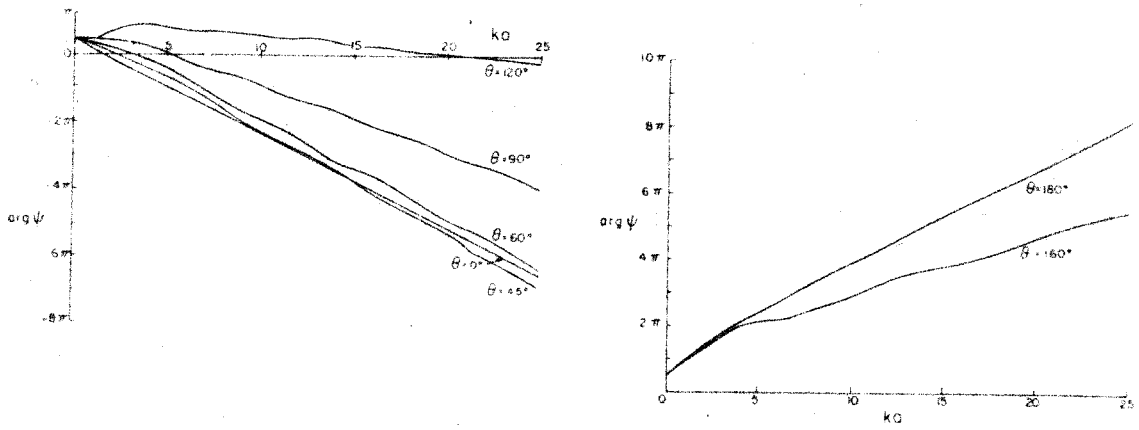

(b) The phase of the far zone pressure field as a function of frequency due to a 40^{o} cap set in the surface of a rigid sphere.

Fig. 3

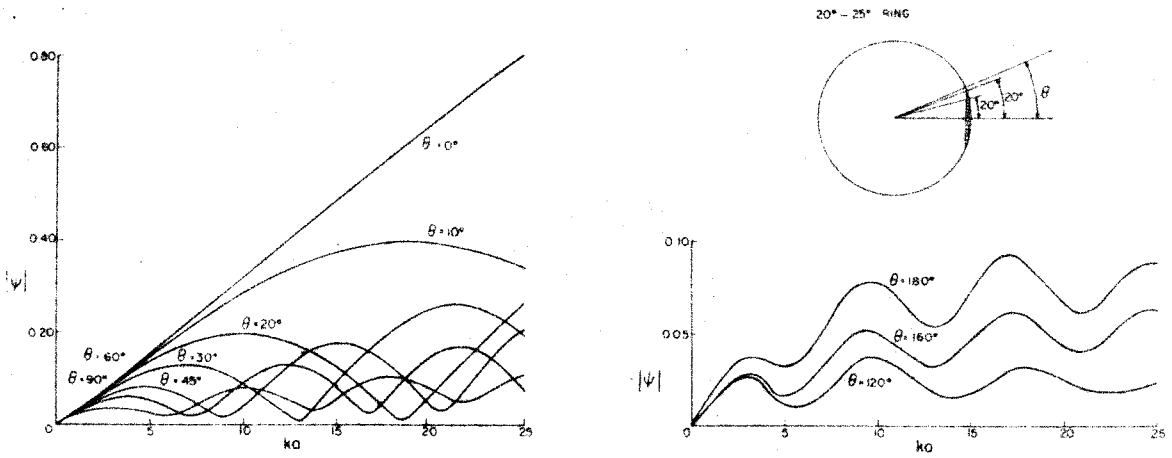

(a) The far zone pressure amplitude as a function of frequency due to a 20° - 25° ring set in the surface of a rigid sphere.

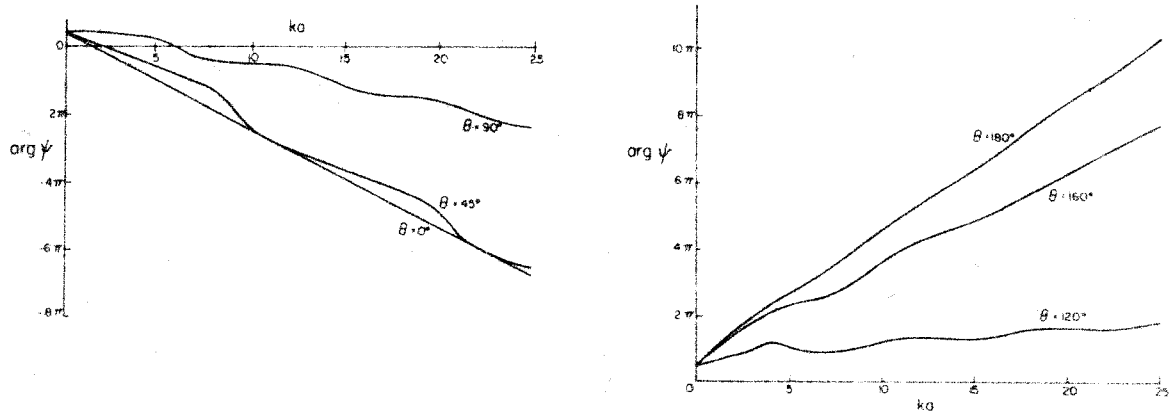

(b) The phase of the far zone pressure field as a function of frequency due to a 20° - 25° ring set in the surface of a rigid sphere.

Fig. 5

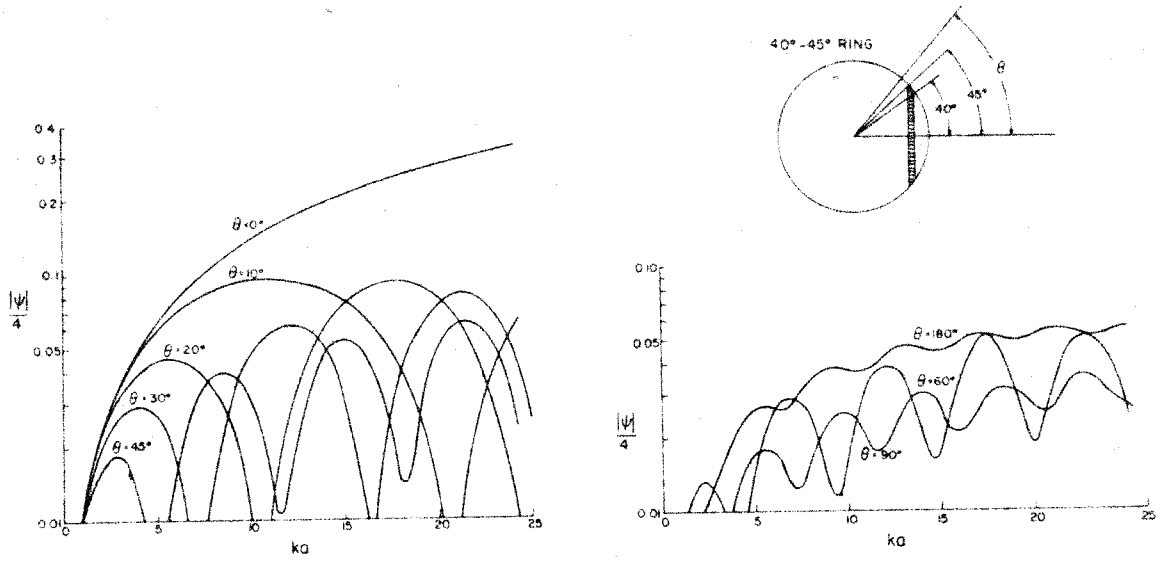

(a) The far zone pressure amplitude as a function of frequency due to a 40° - 45° ring set in the surface of a rigid sphere.

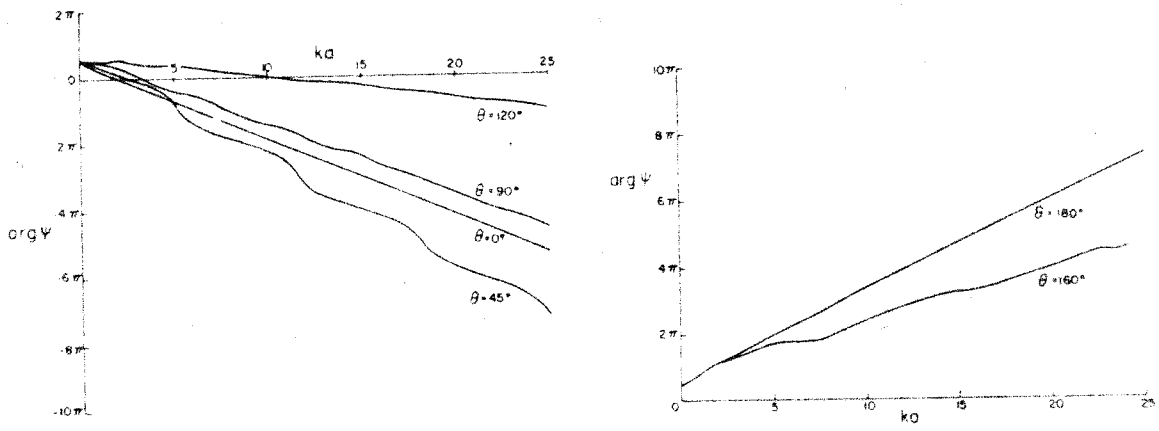

(b) The phase of the far zone pressure field as a function of frequency due to a 40° - 45° ring set in the surface of a rigid sphere.

Fig. 6

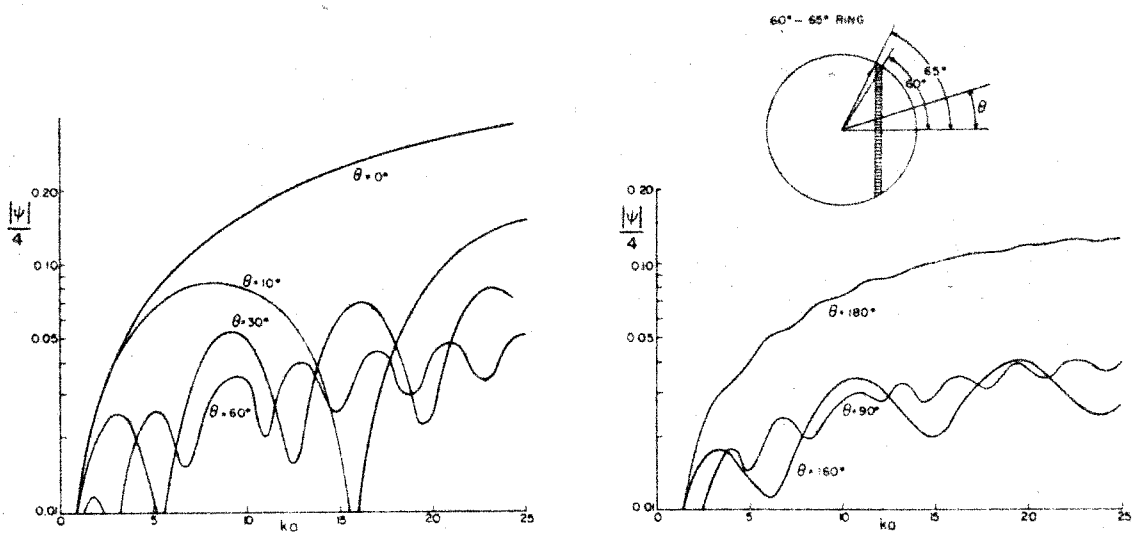

(a) The far zone pressure amplitude as a function of frequency due to a 60^{o} - 65^{o} ring set in the surface of a rigid sphere.

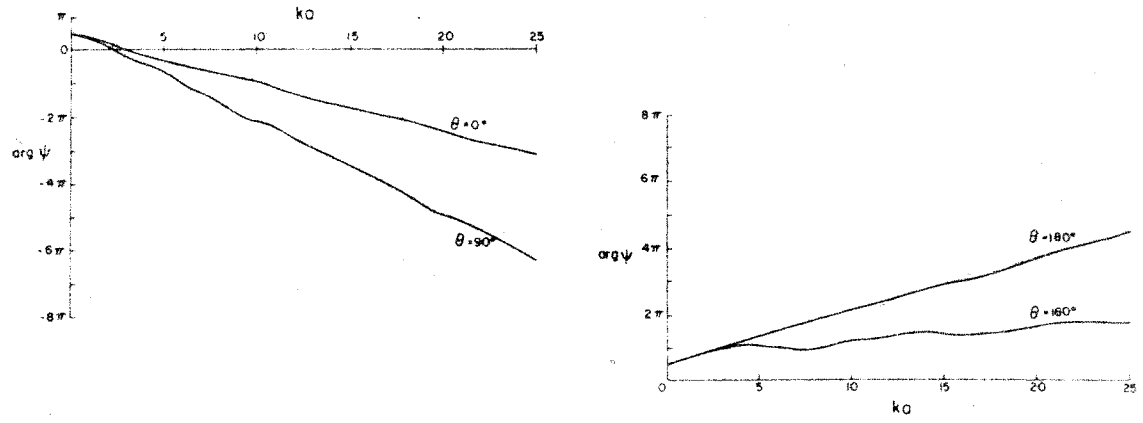

(b) The phase of the far zone pressure field as a function of frequency due to a 60^{o} - 65^{o} ring set in the surface of a rigid sphere.

Fig. 7

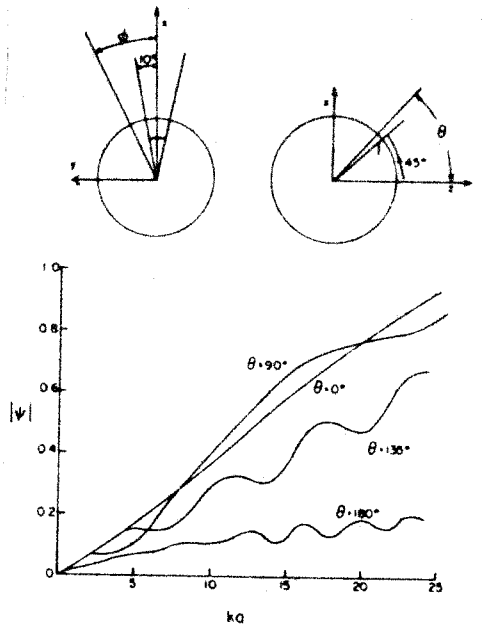

(a) The far zone pressure amplitude as a function of frequency due to a plane line source situated on the plane $\theta_1 = 45^\circ$ between the limits $\phi_1 = \pm 10^\circ$ in the surface of a rigid sphere. The section of the far zone field considered is in the meridian half plane $\phi = 0$.

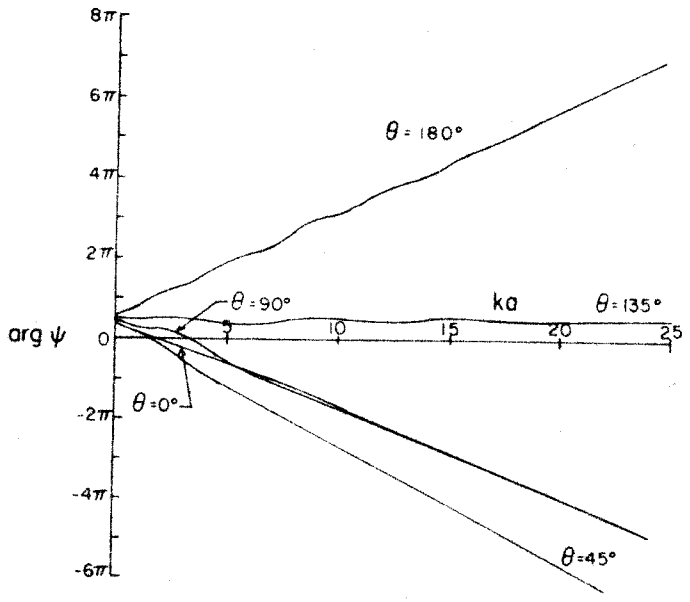

(b) The phase of the far zone pressure field as a function of frequency due to the plane line source defined by $\theta_1 = 45^\circ$, $\phi_1 = \pm 10^\circ$. The section of the far zone field considered is in the meridian half plane $\phi = 0$.

Fig. 8

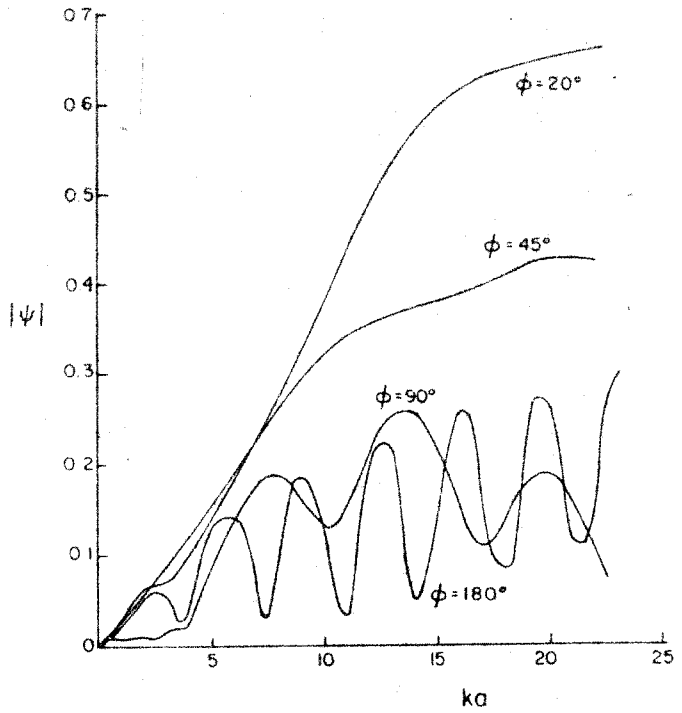

(a) The far zone pressure amplitude as a function of frequency due to the plane line source defined by $\theta_1 = 45^\circ$, $\phi_1 = \pm 10^\circ$. The section of the far zone field considered is in the equatorial plane $\theta = 90^\circ$.

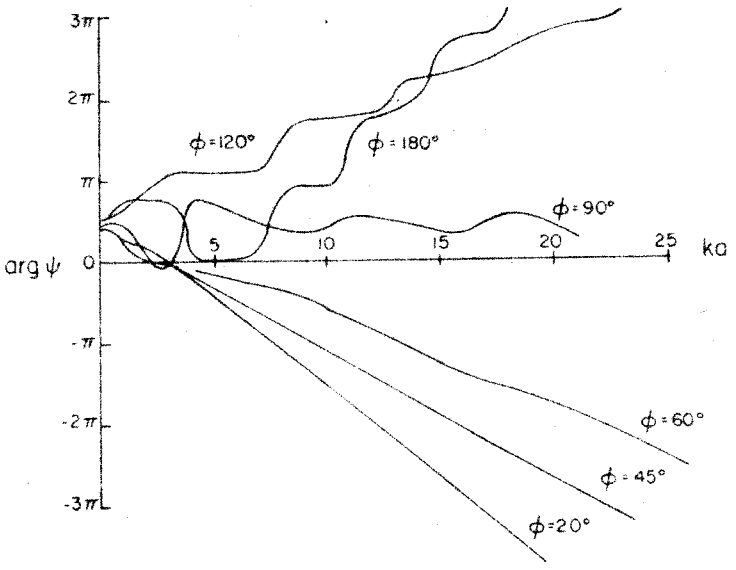

(b) The phase of the far zone pressure field as a function of frequency due to the plane line source defined by $\theta_1 = 45^\circ$, $\phi_1 = \pm 10^\circ$. The section of the far zone field considered is in the equatorial plane $\theta = 90^\circ$.

Fig. 9

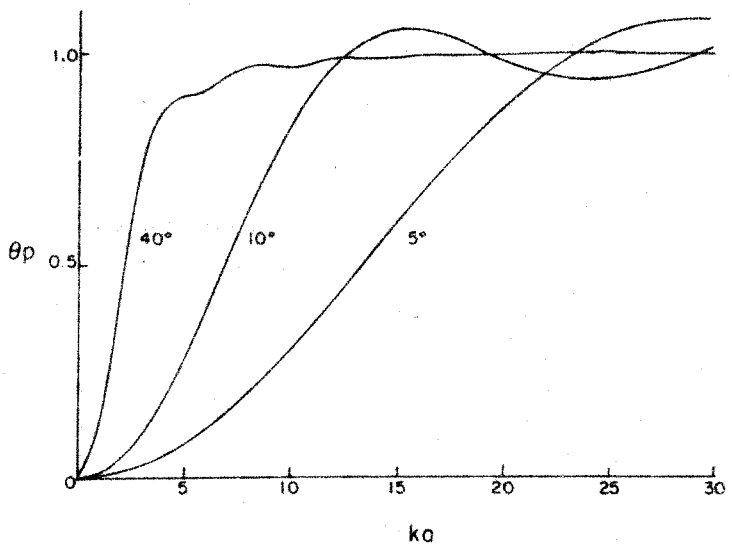

(a) Resistive part θp of the acoustic impedance of the 5°, 10°, 40° caps as a function of frequency.

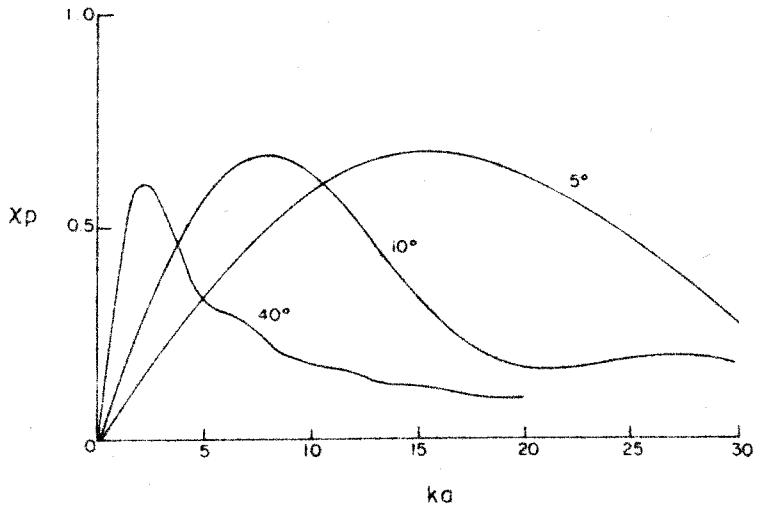

(b) Reactive part Xp of the acoustic impedance of the 5°, 10°, 40° caps as a function of frequency.

Fig. 10

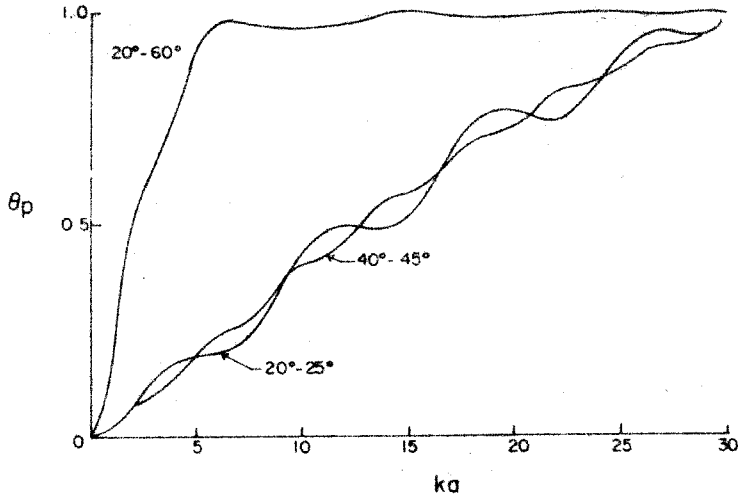

(a) Resistive part θp of the acoustic impedance of the 20° - 25°, 40° - 45°, 20° - 60° rings as a function of frequency.

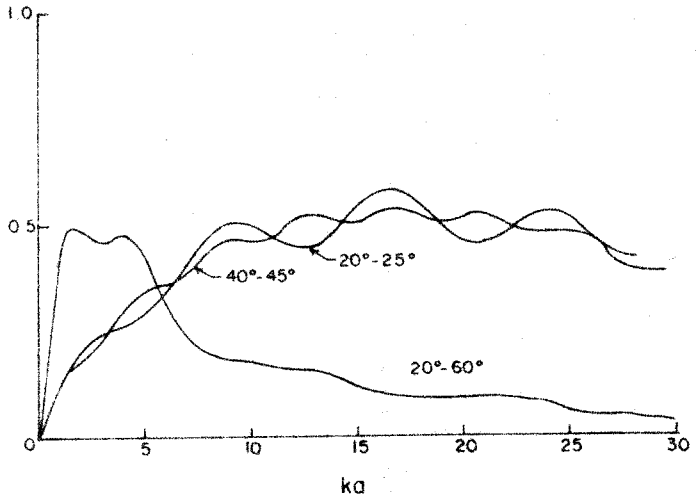

(b) Reactive part χp of the acoustic impedance of the 20° - 25°, 40° - 45°, 20° - 60° rings as a function of frequency.

Fig. 11

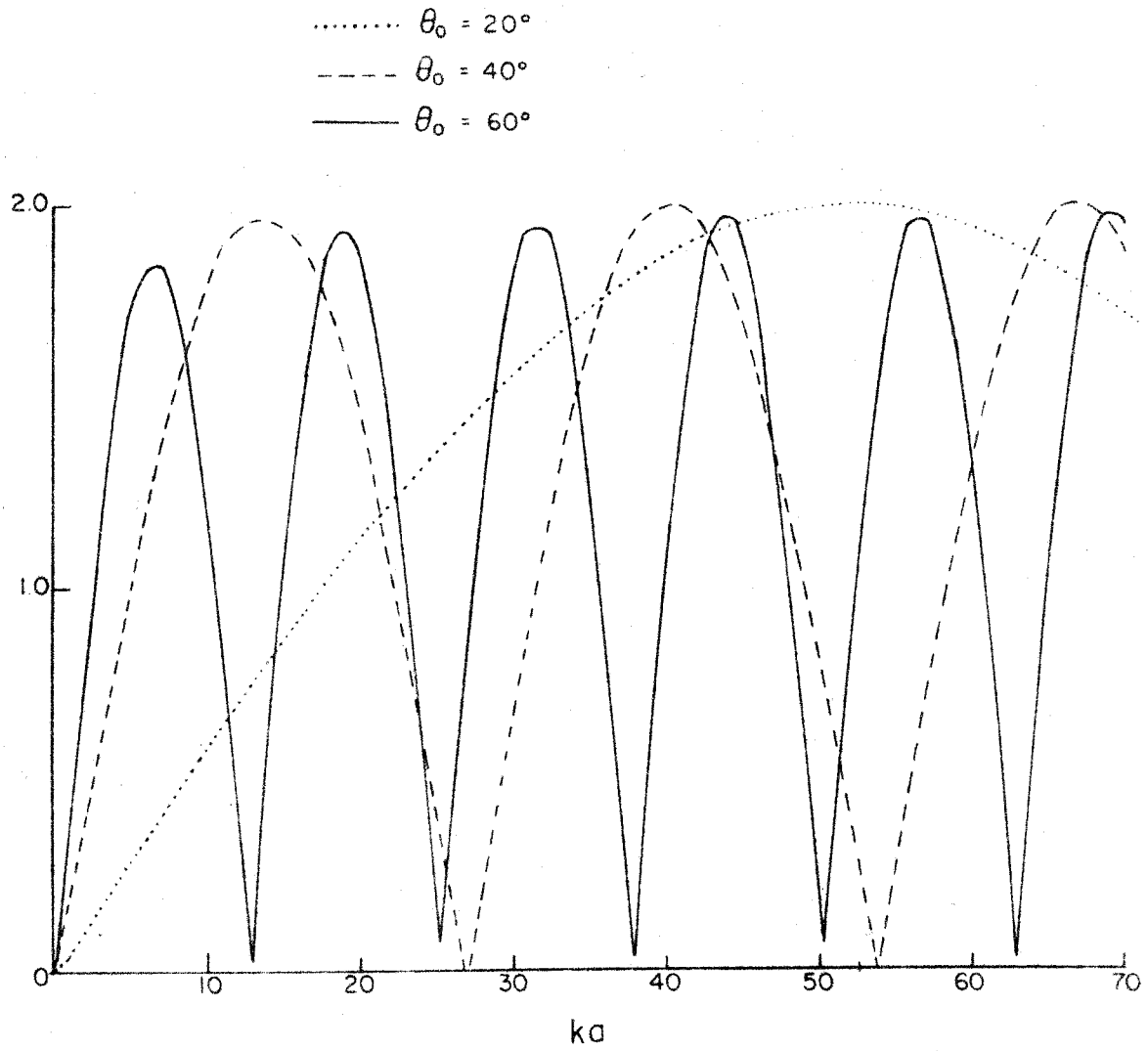

The far zone pressure amplitude on the axis $\theta = 0$ as a function of frequency for caps of increasing size.

Fig. 12

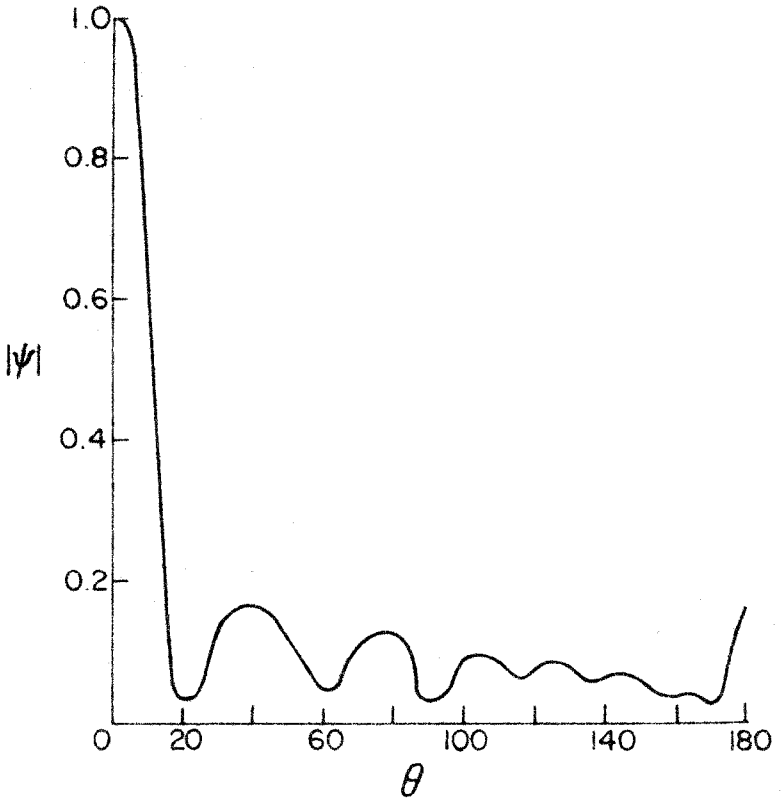

The far zone directional pattern for a 40° cap combined with a 40° - 45° ring for ka = 14.2. The amplitude of vibration of the cap is 1/3 that of the ring and the two elements are 180° out of phase.

Fig. 13

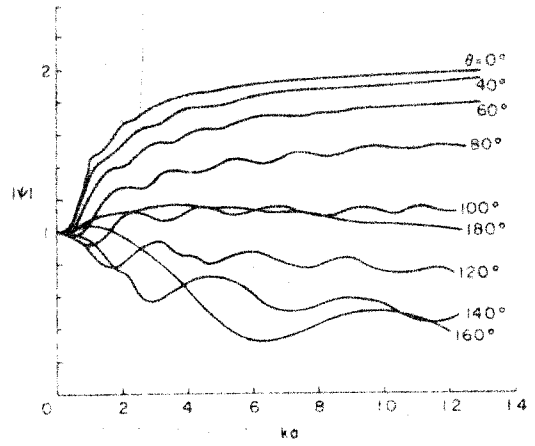

Fig. 14(a) The pressure amplitude on the surface of a rigid sphere due to plane waves incident in the direction $\theta = 180^{\circ}$, as a function of frequency.

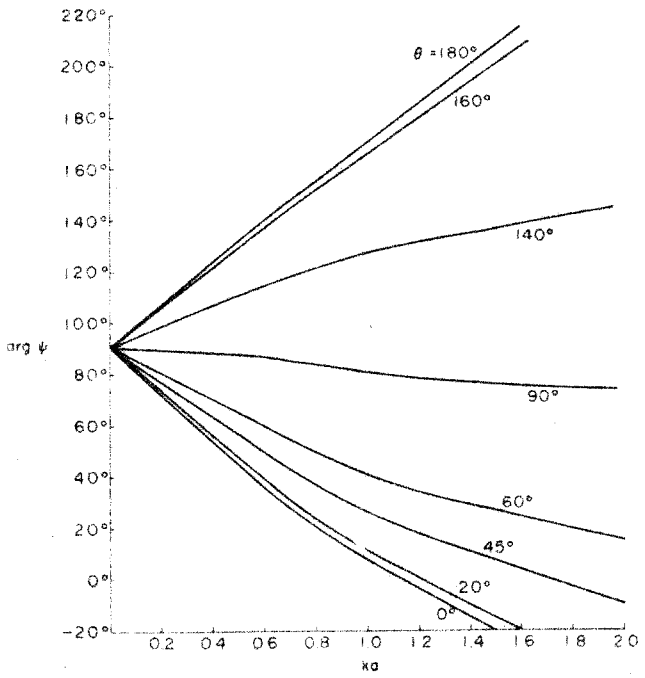

Fig. 14(b) The phase of the far zone pressure field of a point source as a function of frequency in the lower frequency range (or alternatively the phase, with 90° added, of the pressure distribution over a sphere due to incident plane waves).

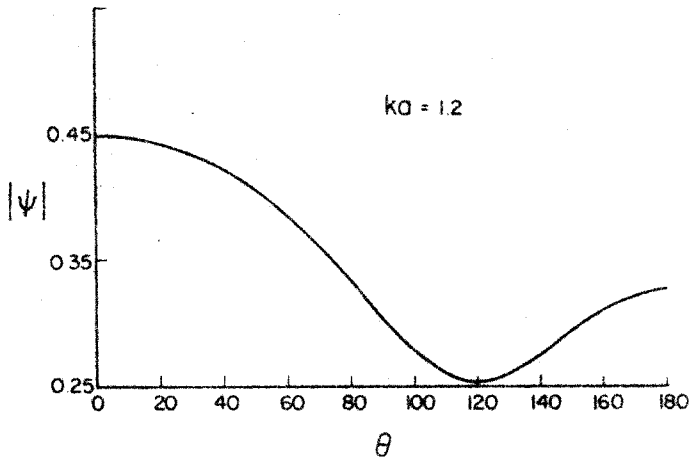

(a) The far zone pressure amplitude as a function of θ due to a point source at a frequency corresponding to ka = 1.2.

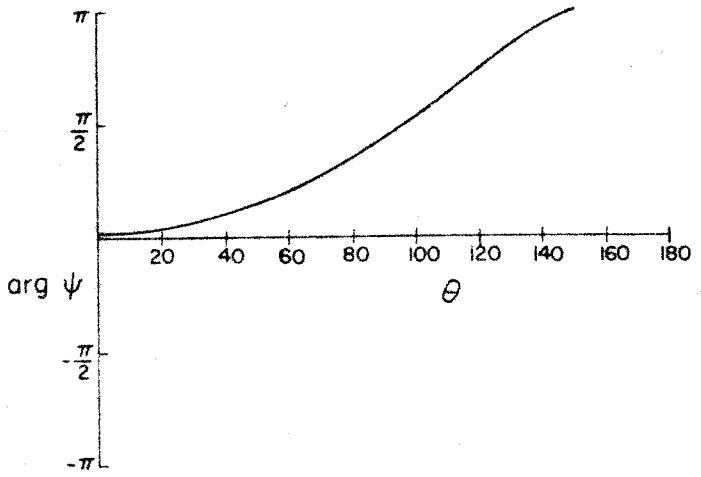

(b) The phase of the far zone pressure field as a function of θ due to a point source at a frequency corresponding to ka = 1.2.

Fig. 15

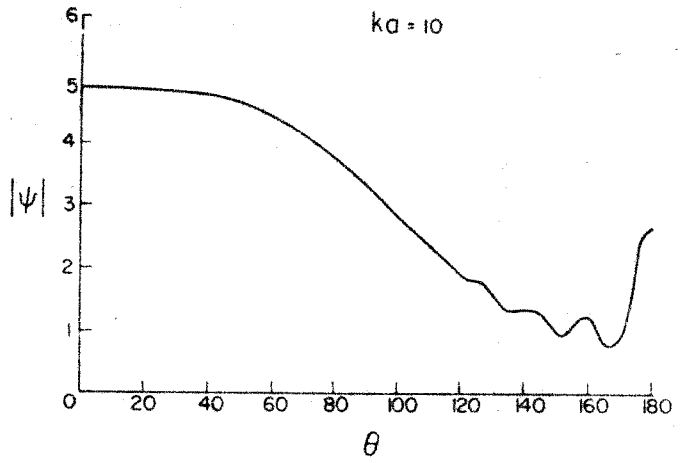

(a) The far zone pressure amplitude as a function of θ due to a point source at a frequency corresponding to ka = 10.

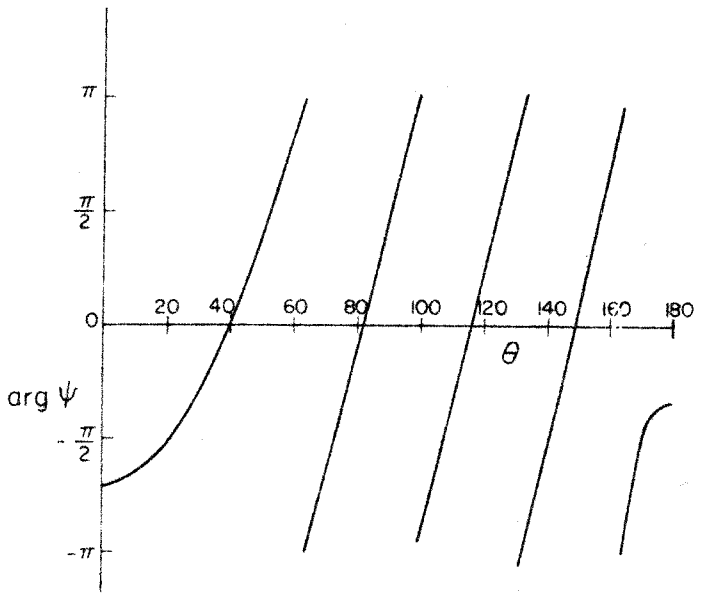

(b) The phase of the far zone pressure field as a function of θ due to a point source at a frequency corresponding to ka = 10.

Fig. 16

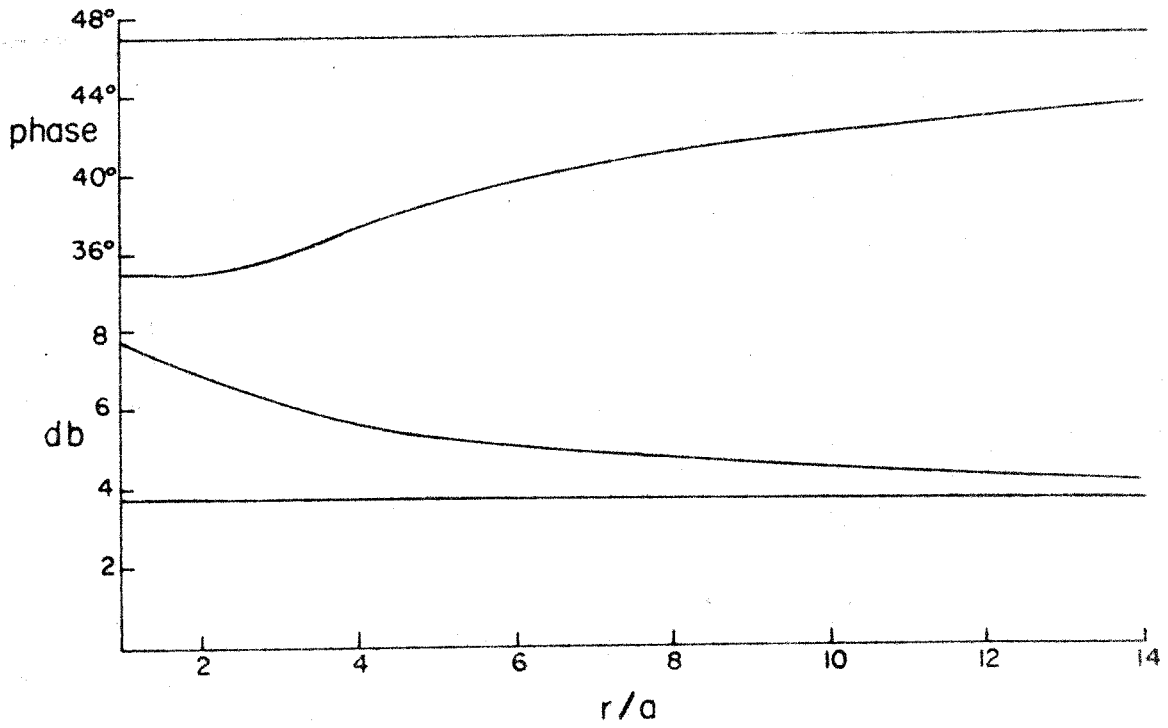

The phase and intensity difference between the two ears as a function of distance, for a point source situated 15° from the line of sight at a frequency corresponding to about 6 k/cs.

Fig. 17

REFERENCES TO PART I

[1] L. D. Hampton and C. M. McKinney, Journ. Acoust. Soc. Amer., 33, 5, 664 - 673 (1961).

[2] J. J. Faran, Journ. Acoust. Soc. Amer., 23, 4, 405 - 418 (1951).

[3] P. M. Morse and H. Feshbach, "Methods of Theoretical Physics" (McGraw-Hill Book Company, New York, 1953), Vol. II, p. 1483.

[4] V. C. Anderson, Journ. Acoust. Soc. Amer., 22, 4, 426 - 431 (1950).

[5] H. Stenzel, "Leitfaden zur Berechnung von Schallvorgagen", (Julius Springer, Berlin, 1939).

[6] Reference [3], Vol. I, p. 142.

[7] Reference [3], Vol. II, p. 1486

[8] Reference [3], Vol. II, pp. 1325, 1573.

[9] Reference [3], Vol. I, pp. 116, 142.

[10] P. M. Morse, "Vibration and Sound", (McGraw-Hill Book Company, New York, 1948) p. 354.

[11] Reference [3], Vol. II, p. 1483.

[12] Reference [3], Vol. II, p. 1554.

[13] American Inst. of Physics Handbook, (McGraw-Hill Book Company, New York, 1957), p. 3 - 80.

[14] D. L. Anderson, Trans. of Engin. Inst. of Canada, 2, 116 - 121 (1958).

[15] R. Hickling, Journ. Acoust. Soc. Amer., 30, 2, 137 - 139 (1958).

[16] Reference [10] pp. 321 - 326, 354 - 357.

[17] Reference [3] Vol. II, p. 1265.

[18] Mathematical Tables Project of the National Bureau of Standards, Tables of Spherical Bessel Funcations, Vols. I and II (New York Columbia University Press, 1947).

[19] Reference [3] Vol. II, p. 1479.

[20] Woodworth and Schlosberg, "Experimental Psychology" (Henry Holt and Co., New York, 1955) pp. 349 - 361.

[21] Lord Rayleigh, "Theory of Sound" (Dover Publications, New York, 1945) Vol. II, pp. 442 - 3.

[22] Lord Rayleigh, Phil. Mag. 6, 13, 214 - 232 (1907).

[23] J. R. Pierce, American Scientist, 38, 1, 40 - 45 (1960).

[24] H. Banister, Brit. Journ. of Psych., 16, 265 - 292 (1926).

[25] A. W. Mills, Journ. Acoust. Soc. Amer., 30, 237 - 246 (1958).

[26] R. G. Klumpp, H. R. Eady, Journ. Acoust. Soc. Amer., 28, 859 - 860 (1956).

PART II - SOME EFFECTS OF THERMAL CONDUCTION AND COMPRESSIBILITY IN THE COLLAPSE OF A SPHERICAL BUBBLE IN A LIQUID

Introduction

Cavities or bubbles can occur spontaneously in a liquid either as the result of a chemical reaction or explosion, or because of temperature and pressure changes in the liquid. The terms cavitation and boiling are usually reserved for the latter processes which require the presence of microscopic nuclei for their inception. In boiling the bubbles contain a relatively large amount of the liquid vapor, whereas in cavitation, which is a rupture of the liquid or of a liquid solid contact, the bubbles contain small amounts of vapor or permanent gas. Cavitation is usually caused by subjecting the liquid to tensile forces. This may occur in several ways, more notably when a liquid flows at high speed past a solid body or when a liquid is subjected to high intensity sonic or ultrasonic sound.

The work presented here is concerned with the collapse of a cavity. If the interior pressure falls to small values when the bubble reaches its maximum size, as in the case of a cavitation bubble or a bubble formed by an explosion, then it is possible for it to collapse again due to ambient pressures in the liquid. In such a collapse the main effect is one of the inertial motion of the liquid rushing in to fill a near vacuum, and high velocities pressures and temperatures will result. As a consequence, various phenomena may occur. One of the best known is the damage experienced by solid surfaces exposed to cavitation. Another, called sonoluminescence, occurs when the gas inside the cavity becomes so highly compressed that it becomes incandescent. Both are

of major interest here and will be discussed more fully in the appropriate sections.

Because of the high pressures generated by a collapsing cavity, the compressibility of the liquid becomes a significant factor. In particular it is possible for shock waves to form and radiate outwards after the cavity has collapsed and rebounded. Also when the gas or vapor inside a collapsing bubble is compressed so that it becomes hot, heat conduction from the gas into the liquid becomes a significant modifying factor. The work presented here is mainly an analysis of these two effects. For simplicity, the bubble or cavity is assumed to be spherical and to be situated in a limitless liquid. The initial conditions prior to collapse are also simplified and hence take no particular account of the origin and previous history of the bubble. Since the effects in question are being considered largely in a qualitative manner, such simplifications are not thought to be critical.

SECTION A - EFFECTS OF THERMAL CONDUCTION IN SONOLUMINESCENCE

1. Introduction

Sonoluminescence is a weak emission of light which occurs when a liquid with dissolved gas is cavitated by a sound field. It is readily observed that the luminescence comes from the cavitation bubbles and also that it occurs in flashes with the same frequency as that of the sound. Although this effect has been known since the early 1930's, it is only recently that quantitative results could be obtained using modern photomultiplier tubes. These results have been summarized and discussed by Jarman[1] who concludes that they can best be explained on the assumption that sonoluminescence is largely thermal in origin. The cavitation bubbles collapse due to a return of positive pressure and compress the gas inside so that it becomes momentarily incandescent. Such high pressures were predicted by Rayleigh[2] a long time ago and arise because of the large inertial forces which are exerted when the liquid advances into the rarefied gaseous phase.

The spectra of sonoluminescence support this hypothesis. All distinctive band and line spectra appear to have been smeared out as though by very high pressures[3] to form a continuous distribution which usually stretches from the infra-red well into the ultra-violet. For example the spectra of sonluminescence for different gases dissolved in water appear to resemble that of a black body radiating between 6,000 K, and 11,000^{o}K[4],[5]. Although there seems to be no distinctive radiation lines or bands, the intensity of the luminescence

TABLE I

Gas	Relative Intensity of Sonoluminescence	Thermal Conductivity (Cal/cm/sec/^{o}C)X 10^{3}	Solubility in Water Henry's Law Const.X 10^{-7}	Molecular Weight
Helium	1	0.3365	10.90	4
Neon	18	0.1092	9.14	20.2
Argon	54	0.0385	2.58	39.9
Krypton	180	0.0212	1.52	83.8
Xenon	540	0.0124	0.742	131.3
Hydrogen	- -	0.414	5.20	2
Oxygen	35	0.0583	2.95	32
Nitrogen	45	0.055	5.75	28

has been found to depend in a striking way on the nature of the dissolved gas[6],[7]. This is shown in Table 1 which lists the relative luminous intensities obtained by Prudhomme and Guilmart[6] for water with different dissolved gases. The luminosity with helium was barely preceptible and with hydrogen could not be observed at all. The cause of this wide variation in intensity has not been very clearly understood, and the theory of the thermal origin of sonoluminescence has been thought to be inadequate because it did not appear to account for it in a straightforward manner. However, such criticism is founded on the assumption that the cavitation bubbles collapse so rapidly that the gas is compressed adiabatically, and in the following analysis of the experiments of Prudhomme and Guilmart it will be shown that this is not the case.

Cavitation bubbles are of two main types, namely the vaporous and the gaseous[8],[9]. The former contain the liquid vapor principally and have a comparatively short lifetime, while the latter contain a significant proportion of permanent gas in addition to the vapor and occur only when there is a sufficient gas content in the liquid. Since attempts to observe sonoluminescence with vaporous cavities have been unsuccessful[1], it is evident that it occurs preferentially with the gaseous type of bubble. Gaseous cavitation bubbles originate as small nuclei full of gas having radii of the order of 10^{-5} cm[8],[9]. For pressure amplitudes larger than a certain threshold, such nuclei will accumulate dissolved gas from the liquid by means of a process described as rectified diffusion[10], in which there is a net inflow into the bubble during a complete cycle of oscillation of the bubble surface reacting under the applied sound field. The theory of this process[10] shows that the rate of growth of such small nuclei will be relatively rapid, so

that the bubbles quickly become large enough to allow the expansion and collapse typical of cavitation. Whether they grow much beyond this stage is uncertain. It is obvious from observation that they do not continue to grow indefinitely and must eventually break up into smaller bubbles which then continue the process.

The size of the cavitation bubbles is actually of critical importance. In their experiments Prudhomme and Guilmart made no direct observation of bubble size. However they did state that the excitation frequency was 960 kc/sec and the power of the transducer was 90 watts, and this information can be used as follows to estimate the maximum size of the bubbles prior to collapse. The experiments were conducted under 1 atmosphere pressure and at room temperature, and Rosenberg[9] has shown that, for these conditions, the cavitation threshold for water saturated with gas occurs at a pressure amplitude of about 1.5 atmospheres. Once cavitation has started it can easily be maintained by amplitudes below this threshold. In the experiments of Prudhomme and Guilmart the acoustic waves were attenuated by being passed through a quartz window and it is apparent that, for a power of 90 watts, the pressure amplitude in the test vessel could not have been much more than a few atmospheres. Rayleigh's[2] formula for the collapse time of a spherical cavity is

$$\tau \sim 0.9\, R_o (\rho/p)^{\frac{1}{2}}$$

where R_o is the radius of the cavity prior to collapse and p and ρ are the ambient pressure and density in the surrounding liquid. For a pressure of only a few atmospheres in water, this relation becomes

$$\tau \sim \tfrac{1}{2}\, 10^{-3}\, R_o \text{ secs}$$

where R_o is in centimeters. Since the acoustic wavelength is obviously much longer than bubble dimensions, this relation can be applied to the cavitation bubbles in the experiments. Now it is evident that these bubbles will only collapse effectively if the collapse time is less than a half cycle of the excitation, and for this to occur the initial radius R_o would have to be less than 10^{-3} cm. Other criteria, from the theory of oscillating bubbles, can be applied to support this estimate. According to the theory[10], the surface of a bubble is an oscillating pressure field becomes unstable when it exceeds a certain critical radius, which in the present case can be estimated to be about 10^{-3}cm. Also the radius at which a bubble resonates under a 960 kc/sec excitation can be shown to be between 10^{-4} and 10^{-3}cm. Finally, Rosenberg[9] has observed that under a 60 kc/sec excitation the maximum size of cavitation bubbles is about 10^{-2}cm. It seems reasonable to expect therefore that, for a 960 kc/sec excitation, the maximum bubble radii should be of the order of 10^{-3}cm.

It is to be expected then that the cavitation bubbles occurring in the experiments of Prudhomme and Guilmart range in size from about 10^{-5}cm to 10^{-3}cm where the bubbles are evolving from nuclei through the acquisition of dissolved gas from the water. No very precise description can be given of this evolution, however. In particular it is difficult to determine just how much gas and vapor will be present in the bubble when its surface goes into large scale oscillation. It obviously starts with exceedingly small amounts which increase by means of rectified diffusion from the dissolved gas in the liquid. In addition the gas content can be increased by the coalescence of several bubbles, since there are a very large number situated close together in a typical

cavitation cloud. Thus it would appear that the gas content of a bubble could vary over quite a wide range. However it will be shown that the amount of gas necessary for effective luminescence is moderately small and restricted between fairly definite limits, so that only a certain proportion of the bubbles will be in the right condition. This agrees with observation since sonoluminescence would presumably be much brighter if all the bubbles in a cavitation cloud could radiate.

Radiation in the visible region of the spectrum occurs when a gas reaches temperatures in excess of about $1,000^{\circ}K$. Prudhomme and Guilmart in fact measured their intensities in the ultra violet, with a photocell operating in the range 190 $m\mu$ to 280 $m\mu$ and having a sharp maximum sensitivity at 230 $m\mu$. Hence the temperature attained by the gas would have to be of the order of $10,000^{\circ}K$[3]. This estimate is in agreement with the spectral distributions mentioned earlier[4],[5]. To reach such temperatures would require an adiabatic compression caused by a spherical bubble collapse of the order of 9/10 of the initial radius, assuming ordinary temperatures initially. If the process is not adiabatic but involves some loss of heat from the bubble, then the collapse will have to proceed further before the right temperatures are reached. In order to obtain such reductions in volume under a constant external pressure of a few atmospheres, it is necessary to limit the initial pressure of the gas to less than 0.1 atmospheres at ordinary temperatures. This estimate is obtained by using Gilmore's theory[11] of a collapsing spherical cavity, in which fairly accurate allowance is made for the compressibility of the liquid. This sets an upper limit on the amount of gas necessary for effective luminescence. A lower limit becomes apparent after the collapse process is considered in more detail.

The collapse of a bubble is generally considered to be quite rapid. However, the inertial forces in the liquid require time to build up and generate high velocities at the cavity wall. The presence of the gas inside does not affect the motion of the interface significantly until the very final stages when it eventually brings it to rest. It is possible to describe this behavior approximately, using Gilmore's theory[11]. For illustration a bubble having an initial radius $R_o = 10^{-3}$ cm under a constant external pressure of 3 atmospheres is used. The collapse time τ is then about $\frac{1}{2}\mu$sec. Inside the bubble there is assumed to be a uniform adiabatic gas of initial pressure 5×10^{-2} atmospheres at ordinary temperatures. Figure 1 shows how the radius R of the bubble will vary with time t for different γ, the ratio of the specific heats of the gas. The temperature of the gas goes as $(R_o/R)^{3(\gamma-1)}$ and the pressure as $(R_o/R)^{3\gamma}$. The motion is seen to be relatively independent of the presence of the gas up to $R/R_o \sim 0.3$. At this stage the elapsed time t is about 0.97τ and the velocity has reached a value of about 7×10^3 cm/sec. i.e. it is still distinctly subsonic with respect to a gas at ordinary temperatures. The most significant point to notice from Fig. 1 however, is that, if some of the energy of the gas molecules is lost, or is absorbed within the molecule because of additional degrees of freedom, then the bubble attains lower final temperatures and collapses to smaller radii. This will profoundly affect the intensity of any resulting luminescence. Now air at ordinary temperatures and at 0.1 atmosphere pressure has a thermal diffusivity of about 3 cm^2/sec. Corresponding to a time of $\frac{1}{2}\mu$sec, the thermal diffusion length is then about 10^{-3} cm i.e. equivalent to the dimensions of the bubble. Thus, since the surrounding water acts as an effective heat sink, it is obvious that significant heat losses from the gas inside the bubble can be expected during

collapse, and that the luminous intensity will be affected correspondingly. If the initial pressure in the gas is much lower than 0.1 atmospheres say about 10^{-3} atmospheres or less, then the thermal diffusivity will be larger and the gas can be expected to remain in thermal equilibrium with the liquid at the bubble wall over most of the motion. This means that it will remain almost isothermal, and that only during the final stages will it approach adiabatic conditions. Hence the final temperatures will not be so high and the final radius will be smaller, so that not much luminescence can be expected as a consequence. This establishes a lower limit on the amount of gas necessary for effective luminescence. Actually for initial pressures of the order of 10^{-3} atmospheres it is inappropriate to consider thermal diffusion in the gas from a continuum standpoint, since the mean free paths are somewhat larger than the dimensions of the bubble. However it can be shown that there is sufficient time for the gas molecules to experience a large number of collisions with the bubble wall during most of the collapse, so that the conclusion is essentially the same.

Since condensation and evaporation rates are comparatively slow, water vapor will behave rather like a permanent gas and, since it is triatomic, it will effectively quench[3] the luminescence of other gases if it is present in any quantity. As has been pointed out earlier, no luminescence could be observed from vaporous cavitation in water[1], and it seems apparent from the experiments of Jarman[12] that the presence of the liquid vapor does indeed diminish sonoluminescence. Also sonoluminescence appears quite distinctive for each dissolved gas and does not appear to arise from a mixture in which one constituent is always the same. For these reasons it is doubtful whether there can be

a high proportion of vapor in the luminescing bubbles. As has already been pointed out, a typical cavitation cloud will contain bubbles whose gas and vapor content can be expected to vary over quite a wide range, and the luminescing bubbles will be those with the right amount of gas combined with only a small amount of vapor.

The fact that loss of heat from the gas inside the bubbles significantly affects the intensity of sonoluminescence, can be used to explain the wide variation in intensity which has been observed for different dissolved gases. This conclusion is supported by Table 1 where there is shown to be a clear inverse relation between the thermal conductivities under ordinary conditions[13] and the observed luminous intensities. It has also been suggested[5] that the solubility of the gas is a contributory factor and that if there is more dissolved gas, then there will be more luminescence. This contention is only partially supported by Table 1 which lists the Henry's Law constant[14] at ordinary temperatures. Also it is not in accord with the relative luminescences observed with different liquids[12]. The amount of dissolved gas can affect the number of the bubbles and, more significantly, their gas content. However these will also depend on the diffusivity of the gas in the liquid which appears[9] to exhibit an opposite trend to that of the solubility, i.e., the smaller molecules are more mobile and accumulate in the bubbles more readily. Hence, provided there is sufficient gas present it is not certain that the luminous intensity should be related to the solubility. In comparison the modifying effect of heat loss from the bubbles is much more definite. According to Table 1, it is possible to obtain a relation between the observed luminous intensities and any parameter which is dependent on the molecular weight. However the

thermal conductivity is itself dependent on the molecular weight, so that it would first be necessary to demonstrate that a parameter relates to a process which can clearly affect the luminescence, before attaching any particular significance to it.

It is evident that the luminous intensity will be dependent on the behavior of the gas during the final stages of collapse, and on the kinds of emission which can occur under such conditions. It has been suggested for instance by Jarman[1] that microshocks may be responsible for part of the luminescence, and since the motion of the bubble wall can be supersonic at this point, this idea would seem to be quite plausible. However the final stages of the collapse and the resulting emission are outside the scope of this paper. It is sufficient for present purposes to point out that whatever takes place in the gas during these stages, will be strongly affected by the heat losses which can occur in the earlier motion.

Although it has been estimated that heat conduction does affect the behavior of the gas inside the bubble, it would be of some interest to examine the process in more detail. In particular it would be interesting to determine how the effect of thermal conduction varies with bubble size, and under what conditions the temperature of neon will become lower than that of nitrogen so as to accord with the relative luminescences given in Table 1. An analysis is therefore presented based on a simplified model of a collapsing spherical cavity in which the equations of motion of a thermally conducting ideal gas are solved numerically up to the stage $R/R_o = 0.3$. During this part of the motion, the bubble wall has a velocity which is much lower than the velocity of sound in the gas. Hence the acoustic waves generated by the motion of

the wall have enough time to be reflected at the center of the cavity, thus avoiding the development of a pressure front. This makes the numerical solution relatively straightforward.

2. Description of the Analytical Model

A spherical cavity in an incompressible liquid contains a thermally conducting ideal gas with negligible quantities of the liquid vapor. It is assumed that both the gas and the liquid are non-viscous, and that prior to collapse they have the same uniform temperature T_o. It is also assumed that during the collapse process, the temperature rise in the liquid at the cavity wall is negligible in comparison to the rise in temperature of the gas. This can be justified on the basis that the heat capacity of the liquid is much greater than that of the gas. Although the thermal conductivity of the liquid is generally about ten times greater than that of the gas, the thermal diffusivity of the gas will still be much greater than that of the liquid. Hence the thermal effects due to a transfer of heat out of the cavity will be confined to a comparatively narrow region of liquid next to the interface[15]. Since the temperature gradient in the liquid has its greatest value at the interface and since it will be about ten times smaller than the gradient in the gas, it follows that the temperature rise at the interface is small in comparison to the temperature rise in the interior of the gas. Hence the condition for the temperature on the boundary T_B can be expressed

$$T_B = T_o \tag{1}$$

In order to generate the collapse, the ambient pressure in the liquid is raised to a uniform value p_∞ while the gas in the interior has

the uniform value $p_o < p_\infty$. Initially the liquid and the gas are at rest. Allowing the pressure difference to take effect, the subsequent motion of the cavity wall is governed by the well-known relation for a collapsing spherical cavity[16]

$$\frac{dU}{dt} = -\frac{1}{R}\left[\frac{p_\infty - p_B}{\rho_L} + \frac{3}{2}U^2\right] \tag{2}$$

where p_B is the pressure exerted by the gas on the cavity wall, U and R are the velocity and radius of the wall and ρ_L is the density of the liquid. At the center of the cavity the boundary conditions are

$$u = 0 \; ; \quad \frac{\partial T}{\partial r} = 0 \tag{3}$$

where u is the velocity, T the temperature and r the radial coordinate.

Since there is a moving boundary, it is necessary to express the equations of motion of the gas in Lagrangian form which for spherically symmetric motion are,

$$\rho r^2 \frac{\partial r}{\partial y} = 1 \; , \tag{4}$$

$$\frac{\partial u}{\partial t} = -r^2 \frac{\partial p}{\partial y} \; , \tag{5}$$

$$C_v \frac{\partial T}{\partial t} = \frac{p}{\rho^2}\frac{\partial \rho}{\partial t} + k \frac{\partial}{\partial y}\left(\rho r^4 \frac{\partial T}{\partial y}\right) \; , \tag{6}$$

$$u = \frac{\partial r}{\partial t} \; , \tag{7}$$

and the equation of state

$$\frac{p}{\rho} = R_g T/M \; , \tag{8}$$

where p and ρ are the density and pressure in the gas and C_v and k are the specific heat at constant volume and thermal conductivity. These last two quantities are assumed to be constant throughout the motion -- an assumption which is not valid when the gas reaches higher temperatures. M is the molecular weight of the gas and y is the Lagrangian independent variable referring to a particle of the gas. R_g is the universal gas constant.

The above set of equations and boundary conditions were expressed in the form of finite difference relations as outlined in the Appendix, and solutions obtained by means of a high-speed digital computer. The initial conditions were chosen in accordance with those discussed in the previous section. The pressure p_∞ was made equal to 3 atmospheres and the initial temperature T_o was 20^oC. The initial pressure p_o inside the cavity was put equal to 0.075 atmospheres. This was chosen only slightly less than the upper limit mentioned in the introduction in order to keep the time of computation to a minimum. Moreover continuum theory is more certain to be applicable when the initial pressure has this value. The calculations were carried out for bubbles containing neon and nitrogen of initial radii 10^{-1}, 10^{-2}, 10^{-3} cm.

3. Discussion of the Results

It is of interest to non-dimensionalize all the variables in the equations given in the previous section. Using the velocity of sound in the gas c_o under the initial conditions, the initial radius R_o, the initial density and temperature of the gas ρ_o and T_o, the dimensionless variable become

$$u' = u/c_o \quad ; \quad r' = r/R_o \quad ; \quad \rho' = \rho/\rho_o \quad ; \quad t' = tc_o/R_o \quad ; \quad T' = T/T_o \quad . \quad (9)$$

Then since $c_o^2 = \gamma p_o/\rho_o = \gamma R_g T_o/M$ where γ is the ratio of the specific heats, it follows from the equations that

$$p' = p/\rho_o c_o^2 = p/\gamma p_o \quad ,$$

$$C_v' = C_v T_o/c_o^2 = MC_v/\gamma R_g \quad , \tag{10}$$

and

$$k' = kT_o/R_o\rho_o c_o^3 = k(MT_o)^{\frac{1}{2}}/R_o p_o \gamma (R_g)^{\frac{1}{2}} \quad . \tag{11}$$

When the variables appear in this form several features become apparent. If the thermal conductivity is negligible, Eq. 6 shows that the gas will behave in the usual adiabatic manner dependent principally upon whether the molecules are monatomic or diatomic. In this case the time will scale with the initial radius R_o, while the relative temperature pressure and velocity distributions will always be of the same magnitude regardless of the initial size of the cavity. On the other hand the effects of thermal conduction are inversely related to scale, When R_o is large the behavior of the gas will be almost adiabatic, and when R_o is small heat conduction will have a strong effect. The influence of heat conduction also depends on the initial pressure and to a lesser degree on the initial temperature.

If $p_o << p_\infty$, it is to be expected that the behavior of the gas will have a negligible effect on the inertial force of the liquid throughout the major part of the collapse. Hence the total collapse time τ is practically independent of the contents of the cavity, and will therefore be proportional to the initial radius R_o. The thermal diffusion length ℓ_D will then be proportional to $R_o^{\frac{1}{2}}$ and the ratio ℓ_D/R_o will vary as $R_o^{-\frac{1}{2}}$. Thus the smaller bubbles will show increased effects of heat con-

duction even though their collapse times are smaller.

Another important feature is that the velocity of sound in the gas remains much higher than the velocity of the bubble wall throughout most of the motion. Under such conditions the pressure in the gas will remain comparatively uniform, because the effects of the disturbance created by the cavity wall have time to be distributed evenly throughout the gas.

These features are all clearly shown in the numerical solutions. When R_o is large the solution is the same as for a uniform adiabatic gas, the differences being found to be within less than 1% at $R/R_o = 0.3$. Figures 2 - 4 give the solutions for $R_o = 10^{-1}$, 10^{-2}, 10^{-3} cm. For $R_o = 10^{-1}$ the thermal conductivity shows a perceptible effect, particularly when the temperature gradients become large. This increases when $R_o = 10^{-2}$. When $R_o = 10^{-3}$, heat conduction modifies the condition of the gas quite significantly, and it is seen that the temperature of neon falls slightly below that of nitrogen. As expected the pressure in the gas remains relatively uniform throughout the motion for all the cases considered. Figure 4 shows how this uniform pressure varies as a function of the bubble radius R, as compared to an adiabatic or an isothermal gas. For the 10^{-3} cm bubble the slope is seen to be almost along the isothermal initially but as the collapse accelerates it alters so that it parallels the adiabatic.

The solution for the 10^{-3} bubble represents the case closest to the conditions of the experiments of Prudhomme and Guilmart. However the average size of the cavitation bubble in these experiments is estimated to be somewhat smaller than 10^{-3} cm, so that the effects of thermal conduction will be even more pronounced. Hence the temperature in the

neon bubbles will fall more distinctly below that in the nitrogen bubbles, thus accounting for the difference in luminous intensity shown in Table I.

APPENDIX

Initially the thermodynamic variables are uniform and have the values ρ_o, T_o, p_o while the initial velocity in the gas is zero. The variable y defined in Eq. 4 is taken to extend from 0 at the center to $\rho_o R_o^3$ at the bubble wall and is divided into n equal intervals Δy. The value of the radial coordinate r at these intervals is then given by

$$r_j^o = (3j\Delta y/\rho_o)^{\frac{1}{3}} \quad : \quad 0 \leqslant j \leqslant n \tag{I. 1}$$

where in the usual notation of a finite difference mesh the superscript i refers to the number of intervals of time Δt from the initial time $t = 0$ and the subscript j to the number of intervals of Δy from the origin $y = 0$. The thermodynamic variables were evaluated at the half intervals $\rho^i_{j+\frac{1}{2}}$, $T^i_{j+\frac{1}{2}}$, $p^i_{j+\frac{1}{2}}$ whereas the velocity u^i_j and the radial coordinate r^i_j were evaluated at the full intervals. In order to preserve accuracy at least in the initial stages, the temperature was divided into two parts so that

$$T^i_{j+\frac{1}{2}} = T_o + \tau^i_{j+\frac{1}{2}} \tag{I. 2}$$

and the $\tau^i_{j+\frac{1}{2}}$ kept as the running variable. For the same reason Eq. 6 was modified so that the term $\frac{\partial \rho}{\partial t}$ was replaced by its equivalent $-\rho\left(\frac{2u}{r} + pr^2 \frac{\partial u}{\partial y}\right)$ derived from Eq. 4. Equations (4) - (8) were then expressed in finite difference form as follows

$$\rho^{i+1}_{j+\frac{1}{2}} = 3\Delta y \Big/ \left(r^{i+1}_{j+1} - r^{i+1}_j\right)\left[\left(r^{i+1}_{j+1}\right)^2 + r^{i+1}_{j+1} r^{i+1}_j + \left(r^{i+1}_j\right)^2\right] \tag{I. 3}$$

$$u_j^{i+1} = u_j^i + \left(r_j^i\right)^2 \Delta t \left(p_{j+\frac{1}{2}}^i - p_{j-\frac{1}{2}}^i\right) \Big/ \Delta y \quad , \tag{I.4}$$

$$\begin{aligned} \tau_{j+\frac{1}{2}}^{i+1} = \tau_{j+\frac{1}{2}}^i - p_{j+\frac{1}{2}}^i \Big[2\left(u_j^i + u_{j+1}^i\right) \Big/ \left(r_j^i + r_{j+1}^i\right) \\ + \rho_{j+\frac{1}{2}}^i \left(r_j^i + r_{j+1}^i\right)^2 \left(u_{j+1}^i - u_j^i\right) \Big/ (4\Delta y) \Big] \Big/ \left[C_v \rho_{j+\frac{1}{2}}^i\right] \\ + k\Delta t \Big[\left(\rho_{j+\frac{3}{2}}^i + \rho_{j+\frac{1}{2}}^i\right) \left(r_{j+1}^i\right)^4 \left(\tau_{j+\frac{1}{2}}^i - \tau_{j-\frac{1}{2}}^i\right) \\ - \left(\rho_{j+\frac{1}{2}}^i + \rho_{j-\frac{1}{2}}^i\right) \left(r_j^i\right)^4 \left(\tau_{j+\frac{1}{2}}^i - \tau_{j-\frac{1}{2}}^i\right) \Big] \Big/ \left[2C_v (\Delta y)^2\right] \end{aligned} \tag{I.5}$$

$$r_j^{i+1} = r_j^i + u_j^i \Delta t \quad , \tag{I.6}$$

$$p_{j+\frac{1}{2}}^{i+1} = \rho_{j+\frac{1}{2}}^{i+1} \frac{R_g}{M} \left(T_o + \tau_{j+\frac{1}{2}}^{i+1}\right) \quad . \tag{I.7}$$

Using these equations and the variables on the ith row, a first estimate was obtained for the variables on the (i + 1)th row. In order to improve the accuracy of the derivatives with respect to the time t, one iteration was performed using this first estimate averaged with values on the ith row. These averages were substituted in the appropriate locations within the above finite difference format and the new values which resulted were then carried on to the next stage. It was found necessary to make one exception in this process however. During the last stages of the calculation towards the end of the collapse, the procedure was found to be unstable unless the expressions in u in Eq. I.5 were replaced by $\left(u_j^{i+1} + u_{j+1}^{i+1}\right)$ and $\left(u_{j+1}^{i+1} - u_j^i\right)$ in the iteration. This change made no apparent difference in the accuracy of the results.

On the cavity wall, the velocity was found from Eq. 2 using the form

$$u_n^{i+1} = u_n^i - \Delta t \left[\frac{(p_\infty - p_R^i)}{\rho_L} + \frac{3}{2} u_n^{i2} \right] \Big/ r_n^i \quad . \tag{I.8}$$

The pressure on the wall p_R^{i+1} was obtained by combining Eq. 2 and Eq. 5 to give

$$p_R^{i+1} = \left[3p_{n-\frac{1}{2}}^{i+1} - \frac{1}{3} p_{n-\frac{3}{2}}^{i+1} + \left\{ \Delta y \left[p_\infty + \frac{3}{2} \left(u_n^{i+1} \right)^2 \right] \right\} \Big/ \left(r_n^{i+1} \right)^3 \right] \Big/ \left\{ \frac{8}{3} + \left[\Delta y / \left(r_n^{i+1} \right)^3 \right] \right\} \tag{I.9}$$

and the derivative $\partial T / \partial y$ on the cavity wall was found using the form

$$\frac{\partial T}{\partial y} \sim \left(3\tau_{n-\frac{1}{2}}^i - \frac{1}{3} \tau_{n-\frac{3}{2}}^i \right) \Big/ \Delta y \tag{I.10}$$

where the temperature on the cavity wall always has the same constant value T_o. An iteration was also performed on these equations in the manner already described.

The above procedure was found to be quite stable provided[17]

$$\Delta t < \alpha_1 C_v (\Delta y)^2 / [2k \rho_r (r_n^i)^4] \tag{I.11}$$

and

$$\Delta t < \alpha_2 \min_j \left(r_{j+1}^i - r_j^i \right) \Big/ c_{j+\frac{1}{2}}^i \tag{I.12}$$

where

$$c_{j+\frac{1}{2}}^i = \left(\gamma p_{j+\frac{1}{2}}^i / \rho_{j+\frac{1}{2}}^i \right)^{\frac{1}{2}} \quad .$$

The most satisfactory value for the constants α_1 and α_2 was found to be 0.6. The first criterion was generally the predominant one. The number of points n was varied from twenty to fifty. The twenty point

solution showed a reasonable agreement with the fifty point solution, and the examples were calculated therefore for thirty points. The work was performed on an IBM 7090 and the longest example took about three hours.

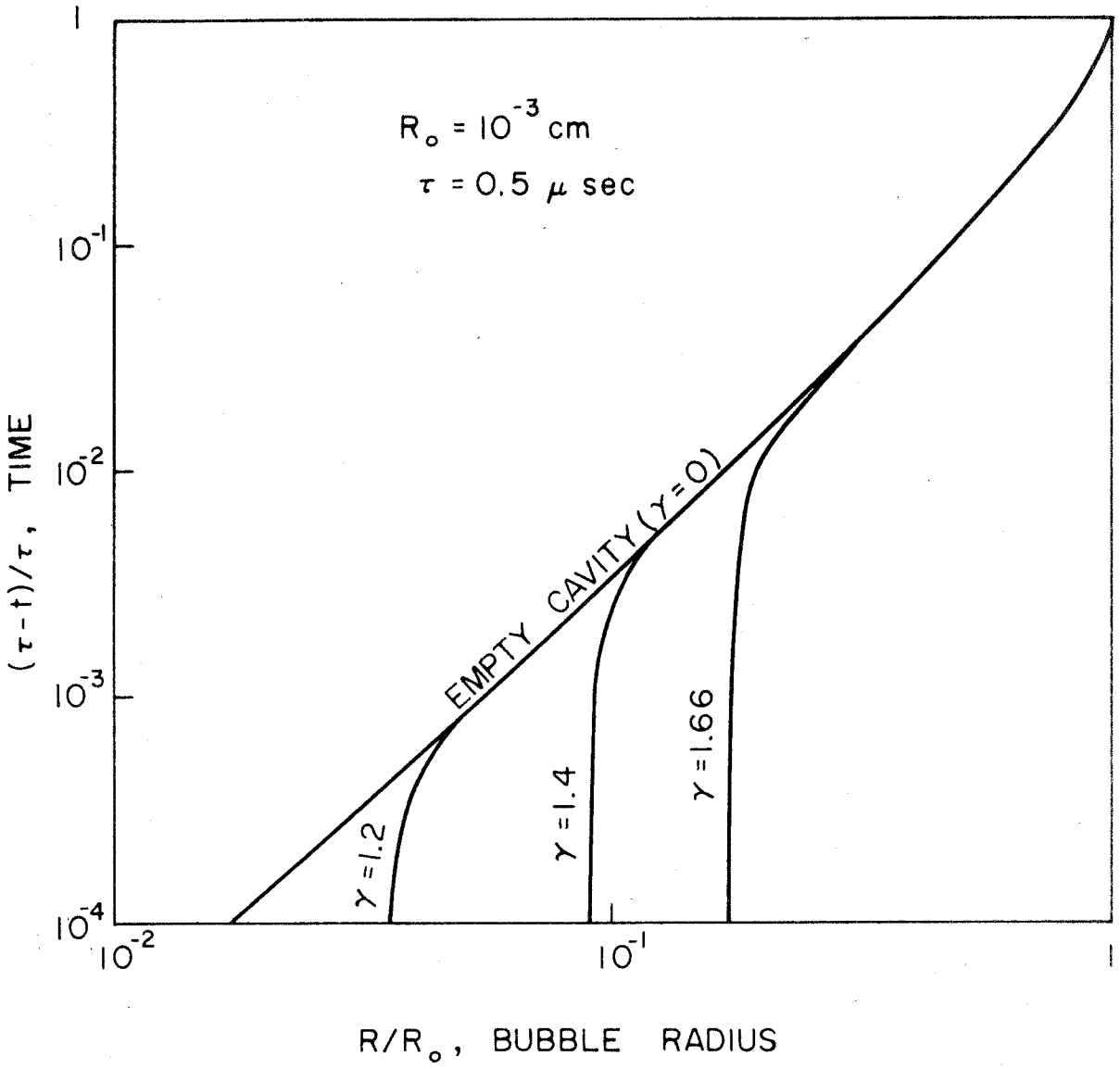

Figure 1. The variation with time of the radius of a spherical bubble containing a uniform adiabatic gas. The bubble is collapsing under a constant external pressure of 3 atmospheres and has an initial internal pressure of 0.05 atmospheres.

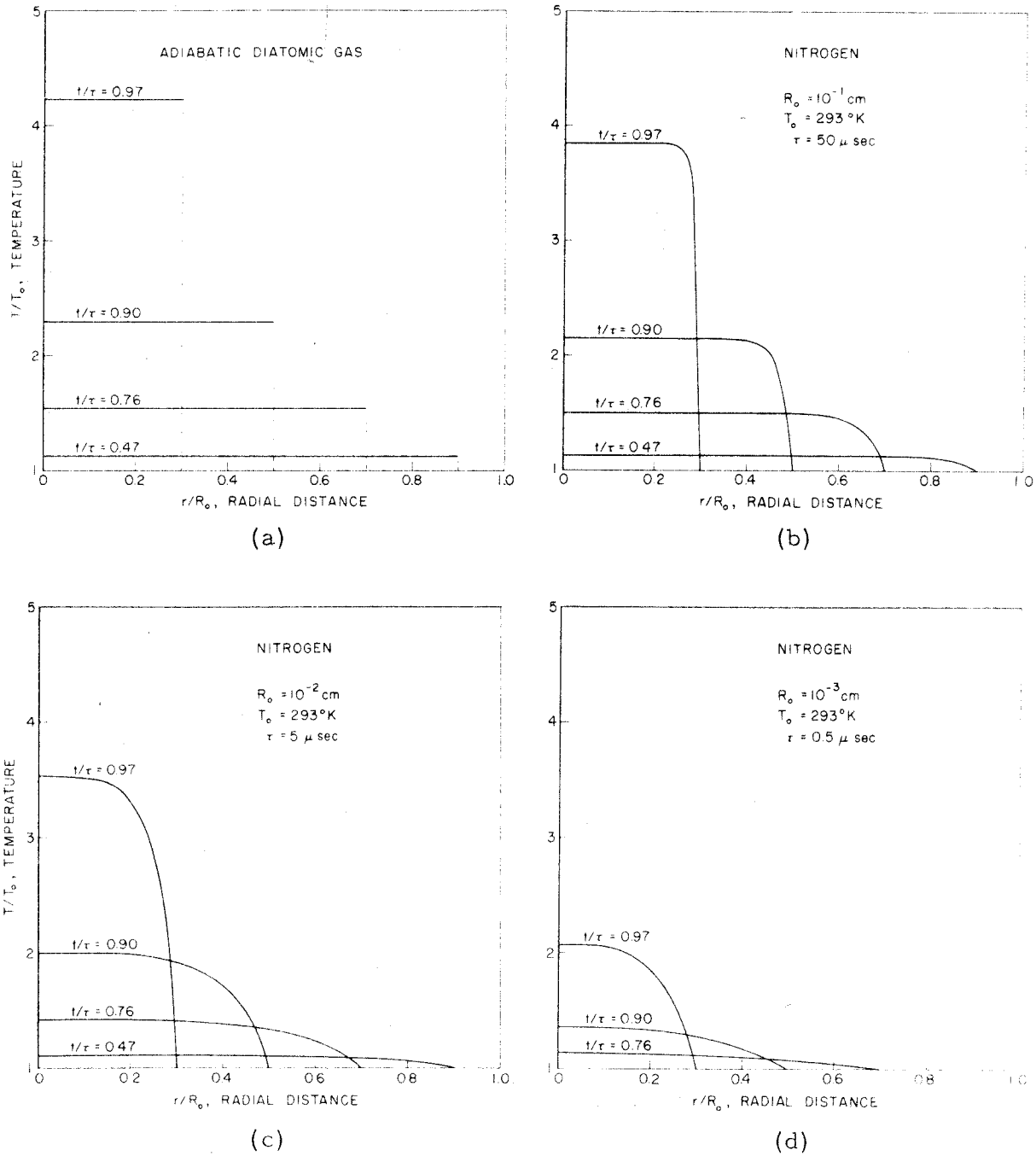

Figure 2. Temperature distributions inside a spherical bubble containing nitrogen at different stages of collapse, for different initial radii. The bubble is subjected to a constant external pressure of 3 atmospheres and has an initial internal pressure of 0.075 atmospheres.

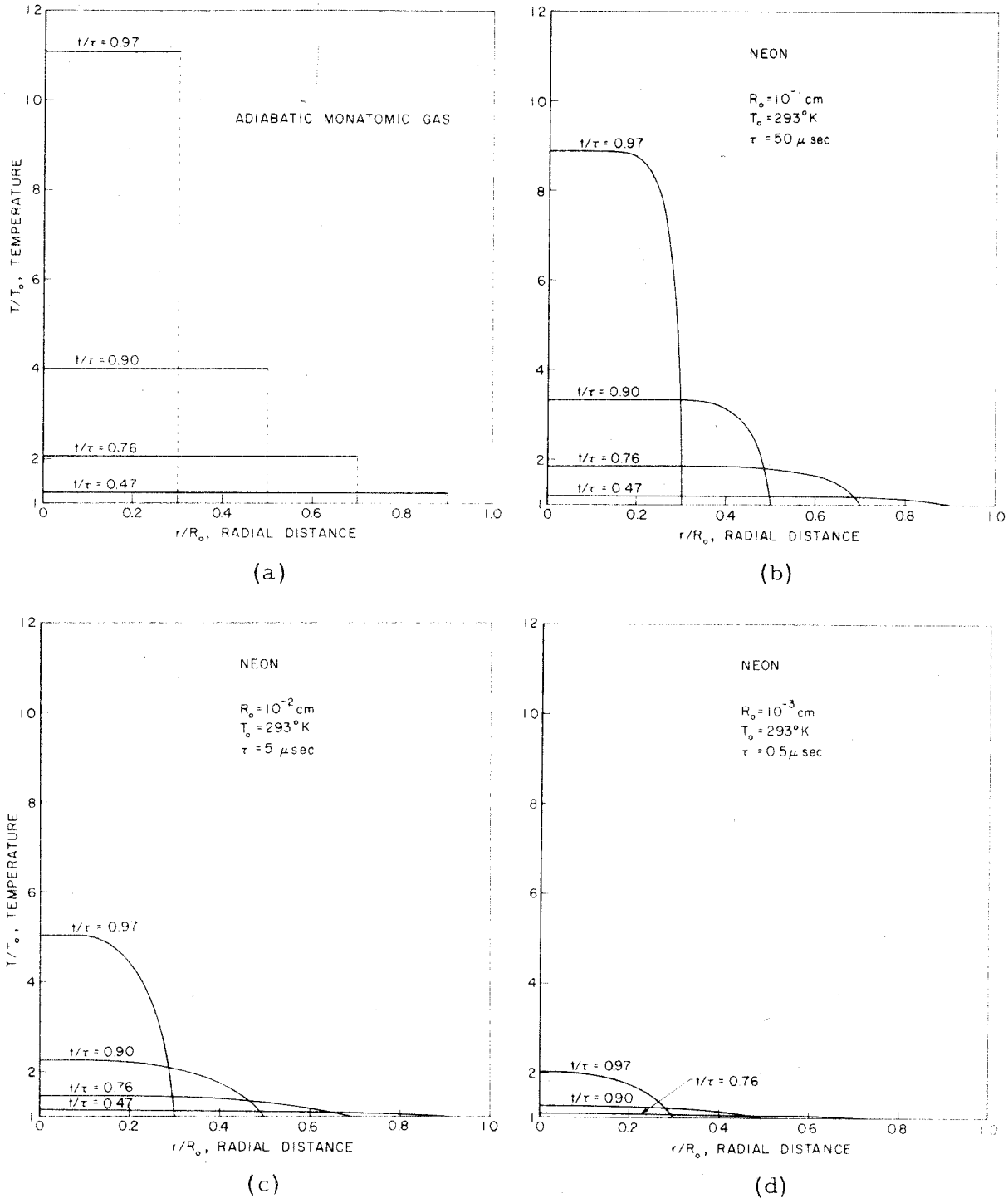

Figure 3. Temperature distributions inside a spherical bubble containing neon at different stages of collapse, for different initial radii. The bubble is subjected to a constant external pressure of 3 atmospheres and has an initial internal pressure of 0.075 atmospheres.

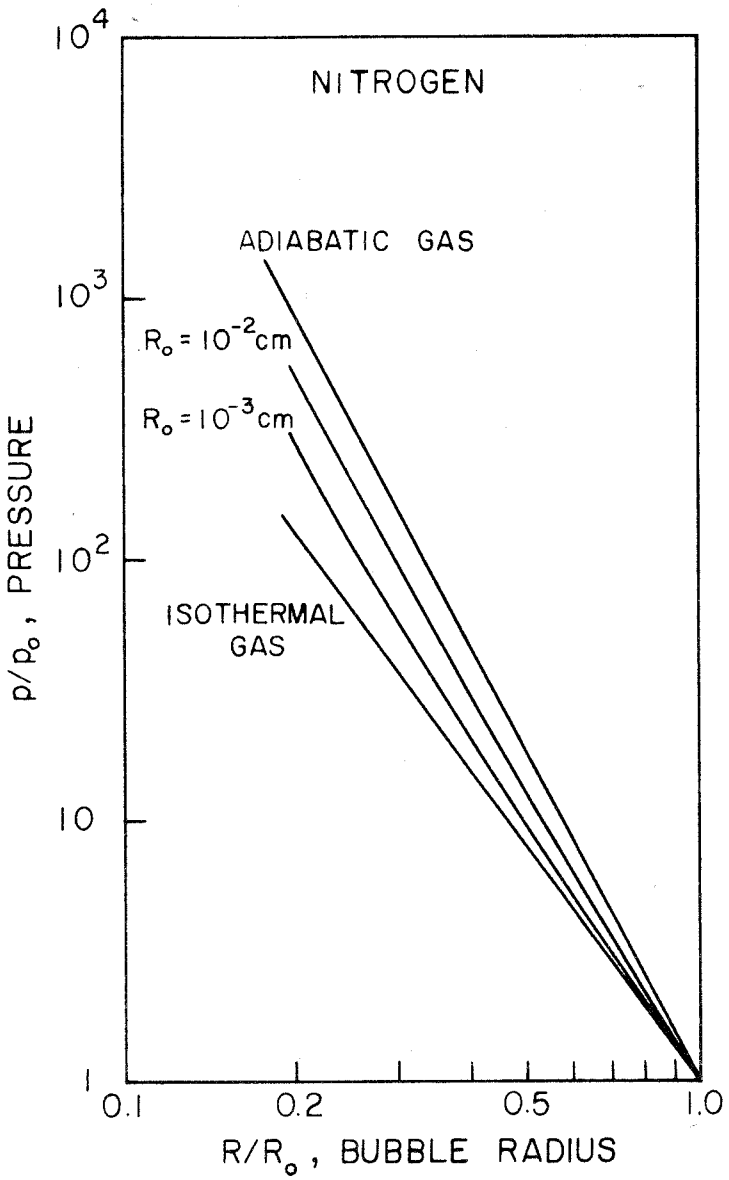

Figure 4. The variation of the uniform pressure inside a spherical bubble containing nitrogen, as a function of the bubble radius. The conditions are the same as those for Fig. 2.

SECTION B - THE COLLAPSE OF A SPHERICAL CAVITY IN A COMPRESSIBLE LIQUID

1. Introduction

The effect of compressibility in the collapse of a cavity in a liquid has been studied for some years. Rayleigh[2] was the first to point out that this was necessary when he showed that pressures in the liquid adjacent to the cavity wall could reach very high values. However a real interest in the problem originated some time later, out of work on underwater explosions[18]. Analytical theories were developed by Herring[19] and Trilling[20] which were first order approximations based on Rayleigh's solution[2] for an incompressible liquid. To obtain higher order approximations the so-called Kirkwood-Bethe hypothesis[18], [21] was postulated. The Kirkwood-Bethe hypothesis forms the basis of a solution by Gilmore[11] which has been used in a modified form by Mellen[22] and by Flynn[23]. This solution has been found to be surprisingly accurate when compared to exact solutions obtained numerically, as will be demonstrated in this paper.

With the advent of high-speed computers numerical solutions of the exact equations of compressible flow became possible, and several integrations of the characteristic equations have been performed. Gilmore[24] obtained some results which he used to compare with his approximate theory, while Hunter[25] performed some numerical work which acted as a basis for a similarity solution valid in the neighborhood

of the final collapse point of an empty cavity. Brand[26] did some further computations. So far however, there has been no numerical solution which describes the rebound of the cavity and the subsequent formation of a shock wave traveling outwards into the liquid. The work of this paper is concerned with such a solution.

Classically the problem to be solved is that of the empty cavity. This is usually quite a good model since the small amounts of gas or vapor, which occur in a typical cavitation bubble, have little effect on the motion of the interface until the final stage of the collapse. However, the contents of a cavity, even though they may be quite rarified initially, will have an important effect on the final pressure, since the further a collapse can proceed before being halted the higher the pressure. The final stage of the collapse will be affected by the behavior of the gas inside the cavity as well as by the quantity. Thus an isothermal gas can be expected to produce a more violent collapse than an equal amount of adiabatic gas. However, it is not the purpose of this paper to discuss the physical behavior at the final collapse point in detail. Such a task would in fact be quite difficult. The main interest here is in the effect of the liquid compressibility, so that the behavior of the contents of the cavity will merely be simulated by a simple gas-like model. The cavity will be assumed to contain a uniform gas whose pressure varies according to the law $p \alpha \rho^{\gamma}$, where ρ is the density. The index γ can be varied so as to simulate the gross behavior of the gas. Thus $\gamma = 1$ implies that the gas is isothermal while $\gamma > 1$ implies that some of the

heat of compression is being retained in the gas. This model has the advantage of avoiding the singularities which would occur at the final collapse point if the cavity were empty. The sudden compression of a gas or vapor inside a cavity can be expected to raise its temperature, and due to conduction and condensation, there will be a consequent rise in temperature in the liquid at the interface. However, such effects will be confined to a very narrow region[27], and they will therefore be neglected. A sudden compression of a liquid does not cause a significant increase in temperature[28], so that it will be assumed to behave according to the well-known law $\rho^n \propto (p+B)$ where B and n are constants. The results presented here are for water with B equal to 3,000 atmospheres and the index n equal to 7. The validity of these values has been discussed elsewhere[18], [25]. It is also assumed that the liquid is inviscid and that the motion remains spherically symmetric at all times. The above description of a collapsing cavity is of course not completely accurate in detail, but it is considered to be sufficiently satisfactory for a study of the effects of liquid compression.

Numerical solutions of the equations of compressible flow for a collapsing cavity in water were obtained for both the characteristic and the Lagrangian forms of the equations. A comparison between the two provided a check on the numerical accuracy. The Lagrangian solution was carried beyond the final collapse point into the region where the liquid rebounds and generates a compression wave which

travels outwards from the collapse center. The solution was terminated when the compression wave had steepened into a shock front. It could probably have been continued beyond this stage by using techniques such as those proposed by von Neumann and Richtmeyer[29] and Lax[30], where an artificial viscosity is introduced into the equations of motion to produce a continuous variation through the shock. However, enough information had already been obtained to estimate the order of magnitude of peak intensities at a distance from the collapse center so that no attempt was made to undertake this additional calculation.

One of the principal purposes of this analysis was to determine whether shocks emanating from the collapse of a cavitation bubble could provide a mechanism for cavitation damage. The results given here indicate that such shocks are in fact strong enough to cause damage to metals and other solids in the bubble's vicinity.

2. Formulation of the Problem

A spherical cavity containing a uniform gas is assumed to expand or contract in an infinite volume of liquid. For cavitation bubbles the effect of gravity is generally quite small, so that it will be neglected along with other asymmetric effects. Since the motion is spherically symmetric, it will be irrotational i.e.

$$\text{curl } \vec{u} = 0 \tag{1}$$

where $\vec{u}$ is the velocity vector. If the center of the bubble is chosen as

the center of a system of spherical polar coordinates, then $\vec{u}$ will have only a single component u lying in the radial direction. The equations of motion expressing the conservation of mass and momentum for a spherically symmetric system are

$$\frac{D\rho}{Dt} = -\rho\left[\frac{\partial u}{\partial r} + \frac{2u}{r}\right] , \tag{2}$$

$$\rho \frac{Du}{Dt} = -\frac{\partial p}{\partial r} , \tag{3}$$

where p and ρ are the pressure and density in the liquid, and the operator

$$\frac{D}{Dt} = \frac{\partial}{\partial t} + u \frac{\partial}{\partial r} \tag{4}$$

is the derivative with respect to time following the motion of the liquid. It is assumed that the liquid is isentropic[18] and that the density and pressure are related by an equation of state of the form

$$\frac{p+B}{p_\infty+B} = \left(\frac{\rho}{\rho_\infty}\right)^n \tag{5}$$

where p_∞ and ρ_∞ are the pressure and density in the liquid at infinity. For water the constant B is given a value of 3,000 atmospheres while the index n has the value 7. The use of this equation has been justified by several authors[18], [25] and is based on the fact that entropy changes are small even when very large pressure jumps are present. The upper limit on the accuracy of the formula appears to be for pressures of about 10^5 atmospheres. The velocity of sound c in the liquid is defined by

$$c^2 = \frac{dp}{d\rho} = \frac{n(p+B)}{\rho} . \tag{6}$$

The velocity of sound at infinity is therefore given by

$$c_\infty = [n(p_\infty + B)/\rho_\infty]^{\frac{1}{2}} \quad .$$

The equations of motion given above are in the Eulerian form which describes what is happening at a particular point in space and how it varies with time. However, it is preferable here to use the Lagrangian form where the properties of the fluid are obtained by following the motion. To do this, it is necessary to ascribe to each particle of fluid a value of a certain parameter, y, which is defined by the expression

$$y = \int_{r(o,t)}^{r(y,t)} \rho r^2 dr \quad .$$

Hence

$$\rho r^2 \frac{\partial r}{\partial y} = 1 \quad . \tag{7}$$

With this relation, Eq. 4 becomes

$$\left(\rho r^2 \frac{\partial r}{\partial y}\right)_t = 0 \tag{8}$$

but, since Eq. 7 is a solution of this equation, the two conditions are equivalent.

On the walls of the cavity the pressure is given by the relation

$$P = p_o (R_o/R)^{3\gamma} \tag{9}$$

where p_o is the initial pressure inside the cavity prior to collapse and R_o is the initial radius of the cavity. Capital letters are used to denote the values of variables at the cavity wall. Thus R is the radius of the cavity and U its velocity. At infinity the liquid is at rest and the pressure and density have the values p_∞ and ρ_∞. All that now

remains before solving the equations is to specify the pressure and velocity in the liquid at some initial instant. For a cavity in an incompressible liquid, it is usual to suppose that the liquid is initially at rest and at a uniform pressure p_∞ and that the collapse is generated by a pressure discontinuity at the cavity wall i.e. $p_\infty > p_o$. The instant this pressure discontinuity is allowed to take effect, it is felt throughout the entire volume of the liquid because of the incompressibility. The cavity wall then starts to accelerate inwards from rest. For a compressible liquid there would be an initial jump in velocity during an infinitesimal period of time. Gilmore[11] has shown that this instantaneous increase in velocity is given by the relation

$$U_o = \frac{2}{(n-1)} (c_o - c_\infty) \tag{10}$$

where $c_o = [n(p_o+B)/\rho_o]^{\frac{1}{2}}$. The maximum value of p_∞ used here is 10 atmospheres, so that for water, such a jump in velocity will always be quite small compared to sonic velocities. In fact, during the early stages of the collapse, the solution will be indistinguishable from that for the incompressible liquid. Because of their simplicity the same initial conditions will be used in the present analysis and, even though it is not really necessary, the effect of the initial jump in velocity will be included. The possibility of the formation of an initial compression wave in the gas or vapor inside the cavity is neglected. The initial conditions are somewhat artificial and there is not much to be gained here in following up such an implication.

A method widely used in the solution of the equations of compressible flow is the method of characteristics. The characteristic equations for spherically symmetric flow are

$$\frac{\partial r}{\partial \alpha} = (u+c)\ \frac{\partial t}{\partial \alpha}\ , \tag{11}$$

$$\frac{\partial r}{\partial \beta} = (u-c)\ \frac{\partial t}{\partial \beta}\ , \tag{12}$$

and

$$\frac{\partial u}{\partial \alpha} + \frac{c}{\rho}\ \frac{\partial \rho}{\partial \alpha} + \frac{2cu}{r}\ \frac{\partial t}{\partial \alpha} = 0\ ,$$

$$\frac{\partial u}{\partial \beta} - \frac{c}{\rho}\ \frac{\partial \rho}{\partial \beta} - \frac{2cu}{r}\ \frac{\partial t}{\partial \beta} = 0\ .$$

The last two equations are not very suitable for finite difference work since ρ varies quite slowly in the liquid. Since $\delta\rho = \delta p/c^2$, the alternative forms

$$\frac{\partial u}{\partial \alpha} + \frac{1}{\rho c}\ \frac{\partial p}{\partial \alpha} + \frac{2cu}{r}\ \frac{\partial t}{\partial \alpha} = 0 \tag{13}$$

$$\frac{\partial u}{\partial \beta} - \frac{1}{\rho c}\ \frac{\partial p}{\partial \beta} - \frac{2cu}{r}\ \frac{\partial t}{\partial \beta} = 0 \tag{14}$$

are used. Equations 11 and 12 define the system of characteristic lines α and β where α is the outward-going characteristic and β the inward going. The bubble wall motion is defined by the variable ℓ and is determined from the expressions

$$\frac{\partial R}{\partial \ell} = U\ \frac{\partial t}{\partial \ell} \tag{15}$$

and

$$\frac{\partial \rho}{\partial \ell} = \frac{dp}{dR}\ \frac{\partial R}{\partial \ell} \tag{16}$$

Related to the method of characteristics is the approximate theory of Gilmore [11] which is based on the so-called Kirkwood-Bethe assumption [18]. This states that the quantity $r\left[h(p) + \frac{u^2}{2}\right]$ is a constant along an outward going characteristic, where

$$h(p) = \int_{p_\infty}^{p} \frac{dp}{\rho} = \frac{1}{(n-1)} (c^2 - c_\infty^2) \qquad (17)$$

is the enthalpy difference between the liquid at pressure p and at pressure p_∞ under isentropic conditions. This assumption can be expressed in the form of an equation containing the particle derivative as defined in Eq. 4. Since the cavity wall moves with the liquid, and since this motion can be expressed purely as a function of time, such particle derivatives can be changed into ordinary derivatives with respect to time and the equation will become

$$R \frac{dU}{dt} \left[1 - \frac{U}{C}\right] + \frac{3}{2} U^2 \left[1 - \frac{U}{3C}\right] = H \left[1 + \frac{U}{C}\right] + \frac{R}{C} \frac{dH}{dt} \left[1 - \frac{U}{C}\right] \qquad (18)$$

governing the motion of the cavity wall. Given initial values on the boundary, a second ordinary differential equation gives the liquid conditions along an outward-going characteristic line:

$$\frac{du}{dt} = \frac{R(H+U^2/2)(u+c)}{r^2 (c-u)} - \frac{2c^2 u}{r(c-u)} . \qquad (19)$$

This is solved in conjunction with the Kirkwood-Bethe assumption and Eqs. 11 and 17.

The variables used in the above equations were non-dimensionalized with respect to the initial radius R_o, the density ρ_∞, and velocity of sound c_∞ in the following way:

$$\rho = \rho/\rho_\infty \quad ; \quad p' = p/\rho_\infty c_\infty^2 \quad ; \quad u' = u/c_\infty \quad ;$$

$$t' = c_\infty t/R_o \quad ; \quad h' = h/c_\infty^2 \quad ; \quad r' = r/R_o \quad .$$

It will be supposed that all the variables and constants used above have already been non-dimensionalized in this way, and the primes suppressed. The equations of motion will remain unaltered by this change, but the liquid equation of state Eq. 5 becomes

$$n(p + B) = \rho^{n} \quad , \tag{21}$$

and the pressure at the bubble wall given by Eq. 9 becomes

$$P = p_o / R^{3\gamma} \quad . \tag{22}$$

Equations 10 and 17 are modified by setting $c_\infty = 1$.

It will be seen from this non-dimensionalization that the solutions are actually independent of the initial radius R_o, i.e., that the same pressures and velocities are obtained regardless of the scale. (The elapsed time is of course proportional to R_o). This is due to the fact that compressible flow equations contain only first order derivatives. If effects such as heat-conduction, viscosity and surface tension were included, the solutions would become dependent on R_o, the dependence becoming stronger with a decrease in R_o.

Solutions to the problem of bubble collapse were obtained by means of a high-speed computer, using the three methods given above. First of all Gilmore's method was used to establish an approximate solution for the motion of the cavity wall. The initial conditions given above were applied, together with the initial value of the velocity given by Eq. 10. The validity of this solution was checked in relation to simple incompressible flow theory[2] for the early stages of the motion. Some exploratory calculations were then carried out using the method of characteristics in the region where the Mach number U/C at the cavity

wall was of the order of 0.1. These results were compared, both on the wall and in the interior of the liquid, with results obtained by Gilmore's method, and it was established that the method was quite accurate in this region. This result was of course to be expected since it can be shown[11] that Gilmore's theory is accurate to terms at least of the order of $(u/c)^2$. Thereafter, Gilmore's method was used to provide initial values in the subsonic $(U/C \sim 0.1)$ region for the solution of the Lagrangian and the characteristic equations. Such a procedure was necessary because of the large amount of computing time required to perform an exact solution starting from the initial stages of the motion. The Lagrangian and the characteristic solutions were carried to the final collapse point and, since they are both supposed to be exact, they provided a check on the numerical accuracy up to this stage. Comparisons were made for points on the cavity wall and in its vicinity, and the discrepencies which occurred were estimated to be at most about one per cent. The Lagrangian solution was then carried on into the region of rebound up to the point where a shock wave formed. Solutions were obtained for a variety of conditions such as might occur in cavitation. The values used for the ambient pressure p_∞ in the liquid were 1 atmosphere, and 10 atmospheres. The initial pressure p_o in the gas was varied from 10^{-1} atmospheres to 10^{-4} atmospheres, while the index γ for the gas had the values 1 and 1.4. The problems were programmed for an IBM 7090 and the numerical methods are described in the appendices.

3. Calculated Results

The first set of calculations were concerned with the motion of the bubble wall and with the gross effect of the gas content of the bubble.

Figures 1-3 show the variation of the bubble wall Mach number with the radius under a variety of conditions. The amount of gas is determined by the initial pressure p_o, and the behavior of the gas is varied by changing the index γ. Figure 1 shows the collapse of a bubble for different initial pressures p_o with $\gamma = 1.4$, acting under an external pressure p_∞ of 1 atmosphere. It is seen that as the amount of gas diminishes, the motion of the bubble wall becomes more and more rapid during the final stages of the collapse. In the case of the empty cavity, the velocity increases without limit as the bubble grows smaller. The exact solutions are compared with solutions derived from Gilmore's theory and from the theory of an empty cavity in an incompressible liquid[2]. It is seen that the compressibility becomes very important during the final stages of the motion. Figure 2 shows the result of increasing the external pressure p_∞ from 1 atmosphere to 10 atmospheres. A comparison with Fig. 3 shows that such an increase does not affect the collapse so much as a change in γ from 1.4 to 1. Thus a gas which behaves isothermally should in general produce a more violent collapse than an adiabatic gas reacting under a high external pressure. In all these results, it is evident that the predictions of Gilmore's theory, based on the Kirkwood-Bethe assumption, continue to be surprisingly accurate.

For the empty cavity under 1 atmosphere external pressure, the bubble wall velocity tends to infinity as $(R_o/R)^{0.785}$. The value of the index was found to be the same when p_∞ was 10 atmospheres. This result is in good agreement with a similar estimate by Hunter[25]. By comparison, Gilmore's theory predicts a rate varying as $(R_o/R)^{0.5}$, while the incompressible theory gives $(R_o/R)^{1.5}$.

The remaining results are concerned with the flow in the liquid around the collapsing bubble and were obtained for the two cases, $p_o = 10^{-3}$ and 10^{-4} atmospheres, with $\gamma = 1.4$ and an external pressure of 1 atmosphere. In both these cases the liquid rebounds and forms a compression wave which moves outwards and steepens into a shock front. The occurrence of the shock front causes the numerical solution to become unstable, so that the results are only presented up to this point. Methods are available[29], [30] for overcoming this instability, and proceeding with the solution. But this continuation would have involved an additional program of computation and, since it is not really necessary for the purposes of this paper, it was not pursued. Figure 4 - 7 show the distributions of Mach number and pressure in the liquid. These are given for successive instants in time which is expressed in terms of τ, the time required for the bubble to collapse from the initial radius R_o to the final minimum radius. The formula used to determine the time scale is $(\tau - t)10^4/\tau$ where t is the time elapsed from the start of the motion. The collapse time τ was determined accurately from the numerical solutions. However it can also be estimated approximately, using Rayleigh's[2] theory for an empty cavity in an incompressible liquid. The approximate formula is

$$\tau \sim 0.91\, R_o(\rho_\infty/p_\infty)^{\frac{1}{2}} \quad .$$

Estimates from this agree to within less than 1% with values obtained in the calculated examples.

Figures 5(b) and 7(b) show the pressure wave forming and traveling outwards into the liquid. Because of the compressibility, the change in the direction of motion of the interface is communicated to the liquid

only by the passage of the pressure wave, and hence a reversal of flow occurs through it, as shown in Figs. 4 and 6. The shock wave forms quite rapidly when the initial pressure is 10^{-4} atmospheres, because the final collapse pressures are high. In the case where the initial pressure is 10^{-3} atmospheres, the pressure front does not steepen so quickly. When $p_o = 10^{-2}$ atmospheres the final pressure at the cavity wall is seen, from Fig. 1, to be about 10^3 atmospheres. For liquid pressures of this magnitude, the compression wave will steepen only very slowly and the rate with which it steepens is reduced as it moves outwards, because of geometric attenuation. For such cases the compression will behave rather like an acoustic wave, which does not alter much in form as it propagates. For larger amounts of gas inside the bubble, the intensity of the compression will diminish even further until only a very weak pulse emanates from the collapse.

Figure 5(b) shows that the acoustic approximation is reasonably valid even in the case where a shock front develops. The pressure front steepens, but the wave remains of approximately the same thickness and attenuates as $1/r$ as it propagates outwards from the collapse center. The last stage of the calculations shows that the peak pressure in the wave is about 1,000 atmospheres at $R/R_o \sim 0.3$. Beyond this point not much change will occur due to dispersion, and the losses due to entropy changes through the shock will be negligible[18]. Hence the pressure pulse will propagate outwards like an acoustic wave, and at $R/R_o \sim 2$ the peak intensity will be of the order of a hundred atmospheres. For smaller amounts of gas inside the bubble, it would be expected that the peak pressures would be somewhat larger even though they are more likely to be affected by dispersion. In both the calculated examples it

was verified that the peak moved with the local velocity of sound.

4. Discussion

It is well-known[31] that cavitation damage is largely due to mechanical causes. However, the precise mechanism is as yet undecided. It has been suggested that the damage is caused by bubbles collapsing asymmetrically on to the solid in such a way that jets of liquid form and strike the surface at high speed. Another mechanism which has been proposed is that the damage is caused by shock waves emanating from bubbles collapsing at a short distance from the solid. The results given in the previous section showed that it would be possible to obtain a shock wave, resulting from the collapse of a cavitation bubble with a peak intensity of the order of a hundred atmospheres or more at a distance of $2R_o$ from the collapse center. A boundary situated at such a distance would not interfere very significantly with the process of collapse. On the other hand the solid material would in all probability be seriously damaged by the pressure pulses resulting from a series of such collapses.

It is possible that the intensity of the radiated pressure pulses would be somewhat diminished by asymmetric effects occurring during the final stage of the collapse. It has been shown[32] that when its velocity is high the wall of a collapsing cavity will become unstable. For an empty cavity this is estimated[33] to occur at radii less than $R/R_o \sim 0.1$. In all the calculated examples the final collapse radii do in fact fall into this region. However the instability will be diminished because of the slowing down of the bubble wall by the internal gas pressure. If the bubble surface does fracture, the collapse will still proceed, but the core of the collapse would probably consist of some kind

of two-phase mixture which is somewhat less compressible than the pure gas phase. Under such conditions shock waves would still emanate, but possibly with diminished intensity. If it is considered that cavitation damage is a fatigue effect caused by a succession of blows then the estimated intensity of the shock waves could be reduced by a factor of ten or so and still remain an effective cause of damage.

The hypothesis that cavitation damage is caused by shock waves from collapsing cavities is supported indirectly by experimental observation. It has been found[34] that an increased gas content in the liquid reduces cavitation damage. This would relate to the fact that weaker shocks occur when there is a larger amount of gas inside the cavities.

APPENDIX I - THE KIRKWOOD-BETHE SOLUTION

From the theory given in Section 2, the governing equation in non-dimensionalized form for the motion of the cavity wall are:

$$\frac{dU}{dt} = [H(C+U) + \frac{R}{C}\frac{dH}{dt}(C-U) - \tfrac{1}{2}U^2(3C-U)]/R(C-U) \qquad (I.1)$$

$$\frac{dR}{dt} = U \qquad (I.2)$$

$$\frac{dH}{dt} = -3\gamma PU/R[n(P+B)]^{1/n} \qquad (I.3)$$

$$P = p_o/R^{3\gamma} \qquad (I.4)$$

$$C = [n(P+B)]^{(n-1)/2n} \qquad (I.5)$$

together with the initial conditions at $t = 0$,

$$R = 1 \; ; \quad P = p_o \; ; \quad C = C(p_o) \; ;$$

$$U = \frac{2}{(n-1)}[C(p_o)-1] \; ; \quad H = \frac{1}{(n-1)}[C^2(p_o)-1] \; . \qquad (I.6)$$

These equations were solved at intervals Δt by a simple step by step iterative procedure starting from the initial values Eq. I.6. A first estimate of U at $t = \Delta t$ was obtained by substituting the initial values into Eq. I.1. This was averaged with the initial value of U and used in Eq. I.2 to obtain a first estimate of R at $t = \Delta t$. The values of R were then averaged in the same way as the values of U and used in Eqs. I.4 and I.5 to get correspondingly averaged values of P and C. The averaged values obtained so far were then used in Eq. I. 3 to obtain an averaged form of dH/dt and a first estimate of H at $t = \Delta t$. This procedure was repeated step by step for each interval Δt. In approaching

the collapse point, the variation with time becomes quite rapid, and it is necessary to keep reducing the interval Δt in order to preserve accuracy. This was done by repeatedly carrying the solution up to the point where U becomes positive, then returning to a suitable earlier point and repeating the last stages of the calculation for a new interval $\Delta t/5$, where Δt was the previous interval.

The solution for the motion of the cavity wall provides the initial values for the following set of equations, which can be solved along an out-going characteristic in the interior of the liquid,

$$\frac{du}{dt} = \left[\frac{(c+u)}{r} Y - 2c^2u\right] / r(c-u) \qquad (I.7)$$

$$\frac{dp}{dt} = [n(p+B)]^{1/n} \left[4c^2u^2 - \frac{(c+u)^2}{r} Y\right] / r(c-u) \qquad (I.8)$$

$$\frac{dr}{dt} = (u+c) \qquad (I.9)$$

$$C = [n(p+B)]^{(n-1)/2n} . \qquad (I.10)$$

The constant Y is derived from the initial conditions and is given by

$$Y = R(H+U^2/2) \qquad (I.11)$$

where R, H, U are values on the cavity wall. This set of equations was solved in the manner already described.

APPENDIX II - THE SOLUTION OF THE CHARACTERISTIC EQUATIONS

The non-dimensionalized equations for the characteristic solution are

$$\frac{\partial r}{\partial \alpha} = (u+c)\ \frac{\partial t}{\partial \alpha} \tag{II.1}$$

$$\frac{\partial r}{\partial \beta} = (u-c)\ \frac{\partial t}{\partial \beta} \tag{II.2}$$

$$\frac{\partial u}{\partial \alpha} + \frac{1}{\rho c}\ \frac{\partial p}{\partial \alpha} + \frac{2cu}{r}\ \frac{\partial t}{\partial \alpha} = 0 \tag{II.3}$$

$$\frac{\partial u}{\partial \beta} - \frac{1}{\rho c}\ \frac{\partial p}{\partial \beta} - \frac{2cu}{r}\ \frac{\partial t}{\partial \beta} = 0 \tag{II.4}$$

with

$$\rho^n = n(p+B) \tag{II.5}$$

$$c = [n(p+B)]^{(n-1)/2n} \ . \tag{II.6}$$

The method used to solve this system is the one used by Gilmore[24] and later by Brand[26]. The initial points lie along an out-going characteristic line α, with the analytic continuation being provided at the intersection with the boundary by the conditions

$$\frac{\partial R}{\partial \rho} = U\ \frac{\partial t}{\partial \ell} \tag{II.7}$$

$$\frac{\partial p}{\partial \ell} = -\ \frac{3\gamma p}{R}\ \frac{\partial R}{\partial \ell} \ . \tag{II.8}$$

This is somewhat shorter than the method used by Hunter[25] who took the initial values to lie along a line $t = \text{const}$. In the present calculations, the initial values were provided by Gilmore's method.

The Eqs. II.1 - II.4 and II.7, II.8 were expressed in finite difference form and applied according to the scheme shown in Fig. 8. The initial line of points along an out-going characteristic are designated by the letter i. The point (i, j) represents the jth point on this line starting from the point on the boundary. The continuation is provided at the boundary at the intersection of the inward-going characteristic through (i, 2) with the boundary. This yields the new point (i + 1, 1). The outward-going characteristic through this new point and the inward-going characteristic through the point (i, 3) intersect at the next new point (i + 1, 2). Repeating this process all the new points on the line (i + 1) are obtained. It is seen that the total number of these points is diminished by 1 compared with the line i. The kind of averaging technique described in the previous appendix was also used here to improve the accuracy.

The fact that one point was lost at each step of the solution proved to be a problem, because it was difficult to decide how many points would be needed to carry the solution to the final stages of the collapse. This was remedied by adding one point at each step using Gilmore's method. This was always done when the Mach number was small so that the new point could be considered to have an accuracy corresponding to the other points on the characteristic line. As the solution approached the last stages of the collapse, the outward-going characteristics began to extend into the region of rebound i.e. into the region $t > \tau$ where τ is the time of collapse. The main criterion for this was the time when the velocity began to turn positive at the end of the line of points. Whenever this occurred, the affected points were discarded. In this way only the points needed to give a solution up to the final stages of collapse were

preserved.

The number of points used was also determined by the motion of the bubble wall. When the collapse becomes more rapid, more points are needed to ensure the proper accuracy. As a check the first and final estimates of the velocity and pressure were compared at each step and, if these differed by a certain percentage, then an interpolation automatically occurred which doubled the total number of points. The additional points were situated at the half intervals.

The techniques described here were tested for a variety of examples, and the accuracy of the results presented is considered to be quite satisfactory. The calculations were performed on an IBM 7090 and each example took about ten minutes.

APPENDIX III - SOLUTION OF THE LAGRANGIAN EQUATIONS

The governing equations for the Lagrangian form of the solution are,

$$\rho r^2 \frac{\partial r}{\partial y} = 1 \tag{III.1}$$

$$\frac{\partial u}{\partial t} = - r^2 \frac{\partial p}{\partial y} \tag{III.2}$$

$$\frac{\partial r}{\partial t} = u \tag{III.3}$$

with

$$\rho^n = n(p+B) \tag{III.4}$$

$$c = [n(p+B)]^{(n-1)/2n} \quad . \tag{III.5}$$

This set of equations is sufficient to determine the variables. Equation III.1 can be used to find ρ, whence Eq. III.4 yields p. However this is not a very satisfactory process, since ρ varies comparatively slowly and is not very suitable as a running variable. Hence instead of Eq. III.1 the following relation was used,

$$\frac{\partial p}{\partial t} = - [n(p+B)] \left[\rho r^2 \frac{\partial u}{\partial y} + \frac{2u}{r} \right] \quad . \tag{III.6}$$

In addition the pressure on the boundary was given by

$$P = p_o / R^{3\gamma} \tag{III.7}$$

The above set of equations were expressed as finite differences. The variables were situated at different points in the finite difference lattice so that the derivatives could be expressed in a difference form

accurate to second order. The arrangement used is shown in Fig. 9. The velocity u was evaluated at the points $(i, j + \frac{1}{2})$, the pressure p at the points $(i + \frac{1}{2}, j)$, and the radial distance r at the points $(i + \frac{1}{2}, j + \frac{1}{2})$, where i, j are the coordinates of a typical point of the lattice. At the boundary the velocity increment was found using a three point difference formula for the derivative $\partial p/\partial y$. An iteration scheme using averaged values was employed, in a manner similar to that described in the previous appendices.

The initial points were obtained using Gilmore's theory. Given a set of points describing the motion of the bubble wall, solutions are found along the outward-going characteristics starting from each of the given points and finishing on a certain line $t = \text{const}$. The points along this line then provide the initial points for the calculation. The increment in y between each of the points is found from Eq. III.1.

Because of the purposes of the calculation, the computations had to be performed over a fairly extensive range of y. However, the need for accuracy decreases in moving away from the bubble wall, and the spacing of the points can be reduced correspondingly. This is already achieved to some extent by the initial points since their spacing with respect to y varies roughly as r^2. However, finer accuracy is required near the boundary when the collapse becomes more rapid. Hence a scheme of interpolation was embarked on, similar to that described in Appendix II for the method of characteristics. When the differences between first and second estimates at the boundary become greater than a certain percentage, interpolations are made between the first twenty-five points closest to the boundary. Hence the total number of points is increased with each interpolation. In order to prevent the loss at each

step in time of the point farthest from the bubble wall, an extrapolation is made assuming the liquid to be incompressible. This assumption is justified because the magnitude of the velocity and pressure in this region is small. The increment in time was determined from the well-known Courant-Levy condition on the relation between sound speed and mesh speed.

The solutions were carried up to the final collapse point and beyond into the region of rebound, where a compression wave forms and moves outwards, eventually turning into a shock front. Beyond this stage the solution could presumably have been carried on using methods such as those of von Neumann and Richtmeyer[29] or Lax[30] where an artificial viscosity term is introduced into the equations of motion to create a smooth transition in flow through the shock. By this means the motion of the shock could have been followed as it moved out into the liquid. This was not attempted here, however, because it was felt that enough information had already been obtained to make an order of magnitude estimate of shock strengths at a distance from the center of collapse, and because to have followed the solution to any extent in this way, would have involved an elaborate reconstruction of the numerical procedures together with an extensive series of test calculations.

Up to the final collapse point the Lagrangian solution could be compared to that obtained from the method of characteristics. Good agreement was found once both programs had been developed and tested. For example in the results presented here the final collapse radii agree to within less than 1%. Other comparisons showed a similar order of agreement. After the final collapse point, the Lagrangian solution showed good agreement with physical considerations. The crest of the

compression wave moved with the local speed of sound, and the attenuation under conditions where dispersive effects were not strong varied approximately in inverse proportion to the distance from the center of collapse.

The calculation time for each of the examples given here was about twenty minutes.

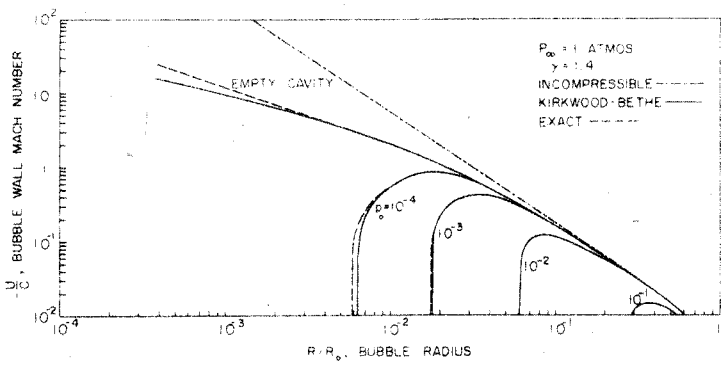

Fig. 1 The bubble wall Mach number as a function of the bubble radius for decreasing gas content. The gas content is determined by its initial pressure p_o in atmospheres. The index γ has the value 1.4 and the ambient pressure p_∞ is one atmosphere.

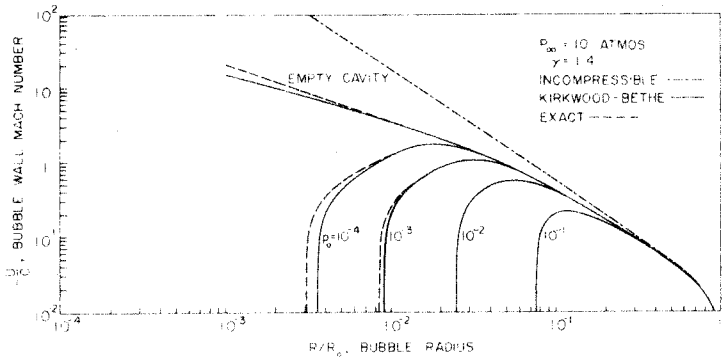

Fig. 2 The bubble wall Mach number as a function of the bubble radius for decreasing gas content. The index γ has the value 1.4 and the ambient pressure p_∞ is 10 atmospheres.

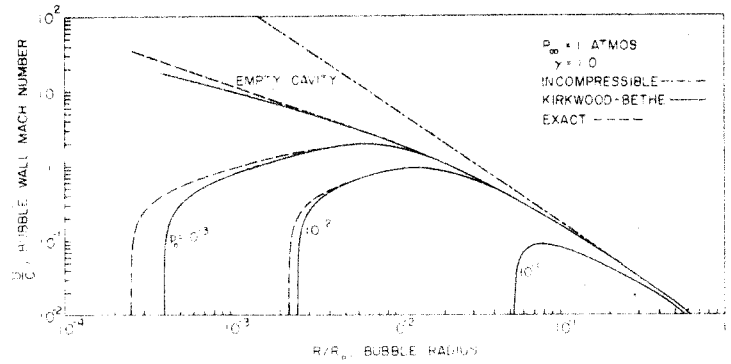

Fig. 3 The bubble wall Mach number as a function of the bubble radius for decreasing gas content. The index γ has the value 1.0 and the ambient pressure p_∞ is 1 atmosphere.

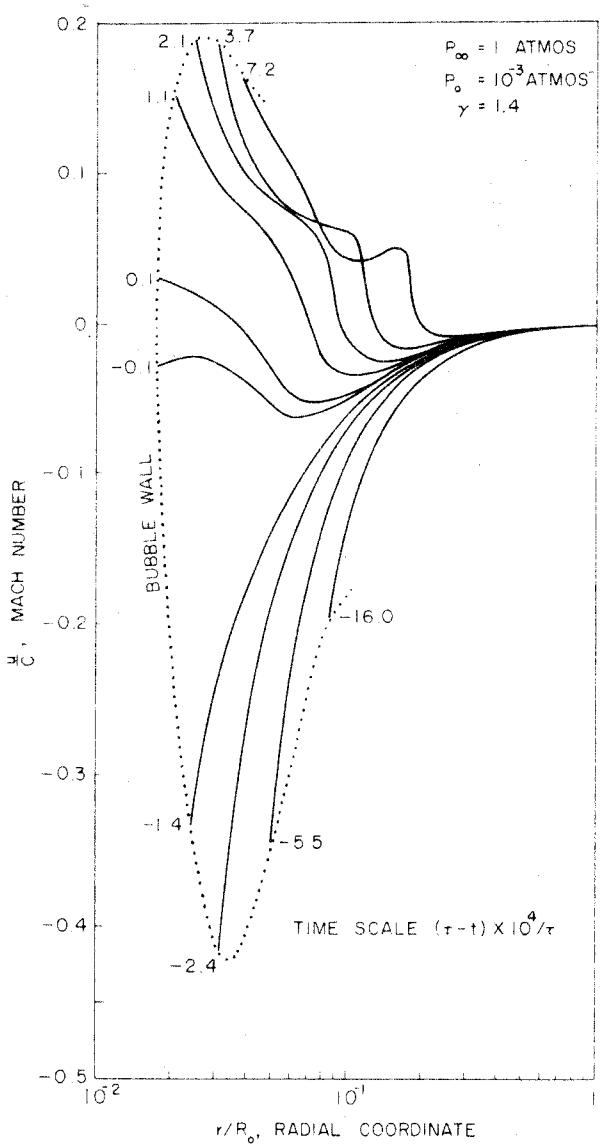

Fig. 4 Variation of Mach number with distance from the bubble wall for different instants in time during the collapse and rebound of the bubble. The initial internal pressure p_o in the gas is 10^{-3} atmospheres. The ambient pressure p_∞ is 1 atmosphere.

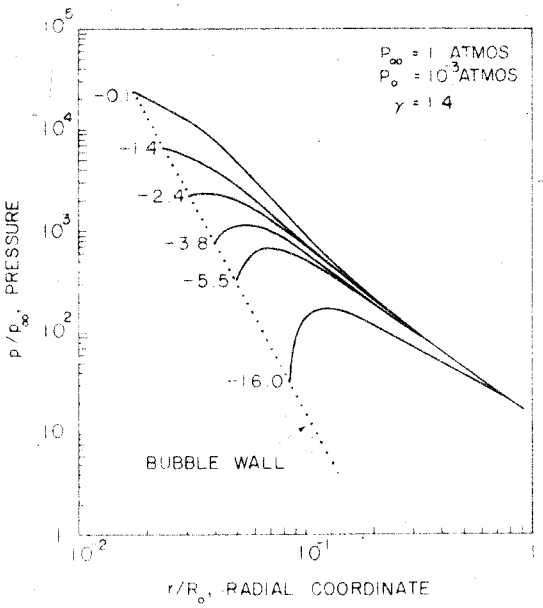

Fig. 5(a) Variation of pressure with distance from the bubble wall for different instants in time during the collapse of the bubble. The conditions correspond to those of Fig. 4.

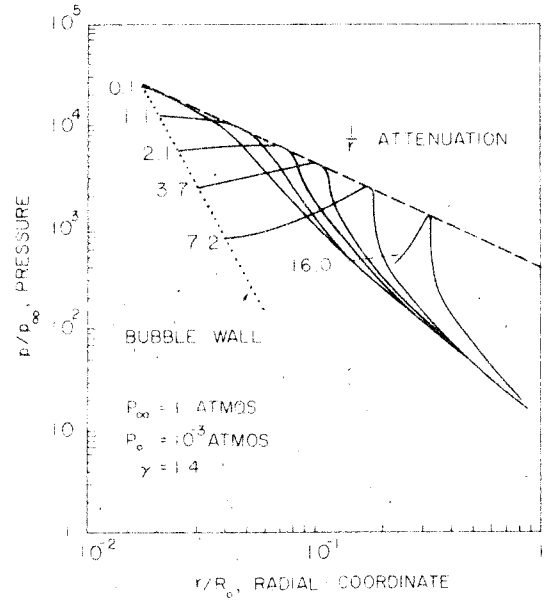

Fig. 5(b) Variation of pressure with distance from the bubble wall for different instants in time during the rebound of the bubble.

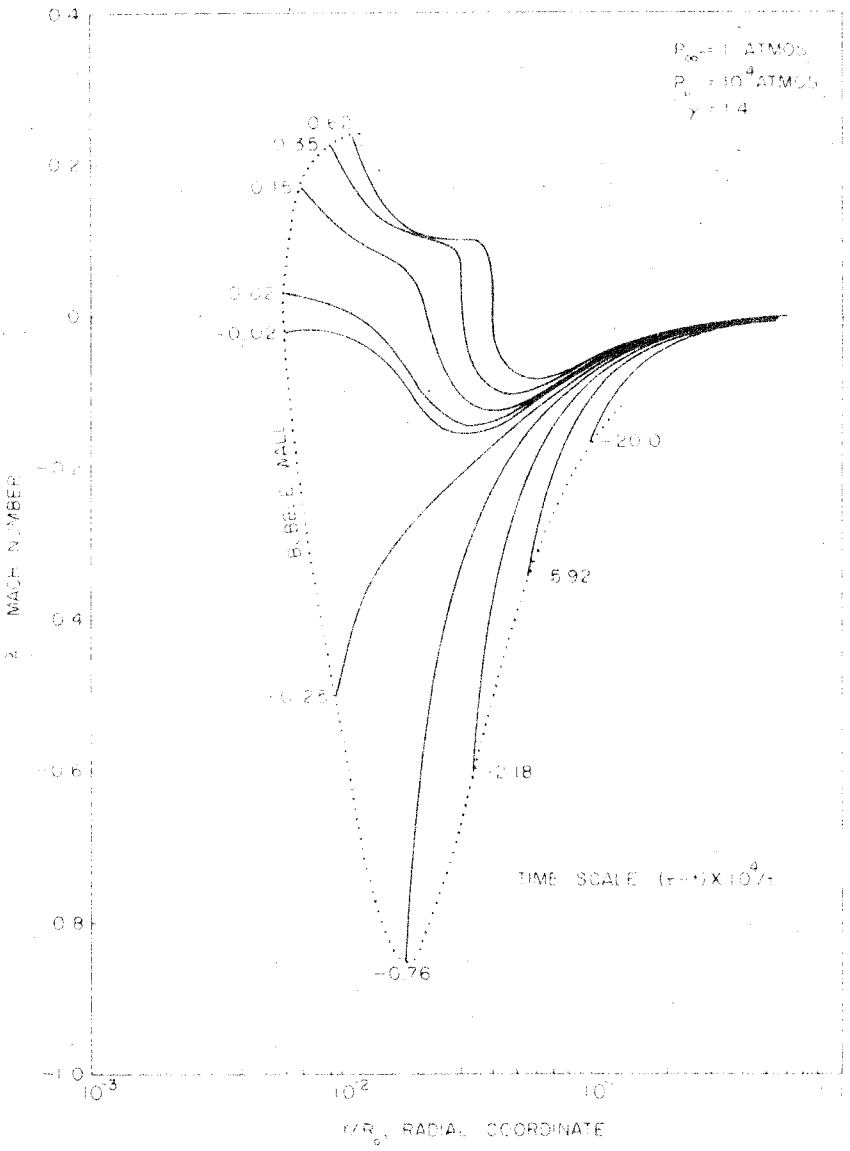

Fig. 6 Variation of Mach number with distance from the bubble wall for different instants in time during the collapse and rebound of the bubble. The initial pressure p_{G_0} in the gas is 10^{-4} atmospheres. The ambient pressure is 1 atmosphere.

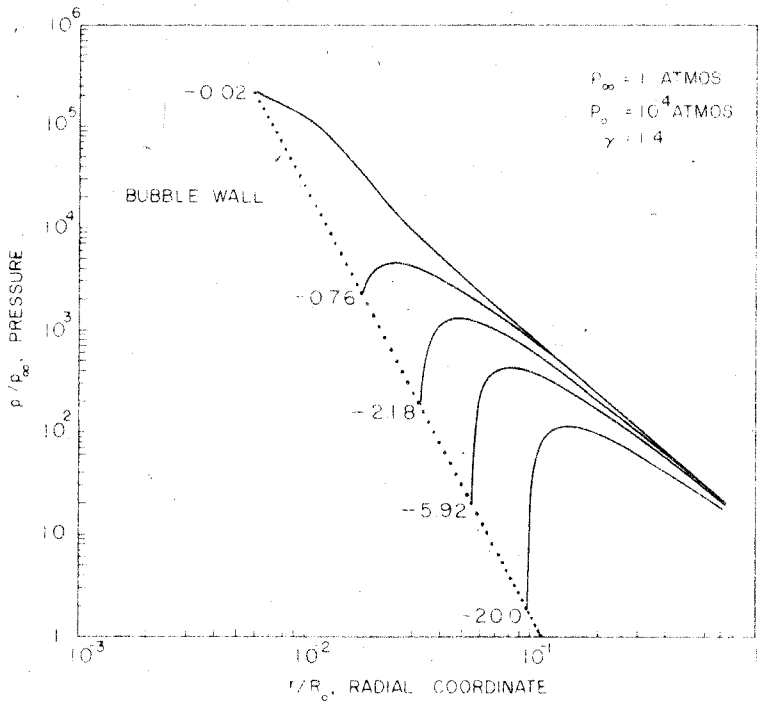

Fig. 7(a) Variation of pressure with distance from the bubble wall for different instants in time during the collapse of the bubble. The conditions correspond to those of Fig. 6.

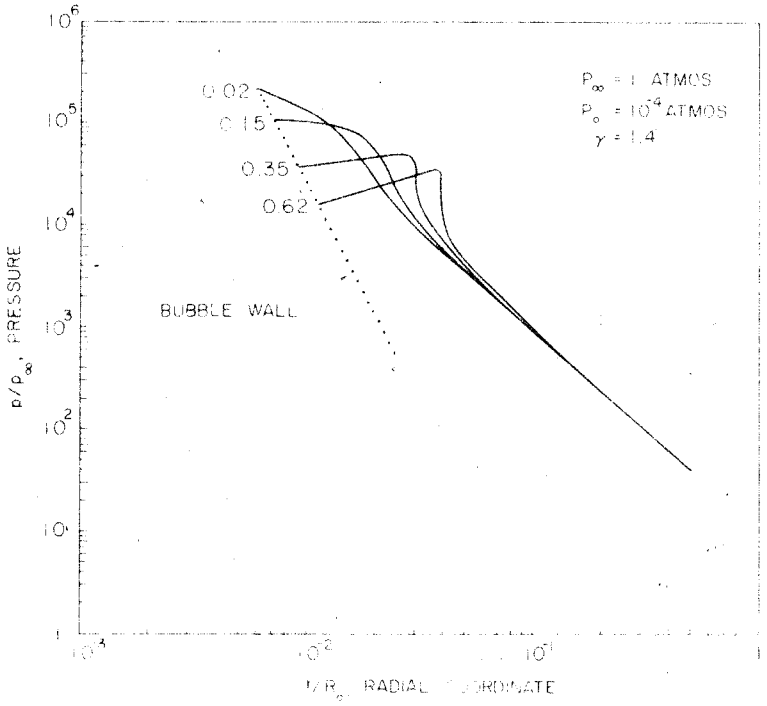

Fig. 7(b) Variation of pressure with distance from the bubble wall for different instants in time during the rebound of the bubble.

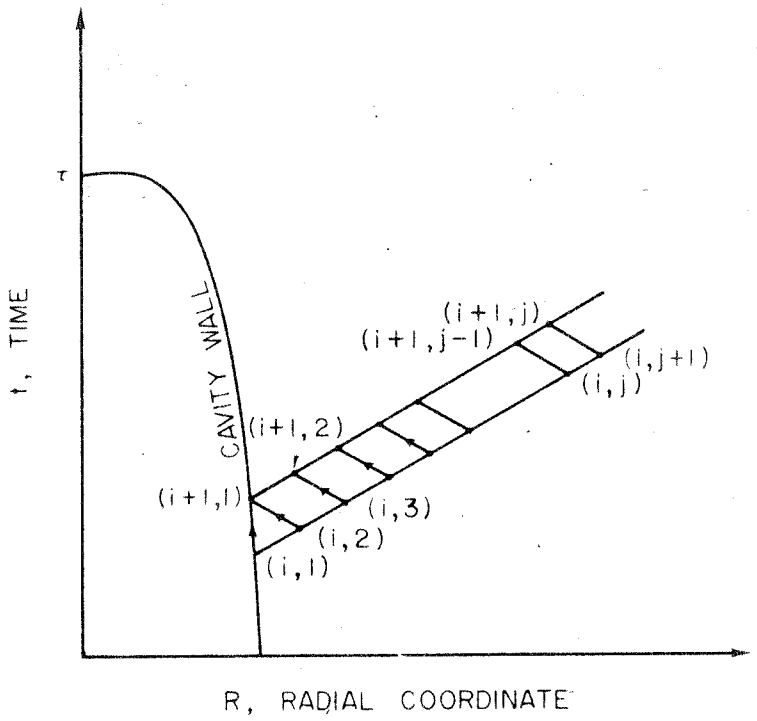

Fig. 8 Finite difference mesh in R - t plane for solution by method of characteristics.

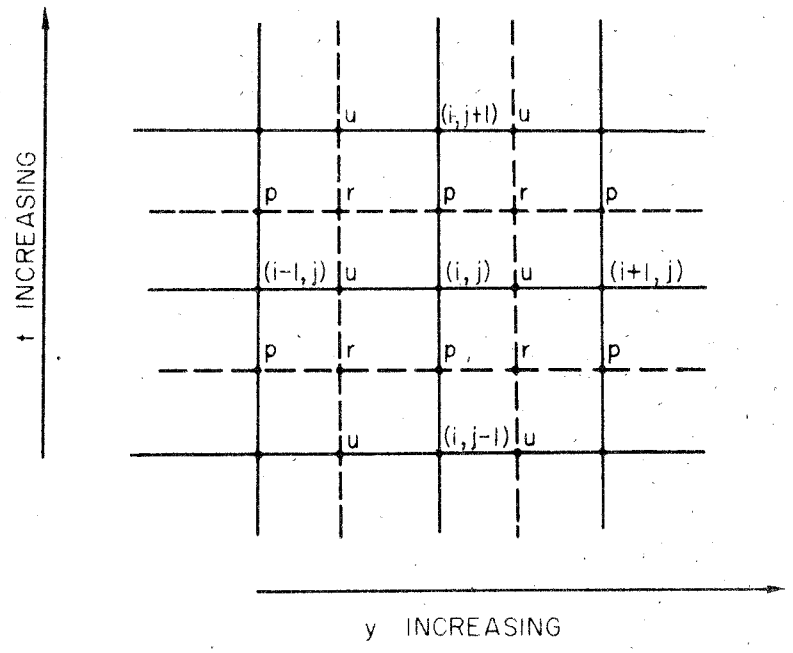

Fig. 9 Finite difference mesh in R - t plane for solution of Lagrangian equations.

REFERENCES TO PART II

[1] P. Jarman, J. Acoust. Soc. Amer., 32, 11, 1459 - 1462 (1960).

[2] Lord Rayleigh, Phil Mag., 34, 94 - 98 (1917).

[3] Yu. N. Ryabinin, "Gases at High Densities and Pressures" Pergamon Press (1961).

[4] P. Gunther, E. Heim and H. V. Borgstedt, Z. Electrochem., 63, 43 - 47 (1959).

[5] D. Srinivasan, The Sonoluminescence of Water, Ph.D. Thesis, University of Missouri (1955).

[6] R. O. Prudhomme and Th. Guilmart, J. Chim. Phys., 54, 336 - 340 (1957).

[7] P. Gunther, W. Zeil, U. Grisaw, E. Heim, Z. Electrochem., 61, 188 - 195 (1957).

[8] F. G. Blake, Tech. Memo. No. 12, Acoustics Research Lab., Harvard University, Cambridge, Mass. (1949).

[9] M. D. Rosenberg, Tech. Memo. No. 26, Acoustics Research Lab., Harvard University, Cambridge, Mass. (1953).

[10] D. Y. Hsieh and M. S. Plesset, J. Acoust. Soc. Amer., 33, 206 - 215 (1961).

[11] F. R. Gilmore, Rept. No. 26-4, Hydrodynamics Laboratory, California Inst. of Technology, Pasadena, Calif. (1952).

[12] P. Jarman, Proc. Phys. Soc. (Lond.), 73, 628 - 640 (1959).

[13] Thorpe's Dictionary of Applied Chemistry, 4th Edit., Longmans Green and Co.

[14] Handbook of Chemistry and Physics, 41st Edit., Chemical Rubber Publishing Company, p. 1708 (1959).

[15] M. S. Plesset and S. A. Zwick, J. Appl. Phys., 23, 95 - 98 (1952).

[16] M. S. Plesset, J. Appl. Mech., 16, 277 - 282 (1949).

[17] R. D. Richtmeyer, "Difference Methods for Initial-Value Problems", Interscience Publishers Inc., New York, 1957, pp. 112, 202.

[18] R. H. Cole, "Underwater Explosions", Princeton University Press (1948).

[19] C. Herring, "Theory of the Pulsations of a Gas Bubble Produced by an Underwater Explosion", OSRD Rept. No. 236 (1941).

[20] L. Trilling, J. Appl. Phys., 23, 14 - 17 (1952).

[21] J. G. Kirkwood and H. A. Bethe, "The Pressure Wave Produced by an Underwater Explosion", OSRD Rept. No. 588 (1942).

[22] R. H. Mellen, Journ. Acoust. Soc. Amer., 28, 447 - 454 (1956).

[23] H. Flynn, Technical Memo No. 38, Acoustics Research Lab., Harvard University (1957).

[24] F. R. Gilmore, Symposium on Naval Hydrodynamics National Acad. Science - - Nat. Res. Council Publication No. 515 (1957) p. 280.

[25] C. Hunter, Journ. Fluid Mech., 8, 241 - 263 (1960).

[26] R. S. Brand, Tech. Rept. No. 34, Division of Applied Mathematics, Brown University (1960).

[27] S. A. Zwick, Rept. No. 21-19, Hydrodynamics Laboratory, California Inst. of Technology, Pasadena, Calif. (1954).

[28] P. W. Bridgman, "The Physics of High Pressures" G. Bell and Sons Ltd., London (1949) p. 141.

[29] J. von Neumann and R. D. Richtmeyer, Journ. Appl. Phys., 21, 232 - 237 (1950).

[30] P. D. Lax, Comm. Pure and Applied Math., 7, 159 - 193 (1954).

[31] M. S. Plesset and A. T. Ellis, Trans. Amer. Soc. Mech. Eng., 77, 1055 - 1064 (1955).

[32] M. S. Plesset and T. P. Mitchell, Quarterly of Appl. Math., 13, 419 - 430 (1956).

[33] M. S. Plesset, Symposium on Cavitation in Real Fluids sponsored by General Motors, (in press) (1962).

[34] M. S. Plesset, Journal of Basic Engineering, 82, 808 - 820 (1960).